7

Solvent Transport Phenomena

Many industrial processes rely on dissolution of raw materials and subsequent removal of solvents by various drying process. The formation of a solution and the subsequent solvent removal depends on a solvent transport phenomena which are determined by the properties of the solute and the properties of the solvent. Knowledge of the solvent movement within the solid matrix by a diffusion process is essential to design the technological processes. Many of the final properties, such as tribological properties, mechanical toughness, optical clarity, protection against corrosion, adhesion to substrates and reinforcing fillers, protective properties of clothing, the quality of the coated surface, toxic residues, morphology and residual stress, ingress of toxic substances, chemical resistance, depend not only on the material chosen but also on the regimes of technological processes. For these reasons, solvent transport phenomena are of interest to modern industry.

7.1 INTRODUCTION TO DIFFUSION, SWELLING, AND DRYING

George Wypych
ChemTec Laboratories, Inc., Toronto, Canada

Small molecule diffusion is the driving force behind movement of small molecules in and out of the solid matrix. Although both swelling and drying rely on diffusion, these processes are affected by the surfaces of solids, the concentration of small molecules in the surface layers, the morphology of the surface, and the interface between phases in which diffusion gradient exists. For these reasons, swelling and drying are treated as specific phenomena.

7.1.1 DIFFUSION

The free-volume theory of diffusion was developed by Vrentas and Duda.[1] This theory is based on the assumption that movement of a small molecule (e.g., solvent) is accompanied by a movement in the solid matrix to fill the free volume (hole) left by a displaced solvent molecule. Several important conditions must be described to model the process. These include the time scales of solvent movement and the movement of solid matrix (e.g. polymer segments, called jumping units), the size of holes which may fit both solvent molecules and jumping units, and the energy required for the diffusion to occur.

The timescale of the diffusion process is determined by the use of the diffusion Deborah, number De, given by the following equation:

$$De = \frac{\tau_M}{\tau_D} \qquad [7.1.1]$$

where:

τ_M	the molecular relaxation time
τ_D	the characteristic diffusion time

If the diffusion Deborah number is small (small molecular relaxation time or large diffusion time) molecular relaxation is much faster than diffusive transport (in fact, it is almost instantaneous).[2] In this case the diffusion process is similar to simple liquids. For example, diluted solutions and polymer solutions above glass transition temperature fall in this category.

If the Deborah number is large (large molecular relaxation time or small diffusion time), the diffusion process is described by Fickian kinetics and is denoted by an elastic diffusion process.[1] The polymeric structure in this process is essentially unaffected and coefficients of mutual and self-diffusion become identical. Elastic diffusion is observed at low solvent concentrations below the glass transition temperature.[2]

The relationships below give the energy required for the diffusion process and compare the sizes of holes required for the solvent and polymer jumping unit to move within the system. The free-volume coefficient of self-diffusion is given by the equation:[2]

$$D_1 = D_o \exp\left[-\frac{E}{RT}\right] \times \exp\left[-\frac{\gamma\left(\omega_1 \hat{V}_1^* + \omega_2 \xi \hat{V}_2^*\right)}{\hat{V}_{FH}}\right] \qquad [7.1.2]$$

where:

D_1	self-diffusion coefficient
D_o	pre-exponential factor
E	energy per molecule required by the molecule to overcome attractive forces
R	gas constant
T	temperature
γ	overlap factor introduced to address the fact that the same free volume is available for more than one molecule
ω	mass fraction (index 1 for solvent, index 2 for polymer)
V*	specific free hole volume (indices the same as above)
ξ	the ratio of the critical molar volume of the solvent jumping unit to the critical molar volume of the polymer jumping unit (see equation [7.1.3])
$\hat{V}_{FH}$	average hole free volume per gram of mixture.

$$\xi = \hat{V}_1^* / \hat{V}_2^* = \hat{V}_1^* M_1 / \hat{V}_2^* M_2 \qquad [7.1.3]$$

where:

M	molecular weight (1 - solvent, 2 - polymer jumping unit)

The first exponent in equation [7.1.2] is the energy term and the second exponent is the free-volume term. Figure 7.1.1 shows three regions of temperature dependence of free-volume: I - above glass transition temperature, II - close to transition temperature, and III - below the transition temperature. In the region I, the second term of the equation [7.1.2] is negligible and thus diffusion is energy-driven. In the region II both terms are significant. In the region III the diffusion is free volume-driven.[3]

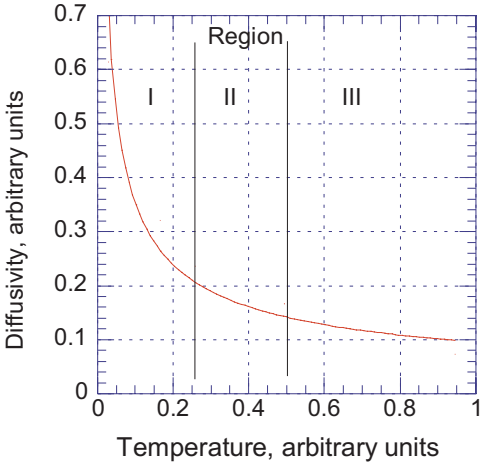

Figure 7.1.1. Temperature dependence of the solvent self-diffusion coefficient. [Adapted, by permission, from D Arnauld, R L Laurence, *Ind. Eng. Chem. Res.*, **31**(1), 218-28 (1992).]

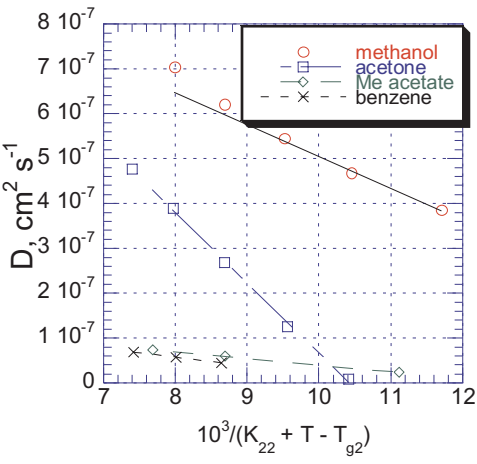

Figure 7.1.2. Free-volume correlation data for various solvents. [Data from D Arnauld, R L Laurence, *Ind. Eng. Chem. Res.*, **31**(1), 218-28 (1992).]

The mutual diffusion coefficient is given by the following equation:

$$D = \frac{D_1 \omega_1 \omega_2}{RT} \left(\frac{\partial \mu_1}{\partial \omega_1} \right)_{T,p} = D_1 Q \qquad [7.1.4]$$

where:

D	mutual diffusion coefficient
μ_1	chemical potential of a solvent per mole
Q	thermodynamic factor.

These equations are at the core of diffusion theory and are commonly used to predict various types of solvent behavior in polymeric and other systems. One important reason for their wide application is that all essential parameters of the equations can be quantified and then used for calculations and modelling. The examples of data given below illustrate the effect of important parameters on the diffusion processes.

Figure 7.1.2 shows the effect of temperature on the diffusivity of four solvents. The relationship between diffusivity and temperature is essentially linear. Only solvents having the smallest molecules (methanol and acetone) depart slightly from a linear relationship due to the contribution of the energy term. The diffusivity of the solvent decreases as temperature decreases. Several other solvents show a similar relationship.[3]

Figure 7.1.3 shows the relationship between the solvent's molar volume and its activation energy. The activation energy increases as the solvent's molar volume increases then levels off. The data show that the molar volume of a solvent is not the only parameter which affects activation energy. Flexibility and the geometry of solvent molecule also affect activation energy.[3] Branched aliphatic solvents (e.g., 2-methyl-pentane, 2,3-dimethyl-butane) and substituted aromatic solvents (e.g., toluene, ethylbenzene, and xylene) show large departures from free volume theory predictions.

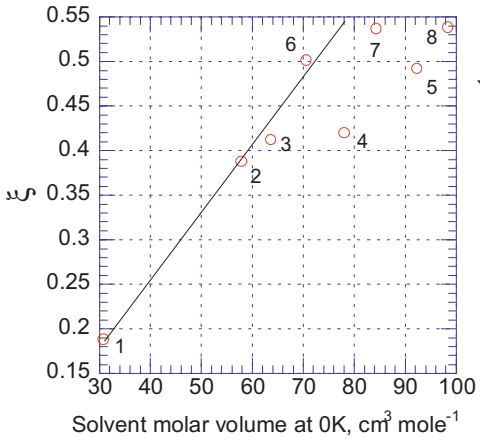

Figure 7.1.3. Parameter ξ vs. solvent molar volume. 1 - methanol, 2 - acetone, 3 - methyl acetate, 4 - ethyl acetate, 5 - propyl acetate, 6 - benzene, 7 - toluene, 8 - ethylbenzene. [Adapted, by permission, from D Arnauld, R L Laurence, *Ind. Eng. Chem. Res.*, **31**(1), 218-28 (1992).]

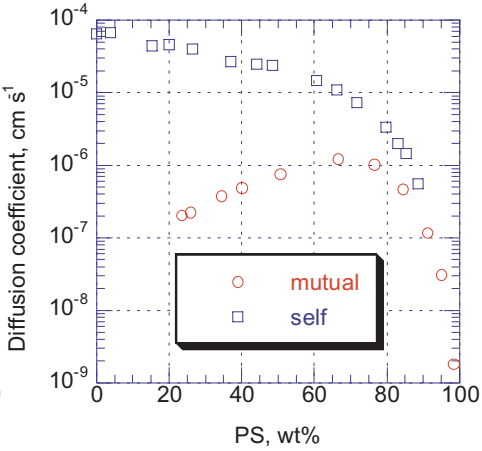

Figure 7.1.4. Mutual and self-diffusion coefficients for polystyrene/toluene system at 110°C. [Adapted, by permission, from F D Blum, S Pickup, R A Waggoner, *Polym. Prep.*, **31** (1), 125-6 (1990).]

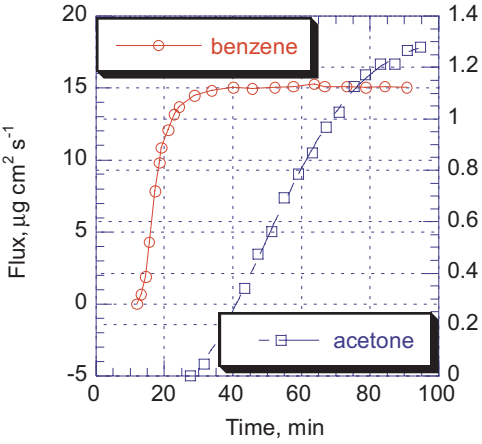

Figure 7.1.5. Flux vs. time for two solvents. [Adapted by permission from C F Fong, , Y Li, De Kee, J Bovenkamp, *Rubber Chem. Technol.*, **71**(2), 285-288 (1998).]

Many experimental methods such as fluorescence, reflection Fourier transform infrared, NMR, quartz resonators, and acoustic wave admittance analysis, are used to study diffusion of solvents.[4-11] Special models have been developed to study process kinetics based on experimental data.

Figure 7.1.4 shows the effect of concentration of polystyrene on mutual and self-diffusion coefficients measured by pulsed-gradient spin-echo NMR. The data show that the two coefficients approach each other at high concentrations of polymer as predicted by theory.[4]

Studies on solvent penetration through rubber membranes (Figure 7.1.5), show that in the beginning of the process, there is a lag time called break-through time. This is the time required for solvent to begin to penetrate the membrane. It depends on both the solvent and the membrane. Of solvents tested, acetone had the longest break-through time in natural rubber and toluene the longest in nitrile rubber. After penetration has started the flux of solvent increases rapidly and ultimately levels off.[7] This study is relevant in testing the permeability of protective clothing and protective layers of coatings.

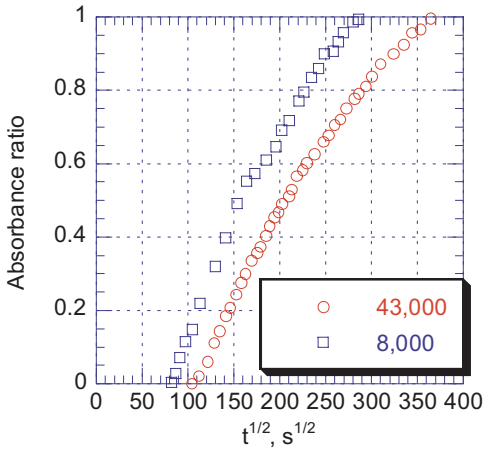

Figure 7.1.6. Absorbance ratio vs. exposure time to water for PMMA of different molecular weights. [Adapted, by permission, from I Linossier, F Gaillard, M Romand, J F Feller, *J. Appl. Polym. Sci.*, **66**, No.13, 2465-73 (1997).]

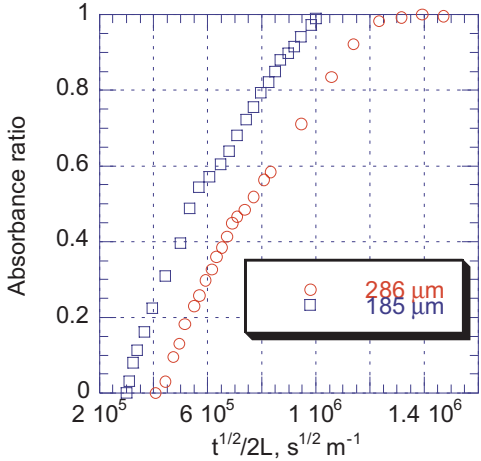

Figure 7.1.7. Absorbance ratio vs. exposure time to water for PMMA films of different thickness. [Adapted, by permission, from I Linossier, F Gaillard, M Romand, J F Feller, *J. Appl. Polym. Sci.*, **66**, No.13, 2465-73 (1997).]

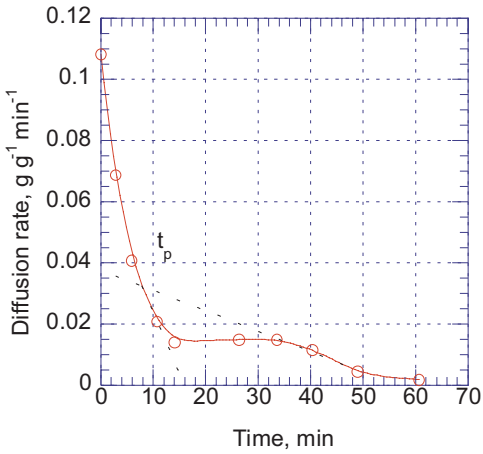

Figure 7.1.8. Relative diffusion rate vs. curing time. [Adapted, by permission, from Jinhua Chen, Kang Chen, Hong Zhang, Wanzhi Wei, Lihua Nie, Shouzhuo Yao, *J. Appl. Polym. Sci.*, **66**, No.3, 563-71 (1997).]

Similar observations were made using internal reflection Fourier transform infrared to measure water diffusion in polymer films.[9] Figure 7.1.6 shows that there is a time lag between the beginning of immersion and water detection in polymer film. This time lag increases as the molecular weight increases (Figure 7.1.6) and film thickness increases (Figure 7.1.7). After an initial increase in water concentration, the amount levels off. Typically, the effect of molecular weight on the diffusion of the penetrant does not occur. High molecular weight polymer has a shift in the absorption peak from 1730 to 1723 cm^{-1} which is associated with the hydrogen bonding of the carbonyl group. Such a shift does not occur in low molecular weight PMMA. Water can move at a higher rate in low molecular weight PMMA. In some other polymers, this trend might be reversed if the lower molecular weight polymer has end groups which can hydrogen bond with water.

Bulk acoustic wave admittance analysis was used to study solvent evaporation during curing.[8] Three characteristic stages were identified: in the first stage viscosity increases accompanied by a rapid decrease in diffusion rate; in the second stage the film is formed, the

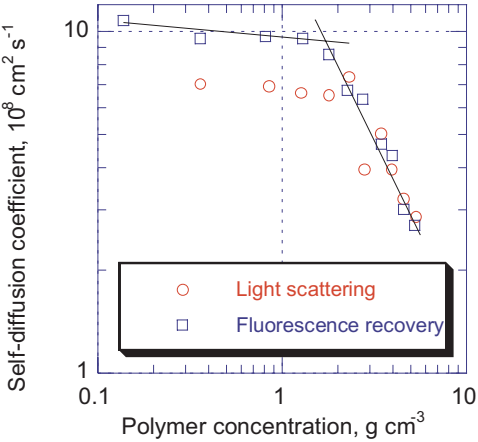

Figure 7.1.9. Self-diffusion coefficient vs. polystyrene concentration. [Adapted, by permission, from L Meistermann, M Duval, B Tinland, *Polym. Bull.*, **39**, No.1, 101-8 (1997).]

surface appears dry (this stage ends when the surface is dry) and the diffusion rate becomes very low; in the third stage solvent diffuses from the cured film. This is a slow process during which diffusion rate drops to zero. These changes are shown in Figure 7.1.8. The diffusion rate during drying decreases as the concentration of polymer (phenol resin) in varnish increases. Also, the time to reach the slope change point in diffusion/time relationship increases as the concentration of polymer increases.[8]

Two methods have been used to measure the diffusion coefficient of toluene in mixtures of polystyrenes having two different molecular weights: one was dynamic light scattering and the other, fluorescence recovery after bleaching.[10] The data show that the relationship between the diffusion coefficient and polymer concentration is not linear. The crossover point is shown in Figure 7.1.9. Below a certain concentration of polymer, the diffusion rate drops rapidly according to different kinetics. This is in agreement with the above theory (see Figure 7.1.1 and explanations for equation [7.1.2]). The slope exponent in this study was -1.5 which is very close to the slope exponent predicted by the theory of reptation (-1.75).

The above data show that theoretical predictions are accurate when modelling diffusion phenomena in both simple and complicated mixtures containing solvents.

7.1.2 SWELLING

Polymers differ from other solids because they may absorb large amounts of solvents without dissolving. They also undergo large deformations when relatively small forces are involved.[12] Swelling occurs in a heterogeneous two phase system a solvent surrounding a swollen body also called gel. Both phases are separated by the phase boundary permeable to solvent.[13]

The swelling process (or solvent diffusion into to the solid) occurs as long as the chemical potential of solvent is large. Swelling stops when the potentials are the same and this point is called the swelling equilibrium. Swelling equilibrium was first recognized by Frenkel[14] and the general theory of swelling was developed by Flory and Rehner.[15,16]

The general theory of swelling assumes that the free energy of mixing and the elastic free energy in a swollen network are additive. The chemical potential difference between gel and solvent is given by the equation:

$$(\mu_1 - \mu_1^0) = (\mu_1 - \mu_1^0)_{mix} + (\mu_1 - \mu_1^0)_{el} \qquad [7.1.5]$$

where:

μ_1 chemical potential of gel
μ_1^0 chemical potential of solvent

The chemical potential is the sum of the terms of free energy of mixing and the elastic free energy. At swelling equilibrium, $\mu_1 = \mu_1^0$, and thus the left hand term of the equation becomes zero. The equation [7.1.5] takes the following form:

$$(\mu_1 - \mu_1^0)_{mix} = -(\mu_1 - \mu_1^0)_{el} = RT[\ln(1-v_2) - v_2 + \chi v_2^2] \qquad [7.1.6]$$

where:

v_2	$= n_2V_2/(n_1V_1 + n_2V_2)$ volume fraction of polymer
n_1, n_2	moles of solvent and polymer, respectively
V_1, V_2	molar volumes of solvent and polymer, respectively
R	gas constant
T	absolute temperature
χ	Flory-Huggins, polymer-solvent interaction parameter.

The interaction between the solvent and solid matrix depends on the strength of such intermolecular bonds as polymer-polymer, solvent-solvent, and polymer-solvent. If interaction between these bonds is similar, the solvent will easily interact with polymer and a relatively small amount of energy will be needed to form a gel.[12] The Hildebrand and Scatchard hypothesis assumes that interaction occurs between solvent and a segment of the chain which has a molar volume similar to that of solvent.[12] Following this line of reasoning the solvent and polymer differ only in potential energy and this is responsible for their interaction and for the solubility of polymer in the solvent. If the potential energies of solvents and polymeric segments are similar they are readily miscible. In crosslinked polymers, it is assumed that the distance between crosslinks is proportional to the molecular volume of the polymer segments. This assumption is the basis for determining molecular mass between crosslinks from results of swelling studies.

The result of swelling in a liquid solvent (water) is determined by equation:[13]

$$\left(\frac{\partial T}{\partial w_1}\right)_P^{g/l} = \frac{T\left(\frac{\partial \mu_1^g}{\partial w_1}\right)_{T,P}}{\Delta H_1^{g/l}} \qquad [7.1.7]$$

where:

T	thermodynamic (absolute) temperature
w_1	mass fraction of solvent in gel at saturation concentration
g	phase symbol (for gel)
l	symbol for liquid
P	pressure
μ_1^g	chemical potential of solvent in gel phase dependent on temperature
$\Delta H_1^{g/l}$	$= H_1^g - H_{01}^{-l}$ is the difference between partial molar enthalpy of solvent (water) in gel and pure liquid solvent (water) in surrounding

Contrast this with the equation for water in the solid state (ice):

$$\left(\frac{\partial T}{\partial w_1}\right)_P^{g/cr} = \frac{T\left(\frac{\partial \mu_1^g}{\partial w_1}\right)_{T,P}}{\Delta H_1^{g/cr}} \qquad [7.1.8]$$

where: cr phase symbol for crystalline solvent (ice)

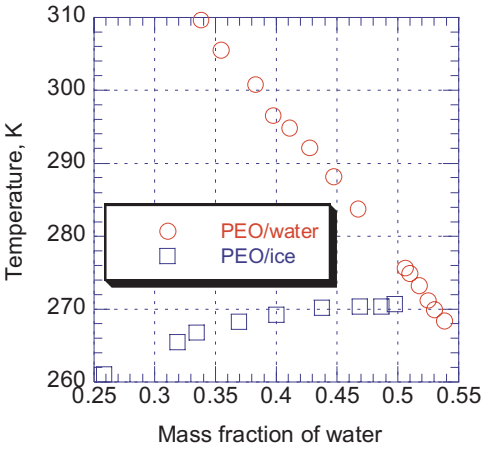

Figure 7.1.10. Swelling of crosslinked polyurethane in water and ice. [Adapted, by permission, from B Hladik, S Frahn, W Borchard, *Polym. Polym. Compos.*, **3**, No.1, 21-8 (1995).]

A comparison of equations [7.1.7] and [7.1.8] shows that the slope and sign of swelling curve are determined by the quantity $\Delta H_1^{g/l \text{ or } cr}$. Since the melting enthalpy of water is much larger than the transfer enthalpy of water, the swelling curves of gel in liquid water are very steep. The sign of the slope is determined by the heat transfer of the solvent which may be negative, positive or zero depending on the quality of solvent. The melting enthalpy is always positive and therefore the swelling curve in the presence of crystalline solvent is flat with a positive slope. A positive slope in temperatures below zero (for ice) means that gel has to deswell (release water to its surrounding, or dry out) as temperature decreases.[13] Figure 7.1.10 illustrates this.

For practical purposes, simple equations are used to study swelling kinetics. The degree of swelling, α, is calculated from the following equation:[17]

$$\alpha = \frac{V_1 - V_0}{V_0} \qquad [7.1.9]$$

where:

V_1 volume of swollen solid at time t=t
V_0 volume of unswollen solid at time t=0

The swelling constant, K, is defined by:

$$K = \frac{k_1}{k_2} = \frac{\alpha}{1-\alpha} \qquad [7.1.10]$$

where:

k_1 rate constant of swelling process
k_2 rate constant of deswelling process

This shows that the swelling process is reversible and in a dynamic equilibrium. The distance of diffusion is time-dependent:

$$distance \propto (time)^n \qquad [7.1.11]$$

The coefficient n is between 0.5 for Fickian diffusion and 1.0 for relaxation-controlled diffusion (diffusion of solvent is much faster than polymer segmental relaxation).[18] This relationship is frequently taken literally[19] to calculate diffusion distance from a measurement of the change of the linear dimensions of swollen material.

The following equation is used to model changes based on swelling pressure measurements:

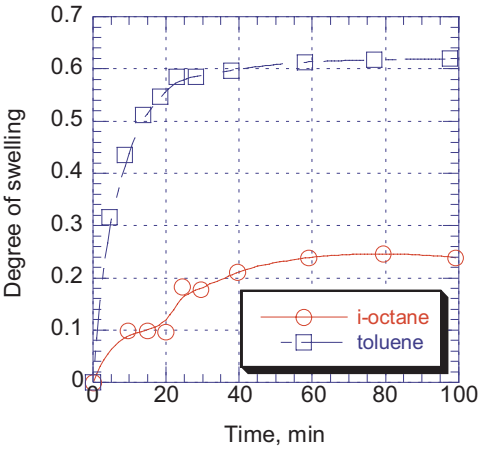

Figure 7.1.11. Swelling kinetics of EVA in toluene and i-octane. [Data from H J Mencer, Z Gomzi, *Eur. Polym. J.,* **30**, 1, 33-36, (1994).]

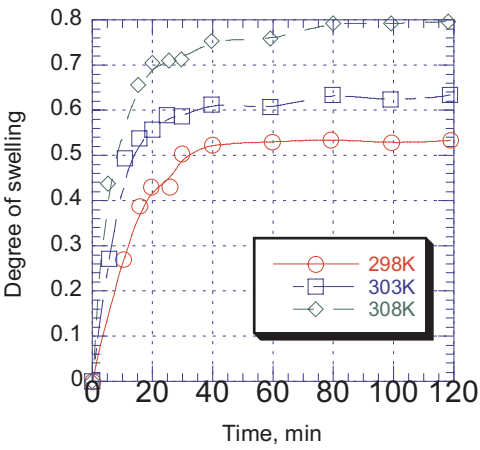

Figure 7.1.12. Swelling kinetics of EVA in tetrahydrofuran at different temperatures. [Adapted, by permission, from H J Mencer, Z Gomzi, *Eur. Polym. J.,* **30**, 1, 33-36, (1994).]

$$\Pi = A\varphi^n = -\frac{RT}{v_1}\left[\ln(1-\varphi) + \varphi + \chi\varphi^2\right] \qquad [7.1.12]$$

where:

Π	osmotic pressure
A	coefficient
φ	volume fraction of polymer in solution
n	= 2.25 for good solvent and = 3 for Θ solvent
v_1	molar volume of solvent
χ	Flory-Huggins, polymer-solvent interaction parameter

The above relationship is used in to study swelling by measuring shear modulus.[20]

Figure 7.1.11 shows swelling kinetic curves for two solvents. Toluene has a solubility parameter of 18.2 and i-octane of 15.6. The degree to which a polymer swells is determined by many factors, including the chemical structures of polymer and solvent, the molecular mass and chain flexibility of the polymer, packing density, the presence and density of crosslinks, temperature, and pressure. In the example presented in Figure 7.1.11 the solubility parameter has a strong influence on swelling kinetics.[17] The effect of temperature on swelling kinetics is shown in Figure 7.1.12. Increasing temperature increases swelling rate. During the initial stages of the swelling process the rate of swelling grows very rapidly and then levels off towards the swelling equilibrium.

In Figure 7.1.13, the diffusion distance is almost linear with time as predicted by equation [7.1.11]. The coefficient n of the equation was 0.91 meaning that the swelling process was relaxation rate controlled.

Figure 7.1.14 shows the relationship between hydrogel swelling and pH. Hydrogels are particularly interesting because their swelling properties are controlled by the conditions around them (e.g. pH).[21-23] Because they undergo controllable volume changes, they find applications in separation processes, drug delivery systems, immobilized enzyme sys-

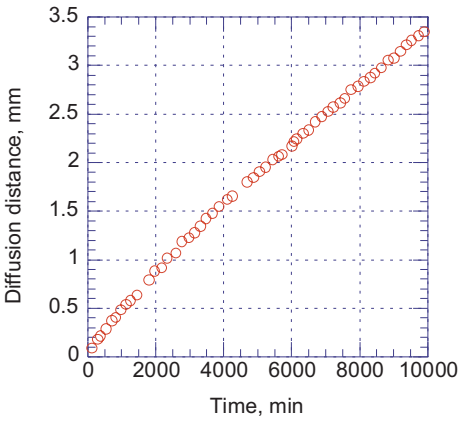

Figure 7.1.13. Diffusion distance of 1,4-dioxane into PVC vs. time. [Adapted, by permission, from M Ercken, P Adriensens, D Vanderzande, J Gelan, *Macromolecules*, **28**, 8541-8547, (1995).]

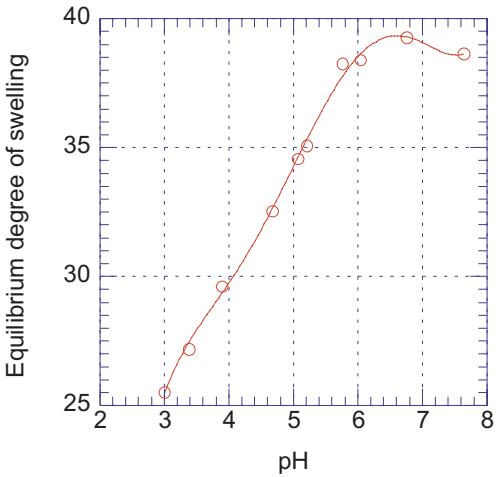

Figure 7.1.14. Effect of pH on the equilibrium swelling of hydrogel. [Data from M Sen, A Yakar, O Guven, *Polymer*, **40**, No.11, 2969-74 (1999).]

tems, etc. Maximum swelling is obtained at pH = 7. At this point there is complete dissociation of the acidic groups present in the hydrogel. The behavior of hydrogel can be modelled using Brannon-Peppas equation.[22]

Figure 7.1.15 shows the 1,1,2,2-tetrachoroethylene, TCE, uptake by amorphous poly(ether ether ketone), PEEK, as a function of time.[24,25] The swelling behavior of PEEK in this solvent is very unusual - the sample mass is increased by 165% which is about 3 times more than with any other solvent. In addition, the solvent uptake by PEEK results in a change in optical properties of the solution from clear to opaque. A clear solution is typical of amorphous PEEK and the opaque solution of crystalline PEEK. It was previously suggested by Fokes and Tischler[26] that polymethylmethacrylate forms weak complexes with various acid species in solution. This may also explain the unusual swelling caused by TCE. Because of the presence of C=O, C-O-C, and aromatic groups, PEEK acts as organic base. TCE is an electron acceptor due to electron-deficient atoms in the molecule.[24] This interaction may explain the strong affinity of solvent and polymer. Figure 7.1.16 illustrates the effect of crystallization. Below 250°C, the carbonyl frequency decreases. But a more rapid decrease begins below 140°C which is glass transition temperature. Above 250°C, the carbonyl frequency increases rapidly. Above the glass transition temperature there is rapid crystallization process which continues until the polymer starts to melt at 250°C then it gradually reverts to its original amorphous structure. The presence of solvent aids in the crystallization process.

7.1.3 DRYING

Solvent removal can be accomplished by one of three means: deswelling, drying or changes in the material's solubility. The deswelling process, which involves the crystallization of solvent in the surrounding gel, was discussed in the previous section. Here attention is focused on drying process. The changes due to material solubility are discussed in Chapter 12.

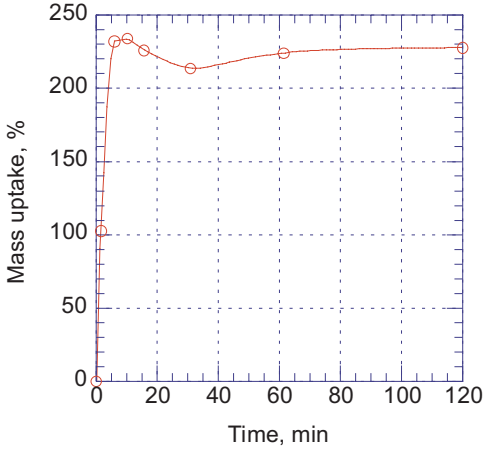

Figure 7.1.15. The mass uptake of TCE by PEEK vs. time. [Adapted, by permission, from B H Stuart, D R Williams, *Polymer*, **35**, No.6, 1326-8 (1994).]

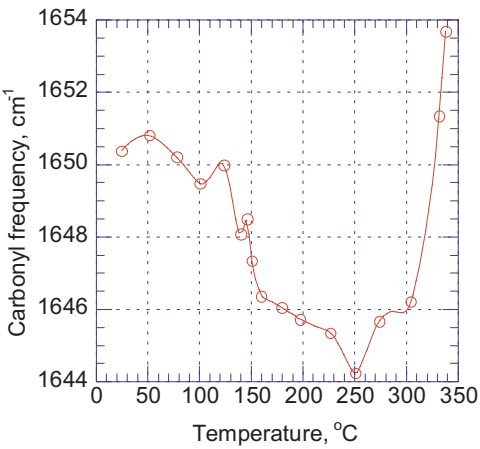

Figure 7.1.16. The frequency of carbonyl stretching mode of PEEK vs. temperature. [Adapted, by permission, from B H Stuart, D R Williams, *Polymer*, **36**, No.22, 4209-13 (1995).]

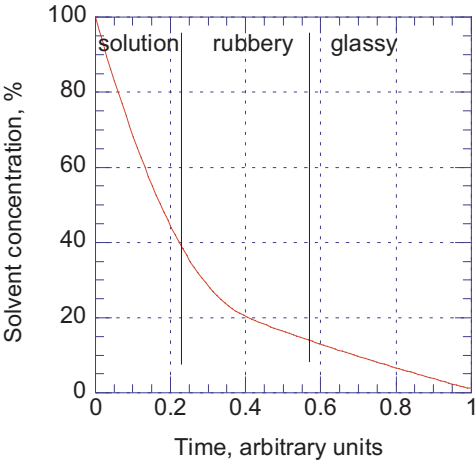

Figure 7.1.17. Solvent concentration vs. drying time.

Figure 7.1.1 can be discussed from a different perspective of results given in Figure 7.1.17. There are also three regions here: region 1 which has a low concentration of solid in which solvent evaporation is controlled by the energy supplied to the system, region 2 in which both the energy supplied to the system and the ability of polymer to take up the free volume vacated by solvent are important, and region 3 where the process is free volume controlled. Regions 2 and 3 are divided by the glass transition temperature. Drying processes in region 3 and to some extent in region 2 determine the physical properties of dried material and the amount of residual solvent remaining in the product. A sharp transition between region 2 and 3 (at glass transition temperature) might indicate that drying process is totally homogeneous but it is not and this oversimplifies the real conditions at the end of drying process. The most realistic course of events occurring close to the dryness point is presented by these four stages:[27,28]

- elimination of the volatile molecules not immobilized by the adsorption onto the polymer
- elimination of adsorbed molecules from the polymer in its rubbery state

- evaporation-induced self association of the polymer with progressive entrapment of adsorbed volatile molecules in the glassy microdomains (during transition from a rubbery to a glassy state)
- elimination of residual molecules entrapped in the polymer.

The last two stages are discussed in Chapter 16 which deals with residual solvent. This discussion concentrates on the effect of components on the drying process and the effect of the drying process on the properties of the product.

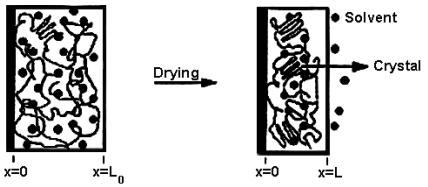

Figure 7.1.18. Schematic representation of drying a polymer slab. [Adapted, by permission, from M O Ngui, S K Mallapragada, *J. Polym. Sci.: Polym. Phys. Ed.*, **36**, No.15, 2771-80 (1998).]

A schematic of the drying process is represented in Figure 7.1.18. The material to be dried is placed on an impermeable substrate. The material consists of solvent and semicrystalline polymer which contains a certain initial fraction of amorphous and crystalline domains. The presence of crystalline domains complicates the process of drying because of the reduction in diffusion rate of the solvent. Evaporation of solvent causes an inward movement of material at the surface and the drying process may change the relative proportions of amorphous and crystalline domains.[29] Equations for the change in thickness of the material and kinetic equations which relate composition of amorphous and crystalline domains to solvent concentration are needed to quantify the rate of drying.

The thickness change of the material during drying is given by the equation:

$$v_1 \frac{dL}{dt} = \left(D \frac{\partial v_1}{\partial x} \right)_{x=L} \qquad [7.1.13]$$

where:

v_1	volume fraction of solvent
L	thickness of slab as in Figure 7.1.18
t	time
D	diffusion coefficient
x	coordinate of thickness

The rate of change of crystalline volume fraction is given by the equation:

$$\frac{\partial v_{2c}}{\partial t} = k_1 v_1 \qquad [7.1.14]$$

where:

v_{2c}	volume fraction of crystalline phase
k_1	rate change of crystalline phase proportional to folding rate

The rate of change of amorphous volume fraction is given by the equation:

$$\frac{\partial v_{2a}}{\partial t} = \frac{\partial}{\partial x}\left(D \frac{\partial v_1}{\partial x} \right) - k_1 v_1 \qquad [7.1.15]$$

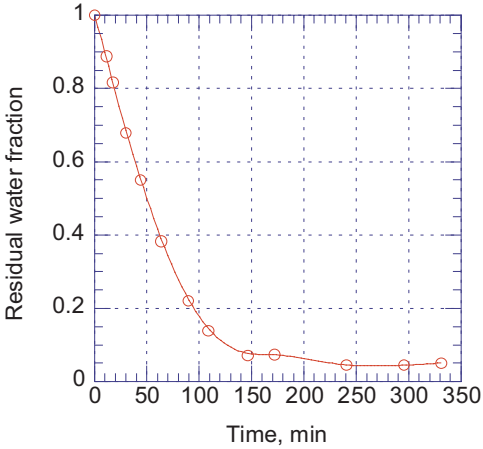

Figure 7.1.19. Fraction of water remaining in PVA as a function of drying time at 23°C. [Data from M O Ngui, S K Mallapragada, *J. Polym. Sci.: Polym. Phys. Ed.*, **36**, No.15, 2771-80 (1998).]

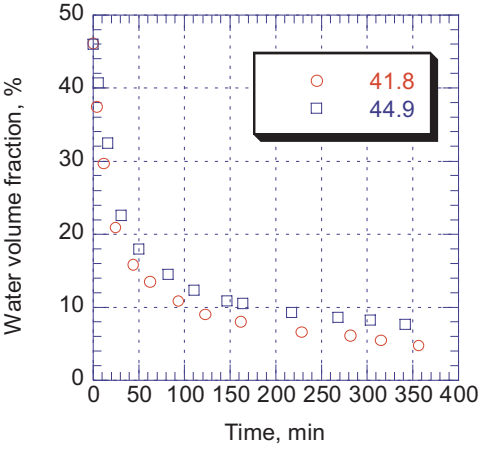

Figure 7.1.20. Water volume fraction vs. drying time for PVA of different crystallinity. [Adapted, by permission, from M O Ngui, S K Mallapragada, *J. Polym. Sci. Polym. Phys. Ed.*, **36**, No.15, 2771-80 (1998).]

where:

v_{2a} volume fraction of amorphous phase

The rate of drying process is determined by the diffusion coefficient:

$$D = D_0 \left[\exp\left(\alpha_D v_1\right)\right](1 - v_{2c}) / \tau \qquad [7.1.16]$$

where:

D_0 initial diffusion coefficient dependent on temperature

α_D constant which can be determined experimentally for spin echo NMR studies[30]

τ constant equal to 1 for almost all amorphous polymers ($v_{2c} \leq 0.05$) and 3 for semi-crystalline polymers

According to this equation, the coefficient of diffusion decreases as crystallinity increases because the last term decreases and τ increases.

Figure 7.1.19 shows that the fraction of solvent (water) decreases gradually as drying proceeds. Once the material reaches a glassy state, the rate of drying rapidly decreases. This is the reason for two different regimes of drying. Increasing temperature increases the rate of drying process.[29]

Figure 7.1.20 shows that even a small change in the crystallinity of the polymer significantly affects drying rate. An increase in molecular weight has similar effect (Figure 7.1.21). This effect is due both to lower mobility of entangled chains of the higher molecular weight and to the fact that higher molecular weight polymers are more crystalline.

Figure 7.1.22 shows that drying time increases as the degree of polymer crystallinity increases. Increased crystallinity slows down the diffusion rate and thus the drying process.

The physical properties of liquids, such as viscosity (Figure 7.1.23) and surface tension (Figure 7.1.24), also change during the evaporation process. The viscosity change for this system was a linear function of the amount of solvent evaporated.[31] This study on waterborne coatings showed that the use of a cosolvent (e.g. i-butanol) caused a reduction in

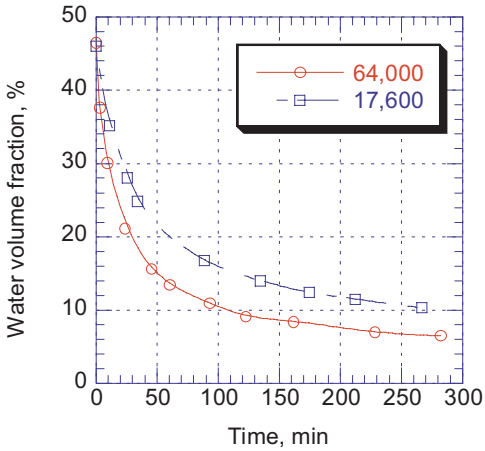

Figure 7.1.21. Water volume fraction vs. drying time for PVA of different molecular weight. [Adapted, by permission, from M O Ngui, S K Mallapragada, *J. Polym. Sci.: Polym. Phys. Ed.*, **36**, No.15, 2771-80 (1998).]

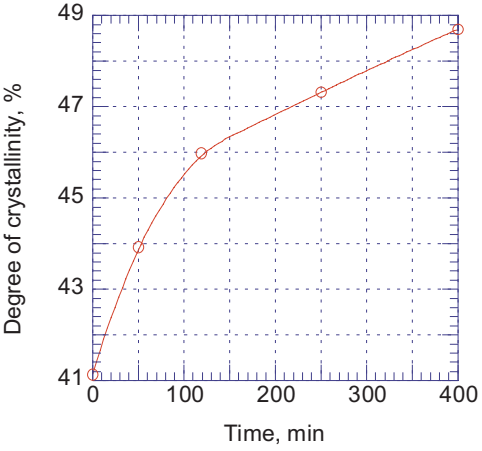

Figure 7.1.22. Degree of crystallinity vs. PVA drying time at 25°C. [Adapted, by permission, from M O Ngui, S K Mallapragada, *J. Polym. Sci.: Polym. Phys. Ed.*, **36**, No.15, 2771-80 (1998).]

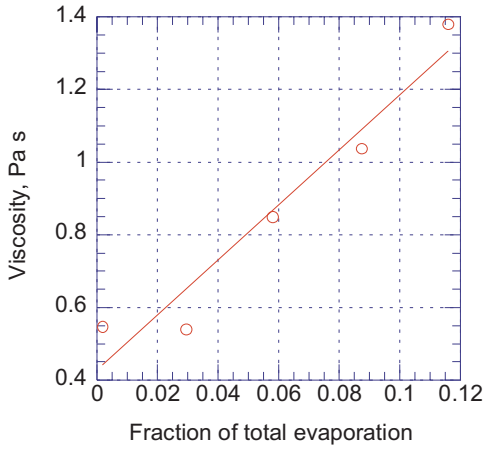

Figure 7.1.23. Viscosity vs. fraction of total evaporation of water from waterborne coating. [Data from S Kojima, T Moriga, *Polym. Eng. Sci.*, **35**, No.13, 1098-105 (1995).]

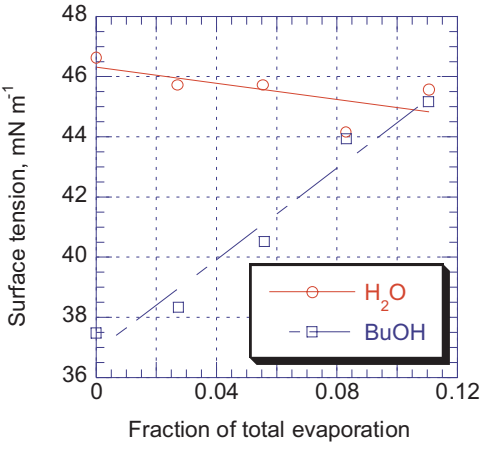

Figure 7.1.24. Surface tension vs. fraction of total evaporation of solvent from waterborne coating. [Data from S Kojima, T Moriga, *Polym. Eng. Sci.*, **35**, No.13, 1098-105 (1995).]

overall viscosity. Micelles of smaller size formed in the presence of the cosolvent explain lower viscosity.[31] Figure 7.1.24 shows that the surface tension of system containing a cosolvent (i-butanol) increases as the solvents evaporate whereas the surface tension of a system containing only water decreases. The increase of surface tension in the system containing cosolvent is due to the preferential evaporation of the cosolvent from the mixture.[31]

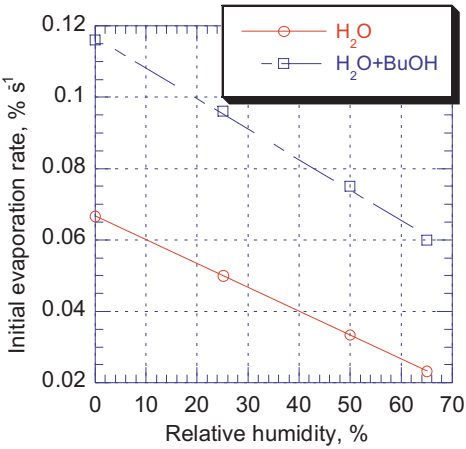

Figure 7.1.25. Initial evaporation rate from waterborne coating vs. relative humidity for two solvent systems. [Data from S Kojima, T Moriga, *Polym. Eng. Sci.*, **35**, No.13, 1098-105 (1995).]

Table 7.1.1. Experimentally determined initial evaporation rates of waterborne coating containing a variety of solvents at 5% level (evaporation at 25°C and 50% RH)

Co-solvent	Initial evaporation rate, μg cm^{-2} s^{-1}
none	3.33
methyl alcohol	4.44
ethyl alcohol	3.56
n-propyl alcohol	4.00
n-butyl alcohol	3.67
i-butyl alcohol	3.67
n-amyl alcohol	3.33
n-hexyl alcohol	3.22
ethylene glycol mono-butyl ester	3.22
ethylene glycol mono-hexyl ester	3.33
butyl carbinol	3.11
methyl-i-butyl ketone	4.89

Table 7.1.1 shows the effect of cosolvent addition on the evaporation rate of solvent mixture.

The initial rate of evaporation of solvent depends on both relative humidity and cosolvent presence (Figure 7.1.25). As relative humidity increases the initial evaporation rate decreases. The addition of cosolvent doubles the initial evaporation rate.

In convection drying, the rate of solvent evaporation depends on airflow, solvent partial pressure, and temperature. By increasing airflow or temperature, higher process rates can be achieved but the risk of skin and bubble formation is increased. As discussed above, Vrentas-Duda free-volume theory is the basis for predicting solvent diffusion, using a small number of experimental data to select process conditions. The design of a process and a dryer which uses a combination of convection heat and radiant energy is a more complex process. Absorption of radiant energy is estimated from the Beer's Law, which, other than for the layers close to the substrate, predicts:[32]

$$Q_r(\xi) = I_0 \alpha \exp\left[-\alpha(\beta h - \xi)\right] \qquad [7.1.17]$$

where:

Q_r	radiant energy absorption
ξ	distance from substrate
I_0	intensity of incident radiation
α	volumetric absorption coefficient
β	fractional thickness of the absorbing layer next to the substrate
h	thickness

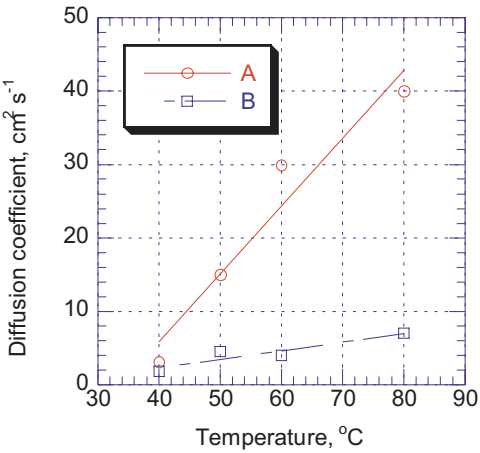

Figure 7.1.26. Diffusion coefficients for two polyurethanes (A & B) dissolved in N,N-dimethylacetamide vs. temperature. [Data from G A Abraham, T R Cuadrado, *International Polym. Process.*, **13**, No.4, Dec.1998, 369-78.]

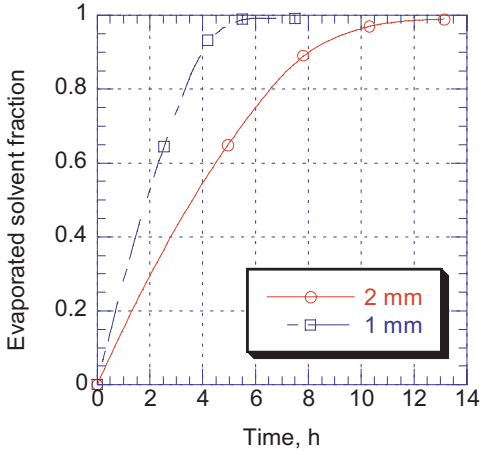

Figure 7.1.27. Effect of film thickness on evaporation rate. [Adapted, by permission from G A Abraham, T R Cuadrado, *International Polym. Process.*, **13**, No.4, Dec.1998, p.369-78.]

The radiant energy delivered to the material depends on the material's ability to absorb energy which may change as solvent evaporates. Radiant energy

- compensates for energy lost due to the evaporative cooling - this is most beneficial during the early stages of the process
- improves performance of the dryer when changes to either airflow rate or energy supplied are too costly to make.

Radiant energy can be used to improve process control. For example, in a multilayer coating (especially wet on wet), radiant energy can be used to regulate heat flow to each layer using the differences in their radiant energy absorption and coefficients of thermal conductivity and convective heat transfer. Experimental work by Cairncross *et al*.[32] shows how a combination dryer can be designed and regulated to increase the drying rate and eliminate bubble formation (more information on the conditions of bubble formation is included in Section 7.2 of this chapter). Shepard[33] shows how drying and curing rates in multilayer coating can be measured by dielectric analysis. Koenders *et al*.[34] gives information on the prediction and practice of evaporation of solvent mixtures.

Vrentas and Vrentas papers provide relevant modelling studies.[35,36] These studies were initiated to explain the earlier observations by Crank[37] which indicated that maintaining a slightly increased concentration of solvent in the air flowing over a drying material may actually increase the evaporation rate. Modelling of the process shows that although the diffusion of solvent cannot be increased by an increased concentration of solvent on the material's surface, an increased concentration of solvent in the air may be beneficial for the evaporation process because it prevents the formation of skin which slows down solvent diffusion.

Analysis of solvent evaporation from paint and subsequent shrinkage[38] and drying of small particles obtained by aerosolization[39] give further insight into industrial drying pro-

cesses. The two basic parameters affecting drying rate are temperature and film thickness. Figure 7.1.26 shows that the diffusion coefficient increases as temperature increases. Figure 7.1.27 shows that by reducing film thickness, drying time can be considerably reduced.[40] Further information on the design and modelling of drying processes can be found in a review paper[41] which analyzes drying process in multi-component systems.

REFERENCES

1 J S Vrentas and J.L. Duda, *J. Polym. Sci., Polym. Phys. Ed*., **15**, 403 (1977); **17**, 1085, (1979).
2 J S Vrentas, C M Vrentas, *J. Polym. Sci., Part B: Polym Phys*., **30**(9), 1005-11 (1992).
3 D Arnauld, R L Laurence, *Ind. Eng. Chem. Res.*, **31**(1), 218-28 (1992).
4 F D Blum, S Pickup, R A Waggoner, *Polym. Prep*., **31** (1), 125-6 (1990).
5 C Bouchard, B Guerrier, C Allain, A Laschitsch, A C Saby, D Johannsmann, *J. Appl. Polym. Sci*., **69**, No.11, 2235-46 (1998).
6 G Fleischer, J Karger, F Rittig, P Hoerner, G Riess, K Schmutzler, M Appel, *Polym. Adv. Technol*., **9**, Nos.10-11, 700-8 (1998).
7 C F Fong, , Y Li, De Kee, J Bovenkamp, *Rubber Chem. Technol*., **71**(2), 285-288 (1998).
8 Jinhua Chen, Kang Chen, Hong Zhang, Wanzhi Wei, Lihua Nie, Shouzhuo Yao, *J. Appl. Polym. Sci*., **66**, No.3, 563-71 (1997).
9 I Linossier, F Gaillard, M Romand, J F Feller, *J. Appl. Polym. Sci*., **66**, No.13, 2465-73 (1997).
10 L Meistermann, M Duval, B Tinland, *Polym. Bull*., **39**, No.1, 101-8 (1997).
11 J S Qi, C Krishnan, J A Incavo, V Jain, W L Rueter, *Ind. Eng. Chem. Res*., **35**, No.10, 3422-30 (1996).
12 Z Hrnjak-Murgic, J Jelencic, M Bravar, *Angew. Makromol. Chem*., **242**, 85-96 (1996).
13 B Hladik, S Frahn, W Borchard, *Polym. Polym. Compos*., **3**, No.1, 21-8 (1995).
14 J Frenkel, *Rubber Chem. Technol*., **13**, 264 (1940).
15 P J Flory, J Rehner, *J. Chem. Phys*., **11**, 521 (1943).
16 P J Flory, *J. Chem. Phys.*, **18**, 108 (1950).
17 H J Mencer, Z Gomzi, *Eur. Polym. J.,* **30**, 1, 33-36, (1994).
18 A G Webb, L D Hall, *Polymer*, **32**(16), 2926-38 (1991).
19 M Ercken, P Adriensens, D Vanderzande, J Gelan, *Macromolecules*, **28**, 8541-8547, (1995).
20 F Horkay, A M Hecht, E Geissler, *Macromolecules*, **31**, No.25, 8851-6 (1998).
21 M Sen, O Guven, *Polymer*, **39**, No.5, 1165-72 (1998).
22 M Sen, A Yakar, O Guven, *Polymer*, **40**, No.11, 2969-74 (1999).
23 Y D Zaroslov, O E Philippova, A R Khokhlov, *Macromolecules*, **32**, No.5, 1508-13 (1999).
24 B H Stuart, D R Williams, *Polymer*, **35**, No.6, 1326-8 (1994).
25 B H Stuart, D R Williams, *Polymer*, **36**, No.22, 4209-13 (1995).
26 F M Fowkes, D O Tischler, *J. Polym. Sci., Polym. Chem. Ed*., **22**, 547 (1984).
27 L A Errede, *Macromol. Symp*., **114**, 73-84 (1997).
28 L A Errede, P J Henrich, J N Schroepfer, *J. Appl. Polym. Sci*., **54**, No.5, 649-67 (1994).
29 M O Ngui, S K Mallapragada, *J. Polym. Sci.: Polym. Phys. Ed*., **36**, No.15, 2771-80 (1998).
30 N A Peppas, J C Wu, E D von Meerwall, *Macromolecules*, **27**, 5626 (1994).
31 S Kojima, T Moriga, *Polym. Eng. Sci*., **35**, No.13, 1098-105 (1995).
32 R A Cairncross, S Jeyadev, R F Dunham, K Evans, L F Francis, L Scriven, *J. Appl. Polym. Sci*., **58**, No.8, 1279-90 (1995).
33 D C Shepard, *J. Coat. Technol*., **68**, No.857, 99-102 (1996).
34 L Khal, E Juergens, J Petzoldt, M Sonntag, *Urethanes Technology*, **14**, No.3, 23-6 (1997).
35 J S Vrentas, C M Vrentas, *J. Polym. Sci., Part B: Polym Phys*., **30**(9), 1005-11 (1992).
36 J S Vrentas, C M Vrentas, *J. Appl. Polym. Sci*., **60**, No.7, 1049-55 (1996).
37 J Crank, *Proc. Phys. Soc*., **63**, 484 (1950).
38 L Ion, J M Vergnaud, *Polym. Testing*, **14**, No.5, 479-87 (1995).
39 S Norasetthekul, A M Gadalla, H J Ploehn, *J. Appl. Polym. Sci*., **58**, No.11, 2101-10 (1995).
40 G A Abraham, T R Cuadrado, *International Polym. Process.*, **13**, No.4, Dec.1998, 369-78.
41 Z Pakowski, *Adv. Drying*, **5**, 145-202 (1992).

7.2 BUBBLES DYNAMICS AND BOILING OF POLYMERIC SOLUTIONS

Semyon Levitsky
Negev Academic College of Engineering, Israel
Zinoviy Shulman
A.V. Luikov Heat and Mass Transfer Institute, Belarus

7.2.1 RHEOLOGY OF POLYMERIC SOLUTIONS AND BUBBLE DYNAMICS

7.2.1.1 Rheological characterization of solutions of polymers

Solutions of polymers exhibit a number of unusual effects in flows.[1] Complex mechanical behavior of such liquids is governed by qualitatively different response of the medium to applied forces than low-molecular fluids. In hydrodynamics of polymers this response is described by rheological equation that relates the stress tensor, σ, to the velocity field. The latter is described by the rate-of-strain tensor, e

$$e_{ij} = \frac{1}{2}\left(\frac{\partial v_i}{\partial x_j} + \frac{\partial v_j}{\partial x_i}\right) \qquad [7.2.1]$$

where:

v_i components of the velocity vector, $\vec{v}$
x_i Cartesian coordinates (i, j = 1, 2, 3)

The tensors σ and e include isotropic, p, e_{kk} and deviatoric, τ, s contributions:

$$\sigma = -pI + \tau, \quad p = -\frac{1}{3}\sigma_{kk}, \quad e = \frac{1}{3}e_{kk}I + s, \quad e_{kk} = \nabla \cdot \vec{v} \qquad [7.2.2]$$

where:

I unit tensor
∇ Hamiltonian operator

For incompressible fluid $\nabla \cdot \vec{v} = 0$, e = s and rheological equation can be formulated in the form of the τ- dependence from e. Compressibility of the liquid must be accounted for in fast dynamic processes such as acoustic waves propagation, etc. For compressible medium the dependence of pressure, p, on the density, ρ, and the temperature, T, should be specified by equation, $p = p(\rho,T)$, that is usually called the equation of state.

The simplest rheological equation corresponds to incompressible viscous Newtonian liquid and has the form

$$\tau = 2\eta_0 e \qquad [7.2.3]$$

where:

η_0 viscosity coefficient

Generalizations of the Newton's flow law [7.2.3] for polymeric liquids are aimed to describe in more or less details the features of their rheological behavior. The most important among these features is the ability to accumulate elastic deformation during flow and thus to exhibit the memory effects. At first we restrict ourselves to the case of small deformation rates to discuss the basic principles of the general linear theory of viscoelasticity

based upon thermodynamics of materials with memory.[2] The central idea of the theory is the postulate that instantaneous stresses in a medium depend on the deformation history. This suggestion leads to integral relationship between the stress and rate-of-strain tensors

$$\tau_{ij} = 2\int_{-\infty}^{t} G_1(t-t')s_{ij}(t')dt', \quad \sigma_{kk} = -3p_0 + 3\int_{-\infty}^{t} G_2(t-t')e_{kk}(t')dt' - 3\int_{-\infty}^{t} G_3(t-t')\frac{\partial\theta}{\partial t'}dt' \quad [7.2.4]$$

where:

θ	$= T - T_0$ deviation of the temperature from its equilibrium value
p_0	equilibrium pressure
G_1, G_2, G_3	relaxation functions

The relaxation functions $G_1(t)$ and $G_2(t)$ satisfy restrictions, following from the entropy production inequality

$$\frac{\partial G_1}{\partial t} \le 0, \quad \frac{\partial G_2}{\partial t} \le 0 \quad [7.2.5]$$

Additional restriction on $G_{1,2}(t)$ is imposed by the decaying memory principle[3] that has clear physical meaning: the state of a medium at the present moment of time is more dependent on the stresses arising at $t = t_2$ than on that stresses arising at $t = t_1$ if $t_1 < t_2$. This principle implies that the inequality $\left(\partial^2 G_{1,2} / \partial t^2\right) \ge 0$ must be satisfied.

The necessary condition for the viscoelastic material to be a liquid means

$$\lim_{t\to\infty} G_1(t) = 0 \quad [7.2.6]$$

Unlike $G_1(t)$, the functions $G_2(t)$ and $G_3(t)$ contain non-zero equilibrium components, such as

$$\lim_{t\to\infty} G_2(t) = G_{20}, \qquad \lim_{t\to\infty} G_3(t) = G_{30} \quad [7.2.7]$$

From the physical point of view this difference between G_1 and $G_{2,3}$ owes to the fact that liquid possesses a finite equilibrium bulk elasticity.

Spectral representations of relaxation functions, accounting for [7.2.5] - [7.2.7], have form ($G_{10} = 0$)

$$G_i(t) = G_{i0} + \int_0^{\infty} F_i(\lambda)\exp(-t/\lambda)d\lambda \quad [7.2.8]$$

where:

λ	relaxation time
$F_i(\lambda)$	spectrum of relaxation times (i = 1, 2, 3)

Equation [7.2.8] defines the functions $G_i(t)$ for continuous distribution of relaxation times. For a discrete spectrum, containing n_i relaxation times, the distribution function takes the form

$$F_i(\lambda) = \sum_{k=1}^{n_i} G_{ik}\,\delta(\lambda - \lambda_{ik}) \quad [7.2.9]$$

where:

G_{ik} partial modules, corresponding to λ_{ik}
$\delta(\lambda - \lambda_{ik})$ Dirac delta function

In this case the integration over the spectrum in Equation [7.2.8] is replaced by summation over all relaxation times, λ_{ik}.

For polymeric solutions, as distinct to melts, it is convenient to introduce in the right-hand sides of equations [7.2.4] additional terms, $2\eta_s s_{ij}$ and $3\rho_0\eta_v e_{kk}$, which represent contributions of shear, η_s, and bulk, η_v, viscosities of the solvent. The result has the form

$$\tau_{ij} = 2\int_{-\infty}^{t}\int_{0}^{\infty} F_1(\lambda)\exp\left(-\frac{t-t'}{\lambda}\right)s_{ij}(t')d\lambda dt' + 2\eta_s s_{ij} \qquad [7.2.10]$$

$$p = p_0 - G_{20}\int_{-\infty}^{t} e_{kk}(t')dt' - \int_{-\infty}^{t}\int_{0}^{\infty} F_2(\lambda)\exp\left(-\frac{t-t'}{\lambda}\right)e_{kk}(t')d\lambda dt' + G_{30}\theta +$$

$$+\int_{-\infty}^{t}\int_{0}^{\infty} F_3(\lambda)\exp\left(-\frac{t-t'}{\lambda}\right)\frac{\partial\theta(t')}{\partial t'}d\lambda dt' - \rho_0\eta_v e_{kk}, \quad p = -1/3\sigma_{kk} \qquad [7.2.11]$$

Equilibrium values of bulk and shear viscosity, η_b and η_p, can be expressed in terms of the relaxation spectra, F_1 and F_2, as:[1]

$$\eta_p - \eta_s = \int_0^{\infty}\lambda F_1(\lambda)d\lambda, \quad \eta_b - \eta_v = \int_0^{\infty}\lambda F_2(\lambda)d\lambda \qquad [7.2.12]$$

In the special case when relaxation spectrum, $F_1(\lambda)$, contains only one relaxation time, λ_{11}, equation [7.2.10] yields

$$\tau_{ij} = 2G_{11}\int_{-\infty}^{t}\exp\left(-\frac{t-t'}{\lambda_{11}}\right)s_{ij}(t')dt' + 2\eta_s s_{ij}, \quad G_{11} = \left(\eta_p - \eta_s\right)/\lambda_{11} \qquad [7.2.13]$$

At $\eta_s = 0$ the integral equation [7.2.13] is equivalent to the linear differential Maxwell equation

$$\tau_{ij} + \lambda_{11}\dot{\tau}_{ij} = 2\eta_p s_{ij} \qquad [7.2.14]$$

Setting $\eta_s = \lambda_2\eta_0/\lambda_1$, $\lambda_1 = \lambda_{11}$, $\eta_p = \eta_0$, where λ_2 is the retardation time, one can rearrange equation [7.2.14] to receive the linear Oldroyd equation[3]

$$\tau_{ij} + \lambda_1\dot{\tau}_{ij} = 2\eta_0\left(s_{ij} + \lambda_{ij}\dot{s}_{ij}\right), \quad \lambda_1 \geq \lambda_2 \qquad [7.2.15]$$

Thus, the Oldroyd model represents a special case of the general hereditary model [7.2.10] with appropriate choice of parameters. Usually the maximum relaxation time in the spectrum is taken for λ_1 in equation [7.2.15] and therefore it can be used for quantitative description and estimates of relaxation effects in non-steady flows of polymeric systems.

Equation [7.2.11], written for quasi-equilibrium process, helps to clarify the meaning of the modules G_{20} and G_{30}. In this case it gives

$$p = p_0 + G_{20}\rho_0^{-1}(\rho - \rho_0) + G_{30}\theta \qquad [7.2.16]$$

Thermodynamic equation of state for non-relaxing liquid at small deviations from equilibrium can be written as follows

$$p = p_0 + \left(\frac{\partial p}{\partial \rho}\right)_{T=T_0}(\rho - \rho_0) + \left(\frac{\partial p}{\partial T}\right)_{\rho=\rho_0}\theta \qquad [7.2.17]$$

The thermal expansion coefficient, α, and the isothermal bulk modulus, K_{is}, are defined as[4]

$$\alpha = -\rho_0\left(\frac{\partial \rho}{\partial T}\right)_{\rho=\rho_0}, \quad K_{is} = \rho_0\left(\frac{\partial p}{\partial \rho}\right)_{T=T_0} \qquad [7.2.18]$$

Therefore, equation [7.2.17] can be rewritten in the form

$$p = p_0 + K_{is}\rho_0^{-1}(\rho - \rho_0) + \alpha K_{is}\theta \qquad [7.2.19]$$

From [7.2.16] and [7.2.18] it follows that $G_{20} = K_{is}$, $G_{30} = \alpha K_{is}$.

In rheology of polymers complex dynamic modulus, G_k^*, is of special importance. It is introduced to describe periodic deformations with frequency, ω, and defined according to:

$$G_k^* = \int_0^\infty \frac{F_k(\lambda)(\omega\lambda)(\omega\lambda + i)d\lambda}{1 + (\omega\lambda)^2} \qquad [7.2.20]$$

Equations of motion of the liquid follow from momentum and mass conservation laws. In the absence of volume forces they mean:

$$\rho\frac{d\vec{v}}{dt} = \nabla \cdot \sigma \qquad [7.2.21]$$

$$\frac{d\rho}{dt} + \rho\nabla \cdot \vec{v} = 0 \qquad [7.2.22]$$

For polymeric solution the stress tensor, σ, is defined according to [7.2.10], [7.2.11]. To close the system, it is necessary to add the energy conservation law to equations [7.2.21], [7.2.22]. In the case of liquid with memory it has the form[2]

$$k\nabla^2\theta - T_0\frac{\partial}{\partial t}\int_{-\infty}^{t} G_3(t-t')e_{kk}(t')dt' = T_0\frac{\partial}{\partial t}\int_{-\infty}^{t} G_4(t-t')\frac{\partial\theta}{\partial t'}dt'$$

$$G_4(t-t') = G_{40} - \int_0^\infty F_4(\lambda)\exp\left(-\frac{t-t'}{\lambda}\right)d\lambda, \quad G_{40} = \rho_0 c_v T_0^{-1} \qquad [7.2.23]$$

where:

k	heat conductivity of the liquid
c_v	equilibrium isochoric specific heat capacity

Equations [7.2.10], [7.2.11], [7.2.21] - [7.2.23] constitute complete set of equations for linear thermohydrodynamics of polymeric solutions.

The non-linear generalization of equation [7.2.4] is not single. According to the Kohlemann-Noll theory of a "simple" liquid,[5] a general nonlinear rheological equation for a compressible material with memory may be represented in terms of the tensor functional that defines the relationship between the stress tensor, σ, and the deformation history. The form of this functional determines specific non-linear rheological model for a hereditary medium. Such models are numerous, the basic part of encountered ones can be found elsewhere.[1,6-8] It is important, nevertheless, that in most cases the integral rheological relationships of such a type for an incompressible liquid may be brought to the set of the first-order differential equations.[9] Important special case of this model represents the generalized Maxwell's model that includes the most general time-derivative of the symmetrical tensor

$$\tau = \sum_k \tau^{(k)}, \quad \tau^{(k)} + \lambda_k F_{abc}\tau^{(k)} = 2\eta_k e \qquad [7.2.24]$$

$$F_{abc}\tau = \frac{D\tau}{Dt} + a(\tau\cdot e + e\cdot\tau) + b\mathrm{I}\,\mathrm{tr}(\tau\cdot e) + c e\,\mathrm{tr}(\tau), \quad \frac{D\tau}{Dt} = \frac{d\tau}{dt} - w\cdot\tau + \tau\cdot w, \quad w = \tfrac{1}{2}\left(\nabla\vec{v} - \nabla\vec{v}^{T}\right)$$

where:

D/Dt	Jaumann's derivative[1]
d/dt	ordinary total derivative
tr	trace of the tensor, $\mathrm{tr}\tau = \tau_{kk}$
w	vorticity tensor
$\nabla\vec{v}^{\,T}$	transpose of the tensor $\nabla\vec{v}$
λ_k, η_k	parameters, corresponding to the Maxwell-type element with the number k

At a = -1, b = c = 0, equations [7.2.24] correspond to the Maxwell liquid with a discrete spectrum of relaxation times and the upper convective time derivative.[3] For solution of polymer in a pure viscous liquid, it is convenient to represent this model in such a form that the solvent contribution into total stress tensor will be explicit:

$$\tau = \sum_k \tau^{(k)} + 2\eta_s e, \quad \tau^{(k)} + \lambda_k\left[\frac{D\tau^{(k)}}{Dt} - \left(\tau^{(k)}\cdot e + e\cdot\tau^{(k)}\right)\right] = 2\eta_k e \qquad [7.2.25]$$

To select a particular nonlinear rheological model for hydrodynamic description of the fluid flow, it is necessary to account for kinematic type of the latter.[7] For example, the radial flows arising from the bubble growth, collapse or pulsations in liquid belong to the elongational type.[3] Therefore, the agreement between the experimental and theoretically predicted dependencies of elongational viscosity on the elongational deformation rate should be a basic guideline in choosing the model. According to data[10-13] the features of elongational viscosity in a number of cases can be described by equations [7.2.25]. More simple version of equation [7.2.25] includes single relaxation time and additional parameter $1/2 \le \alpha \le 1$, controlling the input of nonlinear terms:[7]

$$\tau = \tau^{(1)} + \tau^{(2)}, \quad \tau^{(1)} + \lambda\left[\frac{D\tau^{(1)}}{Dt} - \alpha\left(\tau^{(1)} \cdot e + e \cdot \tau^{(1)}\right)\right] = 2\eta\beta e, \quad \tau^{(2)} = 2\eta(1-\beta)e \quad [7.2.26]$$

Parameter β governs the contribution of the Maxwell element to effective viscosity, η,(Newtonian viscosity of the solution). Equation [7.2.26] is similar to the Oldroyd-type equation [7.2.15] with the only difference that in the former the upper convective derivative is used to account for nonlinear effects instead of partial derivative, $\partial / \partial t$.

Phenomenological parameters appearing in theoretical models can be found from appropriate rheological experiments.[6] Certain parameters, the most important being relaxation times and viscosities, can be estimated from molecular theories. According to molecular theory, each relaxation time λ_k is relative to mobility of some structural elements of a polymer. Therefore, the system as a whole is characterized by the spectrum of relaxation times. Relaxation phenomena, observed at a macroscopic level, owe their origin to the fact that response of macromolecules and macromolecular blocks to different-in-rate external actions is described by different parts of their relaxation spectrum. This response is significantly affected by temperature - its increase "triggers" the motion of more and more complex elements of the macromolecular hierarchy (groups of atoms, free segments, coupled segments, etc).

The most studied relaxation processes from the point of view of molecular theories are those governing relaxation function, $G_l(t)$, in equation [7.2.4]. According to the Rouse theory,[1] a macromolecule is modeled by a bead-spring chain. The beads are the centers of hydrodynamic interaction of a molecule with a solvent while the springs model elastic linkage between the beads. The polymer macromolecule is subdivided into a number of equal segments (submolecules or subchains) within which the equilibrium is supposed to be achieved; thus the model does not permit to describe small-scale motions that are smaller in size than the statistical segment. Maximal relaxation time in a spectrum is expressed in terms of macroscopic parameters of the system, which can be easily measured:

$$\lambda_{11} = \frac{6\left(\eta_p - \eta_s\right)M}{\pi^2 c R_G T} \quad [7.2.27]$$

where:

M	molecular mass of the polymer
c	concentration of polymer in solution
R_G	universal gas constant

The other relaxation times are defined as $\lambda_{1k} = \lambda_{11}/k^2$. In Rouse theory all the modules G_{1k} are assumed to be the same and equal to cR_GT/M.

In the Kirkwood-Riseman-Zimm (KRZ) model, unlike Rouse theory, the hydrodynamic interaction between the segments of a macromolecular chain is accounted for. In the limiting case of a tight macromolecular globe, the KRZ theory gives the expression for λ_{11} that is similar to [7.2.27]:

$$\lambda_{11} = \frac{0.422\left(\eta_p - \eta_s\right)M}{cR_GT} \quad [7.2.28]$$

The differences between other relaxation times in the both spectra are more essential: the distribution, predicted by the KRZ model, is much narrower than that predicted by the Rouse theory.

The KSR and Rouse models were subjected to numerous experimental tests. A reasonably good agreement between the theoretical predictions and experimental data was demonstrated for a variety of dilute polymeric solutions.[14] Further advance in the molecular-kinetic approach to description of relaxation processes in polymeric systems have brought about more sophisticated models.[15,16] They improve the classical results by taking into account additional factors and/or considering diverse frequency, temperature, and concentration ranges, etc. For the aims of computer simulation of the polymeric liquid dynamics in hydrodynamic problems, either simple approximations of the spectrum, $F_1(\lambda)$, or the model of subchains are usually used. Spriggs law[17] is the most used approximation

$$\lambda_{1k} = \lambda_{11} / k^z, \quad z \geq 2 \qquad [7.2.29]$$

The molecular theory predicts strong temperature dependence of the relaxation characteristics of polymeric systems that is described by the time-temperature superposition (TTS) principle.[18] This principle is based on numerous experimental data and states that with the change in temperature the relaxation spectrum as a whole shifts in a self-similar manner along t axis. Therefore, dynamic functions corresponding to different temperatures are similar to each other in shape but are shifted along the frequency axis by the value a_T; the latter is named the temperature-shift factor. With ωa_T for an argument it becomes possible to plot temperature-invariant curves $\mathrm{Re}\{G_1^*(\omega a_T)\}$ and $\mathrm{Im}\{G_1^*(\omega a_T)\}$. The temperature dependence of a_T is defined by the formula

$$a_T = \frac{\rho(T_0)T_0\left(\eta_p(T) - \eta_s(T)\right)}{\rho(T)T\left(\eta_p(T_0) - \eta_s(T_0)\right)} \qquad [7.2.30]$$

The dependence of viscosity on the temperature can be described by the activation theory[19]

$$\eta_p = \eta_{p0} \exp\left[E_p(R_G T_0)^{-1}(T_0 / T - 1)\right], \quad \eta_s = \eta_{s0} \exp\left[E_s(R_G T_0)^{-1}(T_0 / T - 1)\right] \qquad [7.2.31]$$

where:

E_p, E_s activation energies for the solution and solvent, respectively

The E_s value is usually about 10 to 20 kJ/mol. For low-concentrated solutions of polymers with moderate molecular masses, the difference between these two activation energies, $\Delta E = E_p - E_s$, does not exceed usually 10 kJ/mol.[18,20] For low-concentrated solutions of certain polymers in thermodynamically bad solvents negative ΔE values were reported.[20]

The Newtonian viscosity of solution related to the polymer concentration can be evaluated, for example, using Martin equation[18]

$$\eta_p / \eta_s = 1 + \tilde{c} \exp(k_M \tilde{c}), \quad \tilde{c} = c[\eta] \qquad [7.2.32]$$

where:

$\tilde{c}$ reduced concentration of polymer in the solution

$[\eta]$ intrinsic viscosity

Martin equation is usually valid in the range of reduced concentrations, $\tilde{c} \le 10$. For evaluation of [η], the Mark-Houwink relationship[21] is recommended

$$[\eta] = KM^a \qquad [7.2.33]$$

where K and a are constants for a given polymer-solvent pair at a given temperature over a certain range of the molecular mass variation. The parameter a (the Mark-Houwink exponent) lies in the range 0.5 to 0.6 for solutions of flexible chains polymers in thermodynamically bad solvents and in the range 0.7- 0.8 for good solvents. For the former ones the constant $K \approx 10^{-2}$ (if the intrinsic viscosity [η] is measured in cm^3/g), while for the latter $K \approx 10^{-3}$.

Thus, the spectral functions, $F_1(\lambda)$, are comprehensively studied both experimentally and theoretically. The behavior of relaxation functions, $G_2(t)$ and $G_3(t)$, is still much less known. The properties of the function, $G_2(t)$, were mainly studied in experiments with longitudinal ultrasound waves.[22-24] It has been found that relaxation mechanisms manifested in shear and bulk deformations are of a similar nature. In particular, polymeric solutions are characterized by close values of the temperature-shift factors and similar relaxation behavior of both shear and bulk viscosity. The data on the function, $F_3(\lambda)$, indicate that relaxation behavior of isotropic deformation at thermal expansion can be neglected for temperatures well above the glass-transition temperature.[22]

7.2.1.2 Dynamic interaction of bubbles with polymeric liquid

Behavior of bubbles in liquid at varying external pressure or temperature is governed by cooperative action of a number of physical mechanisms, which are briefly discussed below. Sufficiently small bubbles execute radial motions (growth, collapse, pulsations) retaining their spherical shape and exchanging heat, mass and momentum with environment. Heat transfer between phases at free oscillations of gas bubbles is caused by gas heating during compression and its cooling when expanding. Due to the difference in thermal resistance of liquid and gas, the total heat flux from gas to liquid is positive for the oscillation period. This unbalanced heat exchange is the source of so-called heat dissipation. The magnitude of the latter depends on the relation between the natural time of the bubble (the Rayleigh time) $t_0 = R_0(\rho_{f0}/p_{f0})^{1/2}$, governed by the liquid inertia, and the time of temperature leveling in gas (characteristic time of heat transfer in a gas phase), $t_T = R_0^2/a_g$, that is from the thermal Peklet number, $Pe_T = t_T/t_0$,

where:

R	radius of the bubble
a_g	thermal diffusivity of gas, $a_g = k_g/(p_{g0}c_{gp})$
k_g	heat conductivity of gas
c_{gp}	specific heat capacity of gas at constant pressure
0	index, referring to equilibrium state
f	index, referring to liquid
g	index, referring to gas

In the limiting cases $Pe_T >> 1$ and $Pe_T << 1$, when behavior of gas inside the bubble is close to adiabatic and isothermal one, correspondingly, the heat dissipation is small. For a bubble oscillating in a sound field, the above conditions should be changed for $\bar{\omega}\,Pe_T >> 1$ and $\bar{\omega}\,Pe_T << 1$ with $\bar{\omega} = \omega t_0$ being the non-dimensional frequency.

At thermodynamic conditions, close to normal ones, the equilibrium vapor content of the bubble can be neglected, but it grows with temperature (or pressure reduction). In the

vapor presence, the pressure and/or temperature variations inside the oscillating bubble cause evaporation-condensation processes that are accompanied by the heat exchange. In polymeric solutions, transition from liquid to vapor phase and conversely is possible only for a low-molecular solvent. The transport of the latter to the bubble-liquid interface from the bulk is controlled by the diffusion rate. In general case the equilibrium vapor pressure at the free surface of a polymeric solution is lower than that for a pure solvent. If a bubble contains a vapor-gas mixture, then the vapor supply to the interface from the bubble interior is controlled by diffusion rate in the vapor-gas phase. The concentration inhomogeneity within the bubble must be accounted for if $t_{Dg} > t_0$ or $Pe_{Dg} > 1$

where:

t_{Dg}	characteristic time of binary diffusion in vapor-gas phase, $t_{Dg}= R_0^2/D_g$
D_g	diffusion coefficient
Pe_{Dg}	diffusion Peklet number for the vapor-gas phase, $Pe_{Dg}= t_{Dg}/t_0$

Fast motions of a bubble surface produce sound waves. Small (but non-zero) compressibility of the liquid is responsible for a finite velocity of acoustic signals propagation and leads to appearance of additional kind of the energy losses, called acoustic dissipation. When the bubble oscillates in a sound field, the acoustic losses entail an additional phase shift between the pressure in the incident wave and the interface motion. Since the bubbles are much more compressible than the surrounding liquid, the monopole sound scattering makes a major contribution to acoustic dissipation. The action of an incident wave on a bubble may be considered as spherically-symmetric for sound wavelengths in the liquid $l_f >> R_0$.

When the spherical bubble with radius R_0 is at rest in the liquid at ambient pressure, p_{f0}, the internal pressure, p_{in}, differs from p_{f0} by the value of capillary pressure, that is

$$p_{in} = p_{f0} + 2\sigma / R_0 \qquad [7.2.34]$$

where:

σ	surface tension coefficient

If the system temperature is below the boiling point at the given pressure, p_{f0}, the thermodynamic equilibrium of bubble in a liquid is possible only with a certain amount of inert gas inside the bubble. The pressure in vapor-gas mixture follows the Dalton law, that suggests that both the solvent vapor and the gas are perfect gases:

$$p_{in} = p_g + p_v = \left(\rho_g B_g + \rho_v B_v\right) T_m = \rho_m B_m T_m, \quad \rho_m = \rho_g + \rho_v \qquad [7.2.35]$$

$$B_m = \left(1 - k_0\right) B_g + k_0 B_v, \quad B_{g,v} = R_g / \mu_{g,v}$$

where:

k_0	equilibrium concentration of vapor inside the bubble
$\mu_{g,v}$	molar masses of gas and solvent vapor
v	index, referring to vapor

From [7.2.34], [7.2.35] follows the relation for k_0:

$$k_0 = \left[1 + B_v B_g^{-1} \left\{\left(1 + 2\overline{\sigma}\right) / \overline{p}_{v0} - 1\right\}\right]^{-1}, \quad \overline{p}_{v0} = p_{v0} / p_{f0}, \quad \overline{\sigma} = \sigma / \left(p_{v0} R_0\right) \qquad [7.2.36]$$

The equilibrium temperature enters equation [7.2.36] via the dependence of the saturated vapor pressure, p_{v0}, from T_0. Figure 7.2.1 illustrates the relation [7.2.36] for air-vapor bubbles in toluene.[25] The curves 1- 3 correspond to temperatures $T_0 = 363, 378, 383.7$K (the

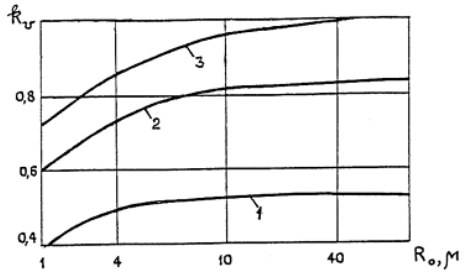

Figure 7.2.1. Dependence of the vapor content of air-vapor bubble in toluene from radius at different temperatures. [Adapted, by permission, from *Nauka i Tekhnica Press*, from the reference 25]

latter value is equal to the saturation temperature T_s for toluene at $p_{f0} = 10^5$ Pa). It follows from the calculated data that the vapor content dependence on the bubble radius is manifested only for minor bubbles as a result of capillary forces. The effect vanish for $R_0 > > 10$ mkm. For $T_0 << T_s$ the k_0 value is small and the bubble can be treated as a pure gas-filled.

The solvent vapor pressure above polymeric solution depends not only from the temperature but also on concentration of polymer. In most cases this dependence differs essentially from the linear Raul's law[21] and can be approximated by the Flory-Huggins equation, that must be used in evaluation of k_0 by the relation [7.2.36]

$$p_{v0} / p^0_{v0} = \phi_1 \exp\left[1 - \phi_1 + \chi(1-\phi_1)^2\right], \quad \phi_1 = \kappa\left[\kappa + (1-\kappa)K_p\right]^{-1}, \quad K_p = v_2 / v_1 \qquad [7.2.37]$$

where:

ϕ_1, κ	volume and mass fraction of the volatile component
p^0_{v0}, p_{v0}	vapor pressure above pure solvent and polymeric solution
v_1, v_2	specific volumes of solvent and polymer
χ	parameter of thermodynamic interaction

At $\phi_1 \to 0$ equation [7.2.37] gives a linear dependence of the relative vapor pressure, p^0_{v0}/p_{v0} on the solvent volume concentration with the angle coefficient $\exp(1+\chi)$. At $\phi_1 \to 1$ solution obeys the Raul's law. Note that the value of ϕ_1 in [7.2.37] is temperature-dependent due to difference in thermal expansion coefficients of components. The χ value for a given solvent depends on the concentration and molar mass of a polymer as well as on temperature. However, to a first approximation, these features may be ignored.[20] Usually χ varies within the range 0.2 - 0.5. For example, for solutions of polyethylene, natural rubber, and polystyrene in toluene χ = 0.28, 0.393 and 0.456, correspondingly.

To describe the dynamic interaction of bubble with polymeric solution it is necessary to invoke equations of liquid motion, heat transfer and gas dynamics. General approach to description of bubble growth or collapse in a non-Newtonian liquid was formulated and developed.[26-31] The radial flow of incompressible liquid around growing or collapsing bubble is described by equations, following from [7.2.21], [7.2.22]:[27]

$$\rho_{f0}\left(\frac{\partial v_r}{\partial t} + v_r \frac{\partial v_r}{\partial r}\right) = -\frac{\partial p_f}{\partial r} + \frac{\partial \tau_{rr}}{\partial r} + \frac{2(\tau_{rr} - \tau_{\phi\phi})}{r} \qquad [7.2.38]$$

$$r\frac{\partial v_r}{\partial t} + 2v_r = 0 \qquad [7.2.39]$$

where:

r, ϕ	radial and angular coordinates of the spherical coordinate system with the origin at the center of the bubble

v_r radial component of velocity in the liquid

The dynamic boundary condition that governs the forces balance at the interface, is:

$$p_g(R,t) = p_f(R,t) + 2\sigma R^{-1} - \tau_{rr}(R,t) \qquad [7.2.40]$$

From [7.2.38] - [7.2.40] follows the equation of bubble dynamics:

$$J + p_f(\infty) - p_g + 2\sigma R^{-1} = S, \quad J = \rho_{f0}\left(R\ddot{R} + \frac{3}{2}\dot{R}^2\right) \qquad [7.2.41]$$

$$S = 2\int_0^\infty (\tau_{rr} - \tau_{\phi\phi})\left(3y + R^3\right)^{-1} dy, \quad y = \frac{1}{3}\left(r^3 - R^3\right)$$

where:

$p_f(\infty)$ pressure in the liquid at infinity
p_g pressure in the bubble
$\dot{R}, \ddot{R}$ derivatives of the bubble radius with respect to time, t

The equation [7.2.41] was investigated[25] for growing and collapsing cavity in a liquid, described by rheological model [7.2.26], at $p_f(\infty) - p_g = \text{const}$. Similar analysis for another rheological model of the solution (the so-called "yo-yo" model of the polymer dynamics) was developed.[32] It was shown that viscoelastic properties of solution can be approximately accounted for only in the close vicinity of the interface, that is through the boundary condition [7.2.40]. In this case the integro-differential equation for R(t), following from [7.2.41], [7.2.26], can be reduced to a simple differential equation. The latter was analyzed accounting for the fact[7] that the effective viscosity η_l of a polymeric solution in elongational flow around collapsing cavity can increase by the factor of 10^2 to 10^3. If the corresponding Reynolds number of the flow $\mathrm{Re} = (\eta_p/\eta_l)\mathrm{Re}_p$ ($\mathrm{Re}_p = t_0/t_p$, $t_p = 4\eta_p(p_f(\infty) - p_g)^{-1}$) is small, the inertial terms in equation [7.2.41] can be neglected. For high-polymer solutions the inequalities $\mathrm{Re} << \mathrm{Re}_p$ and $\mathrm{Re} < 1$ may be satisfied in elongational flow even in the case of $\mathrm{Re}_p >> 1$. Under these assumptions the equation for the relative velocity of the bubble surface takes the form

$$\dot{z} + 2(z - z_1)(z - z_2) = 0, \quad z = \dot{x}/x, \quad x = R/R_0, \quad z_{1,2} = -A/4 \pm \left(A^2/16 + B/2\right)^{1/2}$$

$$A = \bar{\lambda}^{-1}(1-\beta)^{-1}\left(1 - 2k\bar{\lambda}\,\mathrm{Re}_p\right), \quad B = (1-\beta)^{-1}k\bar{\lambda}^{-1}\mathrm{Re}_p, \quad \bar{\lambda} = \lambda/t_0, \quad k = sign\left(p_g - p_f(\infty)\right)$$

Here was adopted for simplicity that $\alpha = 1/2$ and $\bar{\sigma} << 1$ (the latter inequality is satisfied for bubbles with $R_0 > >1$ mkm). Phase plot of this equation is presented in Figure 7.2.2. It is seen that for $k = -1$ (collapsing cavity) $z \to z_1$ as $\bar{t} \to \infty$ if $z_0 > z_2$. The stationary point $z = z_2$ is unstable. The rate of the cavity collapse $z = z_1$ in the asymptotic regime satisfies inequality $z_p \le z_1 \le 0$, where $z_p = -\mathrm{Re}_p$ is equal to the collapse rate of the cavity in a pure viscous fluid with viscosity of polymeric solution η. It means that the cavity closure in viscoelastic solution of polymer at asymptotic stage is slower than in a viscous liquid with the same equilibrium viscosity. On the contrary, the expansion under the same conditions is faster: at $k = 1$ $z_p \le z_1 \le z_x$, where $z_p = \mathrm{Re}_p$ and $z_s = \mathrm{Re}_s = (1-\beta)^{-1}\mathrm{Re}_p$ is the asymptotic rate of the cavity expansion in a pure solvent with the viscosity $(1-\beta)\eta$. This result is explained by different behavior of the stress tensor component τ_{rr}, controlling the fluid rheology effect on the cav-

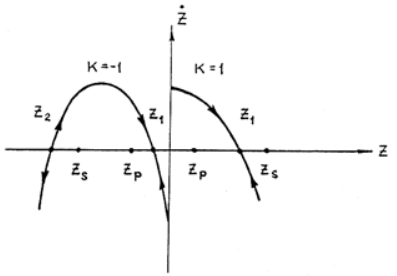

Figure 7.2.2. Phase plane for expanding and collapsing cavity in polymeric solution. [By permission of *Nauka i Tekhnica Press*, from the reference 25]

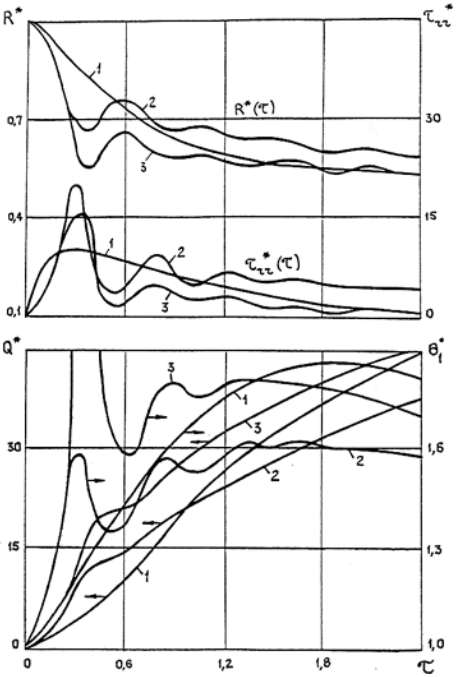

Figure 7.2.3. Heat transfer and rheodynamics at non-linear oscillations of a bubble in polymeric liquid. [By permission of *Nauka i Tekhnica Press*, from the reference 25]

ity dynamics, in extensional and compressional flows, respectively.[9] In the former case, the τ_{rr} value may be considerably greater than in the latter one.

Heat transfer between phases is a strong dissipative factor that in principle can mask the rheological features in bubble dynamics. Nevertheless, even with account for heat dissipation the theoretical dependencies of R(t) are sensitive to rheological properties of solution. Typical results of air bubble dynamics simulations at a sudden pressure change in the solution with $\eta_p >> \eta_s$ are presented on the Figure 7.2.3,

where:

R^*	dimensionless radius of the bubble, $R^* = R/R_0$
τ	dimensionless time, $\tau = t/t_0$
τ^*_{rr}	dimensionless radial component of the extra-stress tensor at the interface, $\tau^*_{rr} = \tau_{rr}(R,t)/p_{f0}$
θ_l^0	dimensionless temperature at the center of the bubble, $\theta_l^0 = T_g(0,t)/T_0$
Q^*	dimensionless heat, transferred to liquid from the gas phase in a time τ, $Q^* = Q/(R_0 T_0 k_g t_0)$
k_g	heat conductivity of gas
Δp_f^*	dimensionless pressure change in the liquid at initial moment of time, $p_f^*(\infty) = 1 + \Delta p_f^* h(t)$, $\Delta p_f^* = \Delta p_f / p_{f0}$
h(t)	unit step function

Calculations have been done for the rheological model [7.2.25] with 20 relaxation elements in the spectrum, distributed according to the law [7.2.29] with z = 2. To illustrate the contribution of rheological non-linearity in equation [7.2.25] the numerical coefficient α (α=1 or 0) was introduced in the term with λ_k, containing material derivative. The value α=1 corresponds to non-linear model [7.2.25], while at $\alpha = 0$ equation [7.2.25] is equivalent to the linear hereditary model [7.2.10] with a discrete spectrum. Other parameters of the system were chosen as follows: $\eta_p = 2$ Pas, $\eta_s = 10^{-2}$ Pas, $\lambda_1 = 10^{-5}$ s, $R_0 = 50$ mkm, $\Delta p_f^* = 10$, $p_{f0} = 10^5$ Pa, $\rho_{f0} = 10^3$ kg/m^3, $T_0 = 293$K, $\sigma = 0.05$ N/m. Thermodynamic parameters of the

air were accepted according to the standard data,[33] the heat transfer between phases was described within homobaric scheme[34] (pressure in the bubble is a function of t only, that is uniform within the volume, while the density and temperature are changed with r and t according to the conservation laws). For the curve 1, $\eta_p = \eta_s = 2$ Pas (pure viscous liquid with Newtonian viscosity of the solution), for curve 2, $\alpha = 1$, for curve 3, $\alpha = 0$, that is, the latter two graphs correspond to viscoelastic solution with and without account for the rheological non-linearity, respectively.

It follows from Figure 7.2.3 that relaxation properties of liquid are responsible for amplification of the bubble pulsations and, as a result, change the heat transfer between phases. Note that in examples, reproduced in Figure 7.2.3, the characteristic time of the pulsations' damping is less than characteristic time of the temperature leveling in gas, t_T (the time moment $\tau = 2.4$, for instance, corresponds to $t/t_T \approx 0.1$). Therefore, after completion of oscillations the temperature in the center of a bubble is reasonably high, and the R* value exceeds the new isothermal equilibrium radius ($R_1^* = 0.453$). The manifestation of rheological non-linearity leads to a marked decrease in deviations of the bubble radius from the initial value at the corresponding instants of time. The explanation follows from stress dynamics analysis in liquid at the interface. At the initial stage, the relaxation of stresses in the liquid slows down the rise in the τ^*_{rr} value in comparison with similar Newtonian fluid. This leads to acceleration of the cavity compression. Since the stresses are small during this time interval, the rheological non-linearity has only a minor effect on the process. Further on, however, this effect becomes stronger which results in a considerable increase of normal stresses as compared with those predicted by the linear theory. It leads to deceleration of the cavity compression and, as a result, to decrease both in the maximum temperature of gas in a bubble and in the integral heat loss.

More detailed information about rheological features in gas bubble dynamics in polymeric solutions can be received within linear approach to the same problem that is valid for small pressure variations in the liquid. The equation describing gas bubble dynamics in a liquid with rheological equation [7.2.10] follows from [7.2.41], [7.2.10] and has the form[35]

$$\rho_{f0}\left(R\ddot{R}+\frac{3}{2}\dot{R}^2\right)=p_{g0}\left(R_0/R\right)^{3\gamma}-p_f(\infty)-2\sigma R^{-1}-4\eta_s R/\dot{R}-$$

$$-4\int_0^\infty F_1(\lambda)\left\{\int_0^t \exp\left(-\frac{t-t'}{\lambda}\right)\dot{R}(t')R^{-1}(t')dt'\right\}d\lambda \qquad [7.2.42]$$

Here is supposed that gas in the bubble follows polytropic process with exponent λ. This equation was solved in linear approximation[35] by operational method with the aim to analyze small amplitude, natural oscillations of the constant mass bubble in relaxing liquid. It was taken $R = R_0 + \Delta R$, $\Delta R/R_0 << 1$, $\Delta R \sim \exp(ht)$ with h being the complex natural frequency. Logarithmic decrement, Λ, and dimensionless frequency, μ, of the oscillations are defined according to formulas

$$\Lambda = -2\pi \mathrm{Re}\{h\}\,\mathrm{Im}^{-1}\{h\}, \quad \mu = (2\pi)^{-1} t_0\,\mathrm{Im}\{h\} \qquad [7.2.43]$$

Typical data for Λ and μ, calculated from the solution of linearized equation [7.2.42] for air bubble in the case of discrete spectrum with n_1 relaxation times, distributed by the Rouse law, are presented in Figures 7.2.4, 7.2.5. The maximum time, λ_1, was evaluated from equations [7.2.27], [7.2.32]. For curves 1- 6 and 1'- 6', n_1 = 1, 5, 10, 20, 50 and 100, correspondingly. Curve 7 refers to Newtonian fluid with $\eta = \eta_p$. For curves 1- 6, A = 200, for curves 1'- 6', A = 1000 with dimensionless parameter $A = p_{f0}M[\eta]/(R_G T_0)$. Other parameters were adopted as follows: $k_M = 0.4$, $\eta_s^* = 10^{-2}$, $\gamma = 1.36$. For atmospheric pressure and $\rho_{f0}=10^3$ kg/m^3 these values correspond approximately to η_s = 0.1 Pas, $R_0 = 10^{-3}$ m. At these parameters, the relative effect of acoustic dissipation on damping of bubble pulsations is small.[31] The value of heat decrement is denoted in Figure 7.2.4 by Λ_1, the value of the rheological one - by Λ_3.

It is seen from the plots that viscoelasticity of the solution is responsible for reduction of rheological dissipative losses. The effect increases with reduced concentration of the polymer, $\tilde{c}$. When the number of relaxation times in the spectrum, accounted for in simulations, grows, the magnitude of Λ_3 also grows. Nevertheless, for all considered values the weakening of the damping, as compared with Newtonian fluid of the same viscosity, is essential. It follows from the analysis that in polymeric solution, pulsations of the bubble are possible even at relatively large c values (to the right of the dashed line in Figure 7.2.4). In this region of reduced concentrations the Newtonian viscosity of the solution is so high that only aperiodic solution for ΔR exists when the liquid follows the Newtonian model. The increase in molecular mass of the dissolved polymer at $\tilde{c}$ = const causes decrease in rheological losses.

The natural frequency of the bubble raises with $\tilde{c}$ and this behavior is qualita-

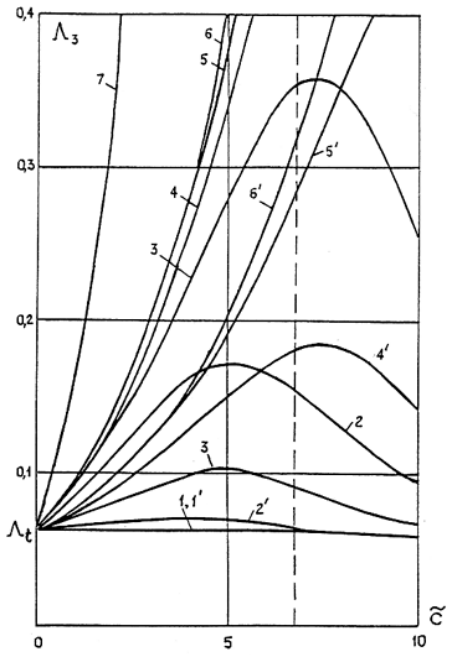

Figure 7.2.4. Rheological dissipative losses versus reduced concentration of a polymer. [By permission of *Nauka i Tekhnica Press*, from the reference 25]

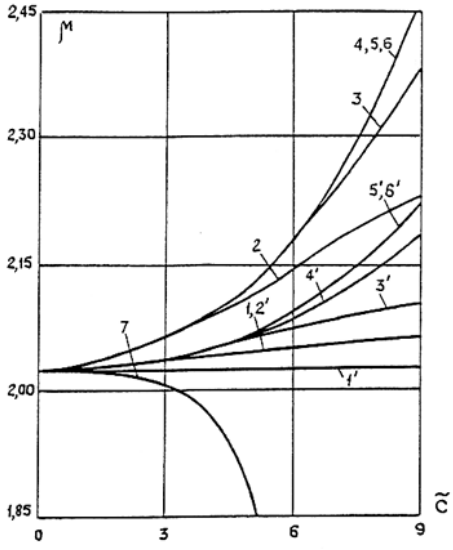

Figure 7.2.5. The effect of reduced polymer concentration on the natural frequency of bubbles. [By permission of *Nauka i Tekhnica Press*, from the reference 25]

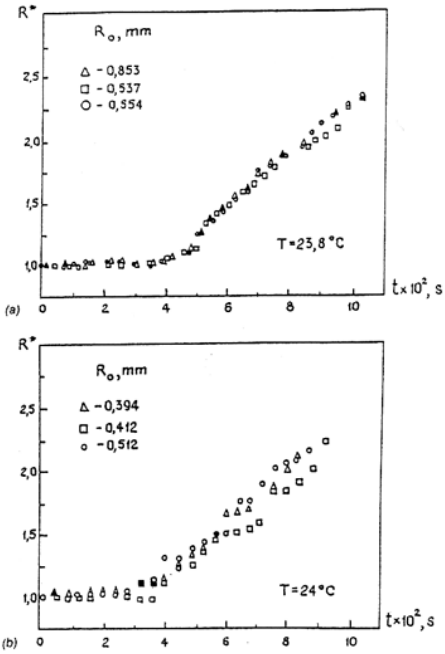

Figure 7.2.6. Expansion of bubbles in water and POE aqueous solution at a pressure drop. (a) - water, (b) - solution of POE with c = 420 ppm. [By permission of the American Institute of Physics from R.Y. Ting, and A.T. Ellis, *Phys. Fluids*., **17**, 1461, 1974, the reference 36]

tively different from the concentration dependence of μ for a bubble in a pure viscous fluid with the same Newtonian viscosity as the solution (curve 7 in Figure 7.2.5).

The rheological properties of polymeric solution highly depend on temperature. Therefore, its variation affects the bubble pulsations. Thermorheological features in bubble dynamics have been studied[35] on the basis of temperature superposition principle, using relations [7.2.30], [7.2.31]. It was shown that the temperature rise leads to decrease of the decrement Λ_3, and this effect is enhanced with the increase of n_1. Note that the higher is the equilibrium temperature of the liquid, the less sensitive are the Λ_3 values to variations in n_1. It is explained by narrowing of the relaxation spectrum of the solution.[25]

Experimental results on bubble dynamics in solution of polymers are not numerous. Existing data characterize mainly the integral effects of polymeric additives on bulk phenomena associated with bubbles while only few works are devoted to studying the dynamics of an individual bubble. The observations of the bubble growth in water at a sudden pressure drop were compared with those for aqueous solution of POE.[36] The results are represented in Figure 7.2.6. It is seen that the effect of polymeric additives is small. This result is explained by rather large value of Reynolds number $Re_p = t_0/t_p$ corresponding to experimental conditions.[36] Therefore, the inertial effects rather than the rheological ones play a dominant role in bubble dynamics. The conclusions[36] were confirmed later[37] when studying the bubbles behavior in aqueous solution of POE (trade mark Polyox WS 301) with the concentration of 250 ppm (for water 1 ppm = 1 g/m^3). A similar result was received also in studies[38] of nucleate cavitation in the PAA aqueous solution with c = 0.1 kg/m^3. The solution viscosity[38] only slightly (by 10%) exceeded that of water.

When the polymer concentration (or molecular mass) is sufficiently high and viscosity of solution exceeds essentially that of solvent, the rheological effects in bubble dynamics become much more pronounced. In Figure 7.2.7, data[39] are presented for the relative damping decrement of free oscillations of air bubble with R_0 = 2.8 mm in aqueous solution of POE via concentration. The dashed line represents theoretical values of the decrement, corresponding to Newtonian liquid with $\eta = \eta_p$. The actual energy losses, characterized by experimental points, remained almost unchanged, despite the sharp rise in the "Newtonian" decrement, Λ_p, with c. This result correlates well with the above theoretical predictions and it is explained by viscoelastic properties of the solution. The same explanation has the phe-

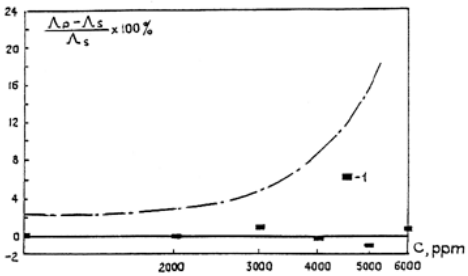

Figure 7.2.7. Relative decrement of free oscillations of air bubble versus concentration of POE in water. [By permission of IOP Publishing Limited from W.D. McComb, and S. Ayyash, *J. Phys. D: Appl. Phys*., **13**, 773, 1980, the reference 39]

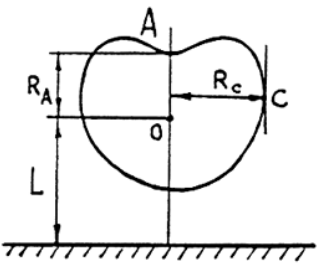

Figure 7.2.8. Geometrical parameters of the collapsing bubble. [By permission of the American Institute of Physics from G.L. Chahine, and D.H. Fruman, *Phys. Fluids*., **22**, 1406, 1979, the reference 37]

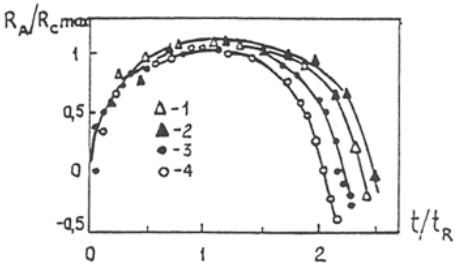

Figure 7.2.9. Collapse of a bubble near a solid wall in water (curves 1 and 4) and in dilute POE aqueous solution (curves 2, 3). [By permission of the American Institute of Physics from G.L. Chahine, and D.H. Fruman, *Phys. Fluids*., **22**, 1406, 1979, the reference 37]

nomenon observed[40] in ultrasonic insonification of liquid polybutadiene with molecular mass $M \sim 10^5$ and $\eta_p \sim 10^6$ Pas. At ultrasound frequency f~18 kHz the acoustic cavitation and well-developed pulsations of bubbles were detected, in spite of for low-molecular liquids with so high viscosity it is completely impossible.[41]

For non-spherical bubbles the effect of polymeric additives becomes essential at lower concentrations, as compared to the spherical bubbles. For example, retardation of the bubble collapse near a solid wall was observed[37,42] in such concentration interval where dynamics of spherical bubbles has remained unchanged. In Figures 7.2.8 and 7.2.9 the data[37] are reproduced, where the Rayleigh time, t_0, was chosen for a scaling time, t_R, and for curves 1- 4 $R_{c,max}/L = 0.5, 0.56, 1.39, 1.25$, respectively. The bubble collapse is accompanied by generation of a microjet towards the wall and addition of polymer led to stabilization of the bubble shape and retardation of the jet formation. This effect is connected with the increase in the elongational viscosity of a polymeric solution in flow around collapsing bubble.

The effect of polymeric additives on collective phenomena, associated with the dynamics of bubbles, can be illustrated by the example of hydrodynamic cavitation, caused by abrupt decrease in local pressure (in flows around bodies, after stream contraction, in jets). It has been found that the use of polymers permits to decrease the cavitation noise, lower the cavitation erosion, and delay the cavitation inception. For example, adding a small amount of POE to a water jet issuing from the orifice caused the decrease of the critical cavitation number, κ_{cr}, by 35-40%.[43,44] In experiments with rotating disk[45] the value of κ_{cr} was decreased by 65% with addition of 500 ppm POE. Note, however, that these features are linked not only to the changes in individual bubble dynamics, but to the influence of macromolecules on the total flow regime as well. In particular, phenomena listed above are

closely connected with the effect of a strong increase in local stresses in a polymer solution flow when the longitudinal velocity gradient reaches the value of reciprocal relaxation time.[3]

7.2.2 THERMAL GROWTH OF BUBBLES IN SUPERHEATED SOLUTIONS OF POLYMERS

Growth of vapor bubbles in a superheated liquid is the central phenomenon in boiling processes. When the bulk superheat is induced by a decrease in pressure, then the initial stage of vapor bubble growth is governed by inertia of the surrounding liquid. During this stage the rheological properties of liquid play important role, discussed in the previous section. The basic features, characterizing this stage, are pressure changes within bubbles and their pulsations. After leveling of pressure in the phases, the process turns into the thermal stage when the cavity growth rate is controlled by ability of the liquid to supply the heat necessary for phase transitions. Expansion of vapor bubble in the thermal regime was examined[46] for the case of liquid representing a binary solution. Similar problem was treated[47] under additional assumption that the convective heat and mass transfer in the two-component liquid phase is insignificant. More recent works on dynamics of vapor bubbles in binary systems are reviewed elsewhere.[48-50]

The features, peculiar to vapor bubbles evolution in polymeric solutions at the thermal stage, owe mainly to the following. First, only the low-molecular solvent takes part in phase transitions at the interface because of a large difference in molecular masses of the solvent and polymer. The second, polymeric solutions, as a rule, are essentially non-ideal and, therefore, saturated vapor pressure of the volatile component deviates from the Raul's law. Finally, the diffusion coefficient in solution is highly concentration dependent that can greatly influence the rate of the solvent transport toward the interface. The role of the listed factors increases at boiling of systems that possess a lower critical solution temperature (LCST) and thus are subjected to phase separation in the temperature range $T < T_s$, where T_s is the saturation temperature. In the latter case the rich-in-polymer phase which, as a rule, is more dense, accumulates near the heating surface (when a heater is placed at the bottom). As a consequence, the growth of bubbles proceed under limited supply of the volatile component.

Consider the expansion of a vapor cavity in a polymer solution with equilibrium mass concentration of the solvent, k_0, at the temperature $T_{f0} > T_s(k_0, p_{f0})$, assuming that both pressure and temperature in the vapor phase are constant

$$p_v = p_{f0}, \quad T_v = T_s(p_{f0}, k_R) = T_{fR}, \quad k_R = k(R, t), \quad T_{fR} = T_f(R, t) \qquad [7.2.44]$$

Parameters k_0, T_{f0} characterize the state of solution far from the bubble (at $r = \infty$). Unlike a one-component liquid, the temperature T_{fR} here is unknown. It is related to the surface concentration of solvent, k_R, by the equation of phase equilibrium at the interface.

Equations for heat transfer and diffusion in the solution have the form

$$\frac{\partial T_f}{\partial t} + v_{fR}\frac{R^2}{r^2}\frac{\partial T_f}{\partial r} = r^{-2}\frac{\partial}{\partial r}\left(a_f r^2 \frac{\partial T_f}{\partial r}\right) \qquad [7.2.45]$$

$$\frac{\partial k}{\partial t} + v_{fR}\frac{R^2}{r^2}\frac{\partial k}{\partial r} = r^{-2}\frac{\partial}{\partial r}\left(Dr^2 \frac{\partial k}{\partial r}\right) \qquad [7.2.46]$$

Since the thermal diffusivity of solution, a_f, is less affected[20] by variations of temperature and concentration over the ranges $T_s(k_R) < T_f < T_{f0}$ and $k_R < k < k_0$, respectively, than the binary diffusion coefficient, D, it is assumed henceforward that a_f = const. Furthermore, since the thermal boundary layer is much thicker than the diffusion layer, it is appropriate to assume that within the latter $D = D(k,T_{fR})$.

The boundary conditions for equations [7.2.45], [7.2.46] are as

$$T_f = T_{f0}, \qquad k = k_0 \qquad \text{at} \qquad r = \infty \tag{7.2.47}$$

$$\dot{R} - v_{fR} = \rho_f^{-1} j, \quad \dot{R} = \rho_v^{-1} j \tag{7.2.48}$$

$$j = \left(\dot{R} - v_{fR}\right)\rho_f k_R + \rho_f D \frac{\partial k}{\partial r}, \quad jl = k_f \frac{\partial T_f}{\partial r} \quad at\ r = R(t) \tag{7.2.49}$$

where:

j	phase transition rate per unit surface area of a bubble
v_{fR}	radial velocity of the liquid at the interface
k_f	heat conductivity of liquid
ρ_f, ρ_v	densities of solution and solvent vapor

Equations [7.2.48] and [7.2.49] yield

$$j = \frac{\rho_f}{1 - k_R} D \frac{\partial k}{\partial r}\Big|_{r=R} \tag{7.2.50}$$

If thermodynamic state of the system is far from the critical one, $\varepsilon = \rho_v / \rho_f << 1$ and it is possible to assume that $v_{fR} = \dot{R}(1-\varepsilon) \approx \dot{R}$. The solution of equations [7.2.45], [7.2.46] is searched in the form $T_f = T(\eta)$, $k = k(\eta)$ with $\eta = r/R(t)$. The concentration dependence of the diffusion coefficient is represented as $D = D_0(1 + f(k))$. The self-similar solution of the problem exists if

$$h = R\dot{R}a_f^{-1} = const, \quad h_1 = R\dot{R}D_0^{-1} = const \tag{7.2.51}$$

In this case the functions $T(\eta)$, $k(\eta)$ satisfy the following equations:

$$\frac{\partial^2 T}{\partial \eta^2} + \left[h\eta + 2\eta^{-1} - (1-\varepsilon)h\eta^{-2}\right]\frac{\partial T}{\partial \eta} = 0 \tag{7.2.52}$$

$$\frac{\partial^2 k}{\partial \eta^2} + \left[\bar{D}^{-1}h_1\eta + 2\eta^{-1} - \bar{D}^{-1}(1-\varepsilon)h_1\eta^{-2}\right]\frac{\partial k}{\partial \eta} + \bar{D}^{-1}\frac{df}{dk}\left(\frac{dk}{d\eta}\right)^2 = 0, \bar{D} = D / D_0 \tag{7.2.53}$$

Equation [7.2.53], as opposed to [7.2.52], is non-linear and cannot be solved analytically for arbitrary function $D = D(k(\eta))$. Note that in the case of the planar non-linear diffusion, if the self-similarity conditions are satisfied, the problem has analytical solution for particular forms of the dependencies $D = D(k)$ (e.g., linear, exponential, power-law, etc[51]). However, the resulting relationships are rather cumbersome. The approximate solution of the problem was derived in the case $J_a >> 1$, using the perturbation method:[52]

$$h = (6/\pi)Ja^2 = (6\pi)Le^{-1}Di^2(1+M_1)^2, \quad Di = \varepsilon^{-1}K_\alpha[1+f(k_R)], \quad K_\alpha = (k_0 - k_R)/(1-k_R) \quad [7.2.54]$$

where:

Ja	Jacob number, $Ja = c_f\Delta T_f(\varepsilon l)^{-1}$
ΔT_f	superheat of the solution with respect to the interface, $\Delta T_f = T_{f0} - T_{fR}$
Le	Lewis number, a_f/D_0
K_α	mass fraction of the evaporated liquid[46]

Here M_1 follows certain cumbersome equation,[52] including f(k). The approximation Ja>>1 corresponds to the case of a thin thermal boundary layer around the growing bubble. Since, for polymeric solutions Le >> 1, the condition of small thickness of the diffusion boundary layer is satisfied in this situation as well.

We start the analysis of the solution [7.2.54] from the approximation f = 0 that corresponds to $D \approx D_0 = \text{const}$. Then from [7.2.54] it follows:

$$K_\alpha = \left(\sqrt{Le}\right)c_f I^{-1}\Delta T \quad [7.2.55]$$

Because of the diffusion resistance, the solvent concentration at the interface is less then in the bulk, $k_R < k_0$. Writing the equation of phase equilibrium in linear approximation with respect to $\Delta k = k_0 - k$, from [7.2.55] one can receive[49,53]

$$\Delta T/\Delta T^* = \left[1 - c_f I^{-1}(1-k_R)\sqrt{Le}\left(\frac{\partial T_s}{\partial k}\right)_{k=k_0}\right]^{-1}, \quad \Delta T^* = T_{f0} - T_s(k_0) \quad [7.2.56]$$

Here ΔT^* represents the superheat of the solution at infinity. For solutions of polymers $\partial T_s/\partial k < 0$ and, therefore, the actual superheat of the liquid $\Delta T < \Delta T^*$. Additional simplification can be achieved if $1 - k_R >> k_0 - k_R$. It permits to assume in [7.2.56] $k_R \approx k_0$ and, hence, to find easily the vapor temperature.

In the diffusion-equilibrium approximation (i.e. $Le \to 0$) $\Delta T = \Delta T^*$. When the diffusion resistance increases, the actual superheat ΔT lowers and, according to [7.2.56], at $Le \to \infty$ $\Delta T \to 0$. However, in the latter case the assumptions made while deriving [7.2.56], are no longer valid. Indeed, the Ja number, connected with the superheat of the solution with respect to the interface, is related to the Ja_0 value, corresponding to the bulk superheat, by $Ja = Ja_0(\Delta T/\Delta T^*)$. Since the ratio $\Delta T/\Delta T^*$ varies in the range (0, 1), then, at small diffusion coefficients, it may be that Ja << 1 even when Ja_0 >> 1. In this case, the asymptotic solution of the problem takes the form[46] h = Ja, and, for thin diffusion boundary layer, it can be received instead of [7.2.54]:

$$h = Ja = (6/\pi)Le^{-1}Di^2(1+M_1) \quad [7.2.57]$$

Finally, at Di << 1 and Ja << 1, the non-linear features in the diffusion transport can be neglected and the expressions for h and k_R (or T_{fR}) take the form

$$h = Ja = Le^{-1}Di \quad [7.2.58]$$

The bubble growth in the thermal regime follows the law[54]

$$R = C\sqrt{t}, \quad C = \sqrt{2a_f h}$$

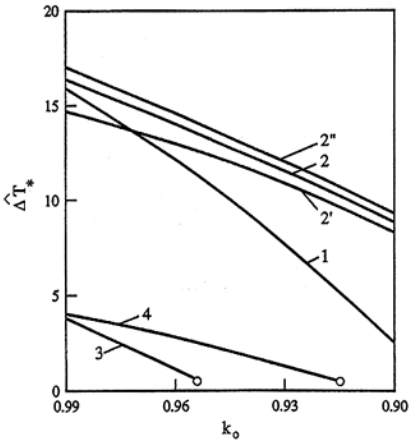

Figure 7.2.10. Limiting superheat at vapor bubble growth in polymeric solution. For all graphs $K_p = 0.7$, the symbol "o" corresponds to $Ja_0 = 1$. [Reprinted from Z.P. Shulman, and S.P. Levitsky, *Int. J. Heat Mass Transfer*, **39**, 631, Copyright 1996, the reference 52, with permission from Elsevier Science]

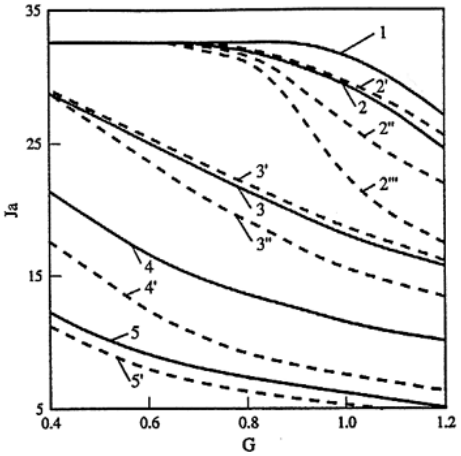

Figure 7.2.11. Dependence of the effective Jacob number for a vapor bubble, growing in a superheated aqueous solution of a polymer, on the parameter G. [Reprinted from Z.P. Shulman, and S.P. Levitsky, *Int. J. Heat Mass Transfer*, **39**, 631, Copyright 1996, the reference 52, with permission from Elsevier Science]

where the constant C can be evaluated through h from [7.2.54], [7.2.57] and [7.2.58]. Note that since $Ja < Ja_0$, the bubble growth rate in a polymer solution is always lower than that in a similar one-component liquid.

The set of equations, formulated above, is closed by the equation of phase equilibrium [7.2.37]. The temperature dependence of the pure solvent vapor pressure is described by equation[54] $p^0_{v0} = A\exp(-B/T)$.

Numerical simulations of vapor bubble growth in a superheated solution of polymer were performed,[52] using iterative algorithm to account for the diffusion coefficient dependence on concentration in the interval (k_R, k_0). The results are reproduced in Figures 7.2.10-7.2.12,

where:

Sn	Scriven number, $Sn = \Delta T/\Delta T^*$
G	dimensionless parameter, $G = \varepsilon Ja_0 Le^{1/2}$
$\Delta\hat{T}^*$	superheat of the solution at infinity, evaluated from the condition Sn = 0.99

A characteristic feature of the liquid-vapor phase equilibrium curves for polymeric solutions in the coordinates p, k or T, k is the existence of plateau-like domain in the region of small polymer concentrations ($k^* \le k_0 \le 1$). For this concentration range, the number Ja_0 can be defined so that at $1 < Ja_0 < Ja_0$ the diffusion-induced retardation of the vapor bubble growth does not manifest itself because of weak dependence of T_s (or p_s) on k_R. The Ja_0 value or the corresponding limiting superheat, $\Delta\hat{T}^*$, can be estimated from the condition Sn = 0.99 (i.e. the deviation of effective superheat, ΔT, from the bulk one, ΔT^*, does not exceed 1%). The dependence of the so-defined parameter, $\Delta\hat{T}^*$, on k_0 is represented in Figure 7.2.10. For curves 1, 2, 2', 2": $l = 2.3\times10^6$ Jkg^{-1}, $c_f = 3\times10^3$ Jkg^{-1}K^{-1}, $a_f = 10^{-7}$ m^{2}s^{-1}, $D_0 = 5\times10^{-11}$ m^{2}s^{-1}; for 3, 4: $l = 3.6\times10^5$ Jkg^{-1}, $c_f = 2\times10^3$ Jkg^{-1}K^{-1}, $a_f = 8\times10^{-8}$ m^{2}s^{-1}, $D_0 = 5\times10^{-11}$

m^2s^{-1}; for 1 - 4: $\alpha = 0$; for 2', 2'': $\alpha = 1, -1$; for 1, 3: $\chi = 0.1$; for 2, 4: $\chi = 0.4$. Here $\alpha = k_R^{-1}\left(d\overline{D}/d\overline{k}\right)_{\overline{k}=\overline{k}_0}$, $\overline{k}=k/k_R$.

It is seen that the $\Delta\hat{T}^*$ value decreases with reduction of k_0 and/or increasing the non-linearity factor, α. Raising the value of the Flory-Huggins constant, χ, causes the $\Delta\hat{T}^*$ value to increase and extends the range $k^* \le k_0 \le 1$. The ΔT^* value essentially depends on the rate of the diffusion mass transfer; reduction of the latter lowers the limiting superheat, that is the value of ΔT^*, below which the bubble grows in a polymeric liquid as though it were a pure solvent. For polymer solutions in volatile organic solvents, the limiting superheat is lower than for aqueous solutions of the same concentrations. Note that for low molecular binary solutions the term "limiting superheat" in the current sense is meaningless in view of pronounced dependence $T_s = T_s(k_0)$ in the entire range of the k_0 variation. The scale of the effect under consideration is closely connected with the deviation of the solution behavior from the ideal one: the larger is deviation the less is the effect. This can be easily understood, since in the case of a very large difference between molecular masses of the solvent and solved substance, typical for a polymer solution, the graph $T_s = T_s(k_0)$, plotted in accordance with the Raul law, nearly coincides with the coordinate axes.[20] For this reason, the bubble growth rate in a polymer solution that obeys the Flory-Huggings law, is always lower than in a similar ideal solution.

The reduction of the diffusion mass transfer rate ($G \sim (Le)^{1/2}$) at a fixed superheat, ΔT^*, leads to a substantial decrease in the effective Jackob's number, Ja. The growth of the content of a polymer in a solution leads to the same result. This follows from Figure 7.2.11 where curves 1 - 5 correspond to $k_0 = 0.99, 0.95, 0.7, 0.5, 0.3$; 2' - 2''': $k_0 = 0.95$; 3' - 3'': $k_0 = 0.7$; 4', 5': $k_0 = 0.5, 0.3$; 1 - 5: $\alpha = 0$; 2' - 3': $\alpha = -0.5$; 2'': $\alpha = 0.8$; 2''', 3'', 4', 5': $\alpha = 2$. For all graphs, $\Delta T^* = 15$ K, $\chi = 0.1$, $K_p = 0.7$.

The influence of non-linearity of diffusional transport is higher for diluted solutions. This is explained by a decrease in the deviation of the surface concentration, k_R, from the bulk k_0 with lowering k_0. This takes place due to simultaneous increase in $|\partial T_s/\partial k|$ that is characteristic of polymeric liquids. The presence of a nearly horizontal domain on the curve Ja = Ja(G) at $k_0 \ge 0.95$ is explained by the existence of the limiting superheat dependent on the Lewis number.

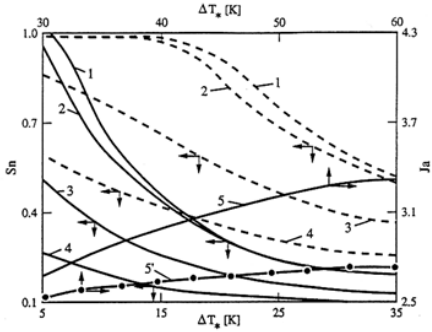

Figure 7.2.12. Effect of the solution bulk superheat on the Scriven and Jacob numbers. (–) - solution of polymer in toluene, (- - -) - aqueous solution. [Reprinted from Z.P. Shulman, and S.P. Levitsky, *Int. J. Heat Mass Transfer*, **39**, 631, Copyright 1996, the reference 52, with permission from Elsevier Science]

The role of diffusion-induced retardation increases with the bulk superheat. This reveals itself in reduction of the number Sn with a growth in ΔT^* (Figure 7.2.12). For solutions of polymers in volatile organic liquids, such as solvents, the effect is higher than in aqueous solutions. For concentrated solutions the difference between the effective ΔT and bulk ΔT^* superheats makes it practically impossible to increase substantially the rate of vapor bubble growth by increasing the bulk superheat. Curves 5 and 5' clearly demonstrate this. They are calculated for solution of polystyrene in toluene at $k_0 = 0.3$, therewith for the curve 5 the dependence of the diffusion coefficient from

temperature and concentration D(T,k) was neglected ($\alpha = 0$), whereas for the curve 5' it was accounted for according to the experimental data.[55] Other curves were evaluated with the following parameter values: curves 1 - 5 correspond to $\alpha = 0$, $k_0 = 0.99, 0.95, 0.7, 0.5, 0.3$; 1 - 4: $\chi = 0.1$. Thermophysical parameters of the liquid and vapor are the same as in the Figure 7.2.10.

Thus, the rate of expansion of vapor bubbles in superheated solution of polymer is lower than in pure solvent due to diffusion resistance. But in diluted solution at rather small superheats the mechanism of diffusional retardation can be suppressed due to a weak dependence of T_s on k_0 in this concentration range. Another important conclusion is that in concentrated solutions it is practically impossible to attain values Ja >> 1 by increasing the superheat because of low values of the corresponding Sn numbers.

7.2.3 BOILING OF MACROMOLECULAR LIQUIDS

Experimental investigations of heat transfer at boiling of polymeric liquids cover highly diluted (c = 15 to 500 ppm), low-concentrated (c ~ 1%), and concentrated solutions (c>10%). The data represent diversity of physical mechanisms that reveal themselves in boiling processes. The relative contribution of different physical factors can vary significantly with changes in concentration, temperature, external conditions, etc., even for polymers of the same type and approximately equal molecular mass. For dilute solutions this is clearly demonstrated by the experimentally detected both intensification of heat transfer at nucleate boiling and the opposite effect, viz. a decrease in the heat removal rate in comparison with a pure solvent.

Macroscopic effects at boiling are associated with changes in the intrinsic characteristics of the process (e.g., bubble shape and sizes, nucleation frequency, etc.). Let's discuss the existing experimental data in more detail.

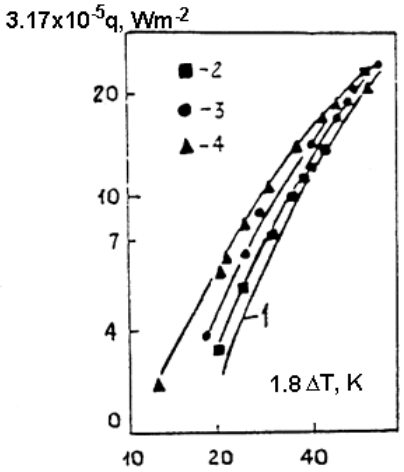

Figure 7.2.13. Effect of the HEC additives on the boiling curve. 1 - pure water; 2, 3 and 4 - HEC solution with c = 62.5, 125 and 250 ppm, correspondingly. [Reprinted from P. Kotchaphakdee, and M.C. Williams, *Int. J. Heat Mass Transfer*, **13**, 835, Copyright 1970, the reference 52, with permission from Elsevier Science]

One of the first studies on the effect of water-soluble polymeric additives on boiling was reported elsewhere.[56] For a plane heating element a significant increase in heat flux at fixed superheat, ΔT = 10-35K, was found in aqueous solutions of PAA Separan NP10 ($M = 10^6$), NP20 ($M = 2\times10^6$), and HEC ($M \sim 7\times10^4$ to about 10^5) at concentrations of 65 to 500 ppm (Figure 7.2.13). The experiments were performed at atmospheric pressure; the viscosity of the solutions did not exceed 3.57×10^{-3} Pas. The following specific features of boiling of polymer solution were revealed by visual observations: (i) reduction in the departure diameter of bubbles, (ii) more uniform bubble-size distribution, (iii) decrease in the tendency to coalescence between bubbles. The addition of HEC led to faster covering of the heating surface by bubbles during the initial period of boiling and bubbles were

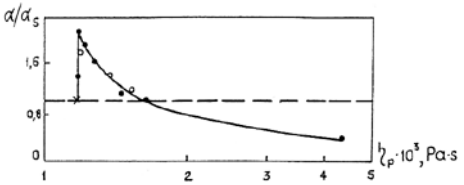

Figure 7.2.14. The relation between the relative heat transfer coefficient for boiling PIB solutions in cyclohexane and the Newtonian viscosity of the solutions measured at T=298 K. ΔT = 16.67 K; ● - PIB Vistanex L-100 in cyclohexane, o - PIB Vistanex L-80 in cyclohexane, x - pure cyclohexane. [Reprinted from H.J. Gannett, and M.C. Williams, *Int. J. Heat Mass Transfer*, **14**, 1001, Copyright 1971, the reference 57, with permission from Elsevier Science]

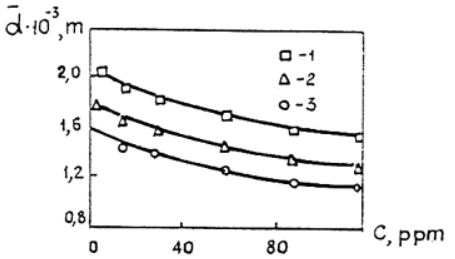

Figure 7.2.15. The average bubble detachment diameter in boiling dilute aqueous solutions of PEO.[59] ΔT = 15K. For curves 1-3 the flow velocity v = 0, 5×10^{-2}, and 10^{-1} m/s, respectively. [Adapted, from S.P. Levitsky, and Z.P. Shulman, **Bubbles in polymeric liquids**, *Technomic Publish. Co.*, Lancaster, 1995, with permission from Technomic Publishing Co., Inc., copyright 1995]

smaller in size than in water and aqueous solutions of PAA.

Non-monotonous change in the heat transfer coefficient, α, with increasing the concentration of PIB Vistanex L80 ($M = 7.2\times10^5$) or L100 ($M = 1.4\times10^6$) in boiling cyclohexane has been reported.[57] The results were received in a setup similar to that described earlier.[56] It was found that the value of α increases with c in the range 22 ppm < c < 300 ppm and decreases in the range 300 ppm < c < 5150 ppm. Viscosity of the solution, corresponding to α_{max} value, according to the data[57] only slightly exceeds that of the solvent (Figure 7.2.14). Within the entire range of concentrations at supercritical (with respect to pure solvent) superheats, the film boiling regime did not appear up to the maximum attainable value ΔT ~ 60K. The growth of polymer concentration in the region of "delayed " nucleate boiling led to a considerable decrease in heat transfer.

These findings[56,57] were confirmed[58] in a study of the nucleate boiling of aqueous solutions of HEC Natrosol 250HR ($M = 2\times10^5$), 250GR ($M = 7\times10^4$), and PEO ($M \sim (2\text{-}4)\times10^6$) at forced convection of the liquid in a tube. A decrease in the size of bubbles in the solution and reduction of coalescence intensity were recognized. Similar results were presented also in study,[59] where the increase in heat transfer at boiling of aqueous solutions of PEO WSR-301 ($M=2\times10^6$) and PAA Separan AP-30 (15 ppm < c < 150 ppm) on the surface of a conical heater was observed. In aqueous solutions of PAA with c > 60 ppm the α value began to decrease. With an increase in c the detachment diameter of bubbles decreased (Figure 7.2.15), the nucleation frequency increased, and the tendency to coalescence was suppressed.

Boiling of PEO solutions with c = 0.002 to 1.28% at atmospheric and sub-atmospheric pressures was examined[60] for subcoolings in the range 0 to 80K. It was demonstrated that at saturated boiling the dependence of the heat transfer coefficient α on the polymer concentration is non-monotonous: as c grows, α first increases, attaining the maximal value at c≈0.04% , whereas at c = 1.28% the value of α is smaller than in water ($\alpha < \alpha_s$) (Figure 7.2.10). With a decrease in pressure the effect of polymeric additives weakens and for solution with greatest PEO concentration (in the investigated range) the α value increases, approaching α_s from below. The critical heat flux densities in PEO solutions are smaller than those for water.

In view of the discussed results, the work[61] attracts special attention since it contains data on boiling of dilute solutions, opposite to those reported earlier.[56-60] The addition of PAA, PEO and HEC to water in concentrations, corresponding to the viscosity increase up to $\eta_p = 1.32\times10^{-3}$ Pas, has brought about reduction in heat transfer. The boiling curve in coordinates q (heat flux) vs. ΔT displaced almost congruently to the region of larger ΔT values with c (Figure 7.2.17a). It was demonstrated[61] that the observed decrease in α with addition of polymer to water can be both qualitatively and quantitatively (with the Rohsenow pool boiling correlation for the heat transfer coefficient[62]) associated with the increase in the solution viscosity (Figure 7.2.17, b). The experiments[61] were performed using a thin platinum wire with diameter 0.3 mm.

Explanation of experimental data needs more detailed discussion of physical factors that can reveal themselves in boiling of polymeric solutions. They include possible changes in capillary forces on interfaces in the presence of polymeric additives; absorption of macromolecules on the heating surface; increase in the number of weak points in the solution, which facilitates increase in the number of nuclei; thermodynamic peculiarities of the polymer-solvent system; the effect of macromolecules on the diffusion mass transfer in evaporation of solvent; hydrodynamics of convective flows in a boiling layer and the motion of bubbles; manifestation of rheological properties of solution.

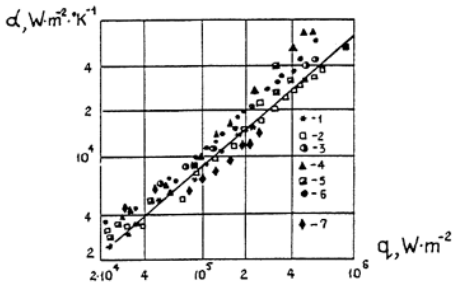

Figure 7.2.16. Heat transfer coefficient for nucleate pool boiling of PEO aqueous solutions. ($p_{f0} = 9.8\times10^3$ Pa). Curve 1 corresponds to pure water, for curves 2 - 7, c = 0.01, 0.02, 0.04, 0.08, 0.16 and 1.28%, respectively. [Adapted, from S.P. Levitsky, and Z.P. Shulman, **Bubbles in polymeric liquids**, *Technomic Publish. Co.,* Lancaster, 1995, with permission from Technomic Publishing Co., Inc., copyright 1995]

The capillary effects were indicated as one of the reasons for the intensification of heat transfer, since many polymers (in particular, HEC, PEO, etc.),[63] similar to low-molecular surfactants,[64] are capable of decreasing the surface tension. As a result, they decrease both the work of the nucleus formation, $W_{cr,}$ and the critical size of bubble, R_{cr}:

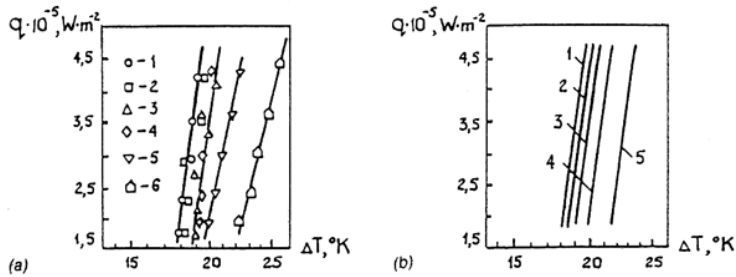

Figure 7.2.17. Boiling curves for aqueous solutions of PAA Separan AP-30. (a) experimental data; for curves 1 - 6 η_r = 1.00, 1.01, 1.04, 1.08, 1.16 and 1.32, correspondingly; (b) calculations made with the use of the Rohsenow pool boiling correlation; for curves 1 - 5, η_r = 1.00, 1.01, 1.04, 1.16 and 1.32, respectively ($\eta_r = \eta_p/\eta_s$). [By permission from D.D. Paul, and S.I. Abdel-Khalik, *J. Rheol*., **27**, 59, 1983, reference 61]

$$W_{cr} = 16/3\pi\sigma^3\Phi(\theta)\left[(dp/dT)\Delta T(1-\rho_v/\rho_f)\right]^2, \quad \Phi(\theta) = 1/4\left(2+3\cos\theta-\cos^3\theta\right) \quad [7.2.59]$$

$$R_{cr} = 2\sigma\left[(dp/dT)\Delta T(1-\rho_v/\rho_f)\right]^{-1}$$

where:

θ	wetting angle
σ	surface tension coefficient

However, it should be noted that the integral effect of the heat transfer enhancement, observed in highly diluted solutions, can not be attributed to the capillary phenomena alone, since the main change in σ occurs in the range of low polymer concentrations[59] ($c < 50$ ppm) and further increase in c does not affect the value of σ, whereas the α value continues to grow. PAA, for example, does not behave like surfactants at all. It should be noted also that in the presence of polymer not only the value of σ changes, but also the wetting angle, θ, in the formula [7.2.59]. The latter may lead to manifestation of different behavior.

Absorption of macromolecules onto a heating surface favors the formation of new centers of nucleation. Together with an increase in nucleation sites in the boundary layer of a boiling liquid it explains the general growth in the number of bubbles. Both this factor and reduction in the σ value for solutions of polymers that possess surface activity, are responsible for a certain decrease in superheat needed for the onset of boiling of dilute solutions.[57,60]

The decrease in the water vapor pressure due to presence of polymer in solution at c~1% can be neglected. However, if the solution has the LCST, located below the heating wall temperature, the separation into rich-in-polymer and poor-in-polymer phases occurs in the wall boundary layer. At low concentration of macromolecules the first of these exists in a fine-dispersed state that was observed, for example, for PEO solutions.[60] The rich-in-polymer phase manifests itself in a local buildup of the saturation temperature, which can be significant at high polymer content after separation; in decrease of intensity of both convective heat transfer and motion of bubbles because of the increase in viscosity; and reduction of the bubble growth rate. The so-called "slow" crisis, observed in PEO solutions[60] is explained by integral action of these reasons. Similar phenomenon, but less pronounced, was observed also at high enough polymer concentrations.[58] It is characterized by plateau on the boiling curves for solutions of PIB in cyclohexane, extending into the range of high superheats.

The main reason for the decrease in heat transfer coefficient at nucleate boiling of polymeric solutions with $c \sim 1\%$ is the increase in liquid viscosity, leading to suppression of microconvection and increasing the resistance to the bubbles' rising. In the presence of LCST, located below the boiling temperature, the role of this factor increases because appearance in the boiling layer of the rich-in-polymer phase in fine-dispersed state. Another reason for the decrease of α in the discussed concentration range is the decrease in the bubble growth rate at the thermal stage, when the superheat $\Delta T > \Delta T^*$ (Section 7.2.2).

In highly diluted solutions the change in Newtonian viscosity due to polymer is insignificant, and though the correlation between heat transfer enhancement and increase in viscosity has been noticed, it cannot be the reason for observed changes of α. In hydrodynamics, the effect of turbulence suppression by small polymeric additives is known, but it also cannot be considered for such a reason because laminarization of the boundary layer leads to reduction of the intensity of convective heat transfer.[65] Nevertheless, the phenomenon of the decrease of hydrodynamic resistance and enhancement of heat transfer in boiling dilute solutions have a common nature. The latter effect was connected

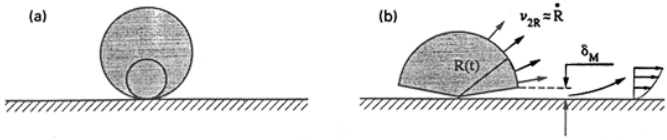

Figure 7.2.18. Growth of vapor bubbles on the heating surface at high (a) and low (b) pressures. [Reprinted from S.P. Levitsky, B.M. Khusid and Z.P. Shulman, *Int. J. Heat Mass Transfer*, **39**, 639, Copyright 1996, the reference 66, with permission from Elsevier Science]

with manifestation of elastic properties of the solution at vapor bubble growth on the heating surface.[66]

The general character of the bubbles evolution at boiling under atmospheric and subatmospheric pressures, respectively, is clarified schematically in Figure 7.2.18. In the first case (at high pressures) the base of a bubble does not "spread"[67] but stays at the place of its nucleation. Under such conditions the decrease in the curvature of the bubble surface with time, resulting from the increase in bubble radius, R, leads to liquid displacement from the zone between the lower part of the microbubble and the heating surface. This gives rise to the local shear in a thin layer of a polymer solution. A similar shear flow is developed also in the second case (at low pressures), when a microlayer of liquid is formed under a semi-spherical bubble. As known, at shear of a viscoelastic fluid appear not only tangential but also normal stresses, reflecting accumulation of elastic energy in the strained layer (the Weissenberg effect[3]). The appearance of these stresses and elastic return of the liquid to the bubble nucleation center is the reason for more early detachment of the bubble from the heating surface, reduction in its size and growth in the nucleation frequency. All this ultimately leads to enhancement of the heat transfer.

The above discussion permits to explain the experimental results.[61] Their reasons are associated with substantial differences in the conditions of boiling on a thin wire and a plate or a tube. Steam bubbles growing on a wire have a size commensurable with the wire diameter (the growing bubble enveloped the wire[61]). This results in sharp reduction of the boundary layer role, the same as the role of the normal stresses. Besides, the bubble growth rate on a wire is smaller than on a plane (for a wire $R \sim t^n$ where $n < 1/4$).[67]

The elastic properties of the solution are responsible also for stabilization of the spherical shape of bubbles observed in experiments on boiling and cavitation. Finally, the observed reduction in a coalescence tendency and an increase in the bubble sizes uniformity can also be attributed to the effects of normal stresses and longitudinal viscosity in thin films separating the drawing together bubbles.

The linkage between the enhancement of heat transfer at boiling of dilute polymer solutions and the elastic properties of the system is confirmed by the existence of the optimal concentration corresponding to α_{max} (Figure 7.2.14). Similar optimal concentration was established in addition of polymers to water to suppress turbulence - the phenomenon that also owes its origin to elasticity of macromolecules.[1,3,9] Therefore, it is possible to expect that the factors favoring the chain flexibility and increase in the molecular mass, should lead to strengthening of the effect.

The data on boiling of concentrated polymeric solutions[20] demonstrate that in such systems thermodynamic, diffusional, and rheological factors are of primary importance.

The diagram of the liquid-vapor phase equilibrium is characterized by a decrease in the derivative dp/dT with the polymer concentration ($dp/dT \to 0$ at $k \to 0$). This leads to increase in both the nucleation energy and the detachment size of a bubble (equation [7.2.59]) and, consequently, to reduction of the bubbles generation frequency. Note that in reality the critical work, W_{cr}, for a polymeric liquid may exceed the value predicted by the formula [7.2.59] because of manifestation of the elasticity of macromolecules.

As known,[62] the heat transfer coefficient in the case of developed nucleate boiling of low-molecular liquids is related to the heat flux, q, by the expression $\alpha = Aq^n$ where $n \approx 0.6\text{-}0.7$. For concentrated polymeric solutions the exponent n is close to zero. The decrease in heat transfer is explained by the increase in the viscosity of the solution near the heating surface, resulting from the evacuation of the solvent with vapor. Another reason for the decrease of α in such systems is the reduction of the bubble growth rate with lowering k_0 and the impossibility to achieve large Ja numbers by rising the solution superheat.

Since in boiling of concentrated polymer solutions the α value is small, the superheat of the wall at a fixed q increases. This can give rise to undesirable phenomena such as burning fast to the heating surface, structure formation, and thermal decomposition. Usually, in this case the heat transfer is intensified by mechanical agitation. Note that one of the promising trends in this field may become the use of ultrasound, the efficiency of which should be evaluated with account for considerable reduction in real losses at acoustically induced flows and pulsations of bubbles in viscoelastic media.[68,69]

Specific features of boiling of high-molecular solutions are important for a number of applications. One of examples is the heat treatment of metals, where polymeric liquids find expanding employment. The shortcomings of traditionally used quenching liquids, such as water and oil, are well known.[70] Quenching in oil, due to its large viscosity and high boiling temperature, does not permit to suppress the perlite transformation in steels. From the other hand, water as a quenching medium is characterized by high cooling rate over the temperature ranges of both perlite and beinite transformations. However, its maximum quenching ability lies in the temperature range of martensite formation that can lead to cracking and shape distortion of a steel article. Besides, the quenching oils, ensuring the so-called "soft" quenching, are fire-hazardous and have ecological limitations.

The polymeric solutions in a certain range of their physical properties combine good points of both oil and water as quenching liquids and permit to control the cooling process over wide ranges of the process parameters. For the aims of heat treatment a number of water-soluble polymers are used, e.g. PVA, PEO, PAA, polymethacrylic acids (PMAA, PAA) and their salts, cellulose compounds, etc.[71-73] The optimal concentration range is 1 to 40% depending on molecular mass, chemical composition, etc. Typical data[73] are presented in Figure 7.2.19, where curves 1-5 correspond to the solution viscosity $\eta_p = (1.25, 2.25, 3.25, 5, 11)\times10^{-3}$ Pas, measured at 40°C. The quenchants based on water-soluble polymers sustain high cooling

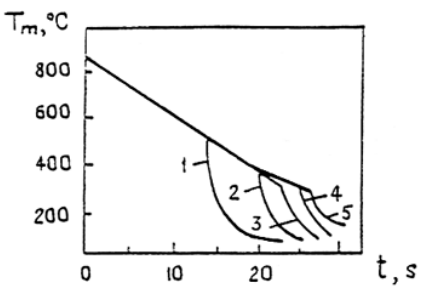

Figure 7.2.19. Cooling curves for a silver specimen quenched in a polymer aqueous solution at 20°C. [Adapted, from S.P. Levitsky, and Z.P. Shulman, **Bubbles in polymeric liquids**, *Technomic Publish. Co.*, Lancaster, 1995, with permission from Technomic Publishing Co., Inc., copyright 1995]

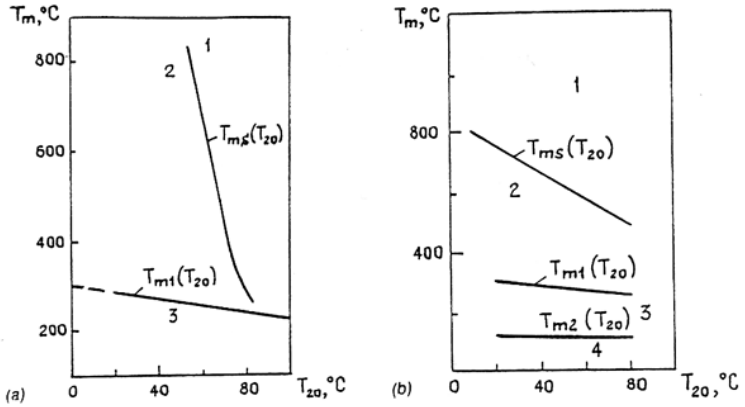

Figure 7.2.20. Stability diagrams for film boiling.[73] Quenching in water (a) and in aqueous polymer solution with $\eta_s = 3.27\times10^{-3}$ Pas at 40ºC; (b): 1, 2 - stable and unstable film boiling, 3 - nucleate boiling, 4 - convection. T_{ms}, T_{m1} and T_{m2} are the surface temperatures of the specimen, corresponding to the destabilization of the regimes 1 - 3, respectively. [Adapted, from S.P. Levitsky, and Z.P. Shulman, **Bubbles in polymeric liquids**, *Technomic Publish. Co*., Lancaster, 1995, with permission from Technomic Publishing Co., Inc., copyright 1995]

rates during the initial stage of quenching that permits to obtain fine-grained supercooled austenite, and relatively low intensity of heat removal at moderate temperatures, when martensite transformations take place.

The main feature of quenching in polymeric solutions is the prolongation of the cooling period as a whole in comparison with water that is explained by extended range of a stable film boiling (Figure 7.2.20). The increase in polymer concentration leads to reduction of α on the stage of nucleate boiling and growth of the temperature, corresponding to the onset of free convection regime.

The effect of polymeric additives on the initial stage of the process was the subject of a special investigation.[74] Experiments were performed with aqueous polymer solutions of Breox, PEO and some other polymers with $M = 6\times10^3$ to 6×10^5 at pressure of 0.1 MPa. The platinum heater with short time lag, submerged in solution, was heated in a pulsed regime with $\dot{T} \sim 10^5$ to 10^6 K/s. The experimental results revealed the existence of a period with enhanced heat transfer (as compared to water) in solutions with $c \sim 1\%$, which lasted for 10 to 100 μs after the onset of ebullition. The sensitivity of heat transfer to the polymer concentration was sufficiently high. After formation of the vapor film the secondary ebullition was observed, which resulted from superheating of the liquid outside the region of concentration gradients near the interface. The mechanism of this phenomena was described.[75] It is associated with the fact that heat transfer has a shorter time lag than mass transfer, and thus the thermal boundary layer in a liquid grows faster than the diffusion one.

The experimental data and theoretical results on the growth of vapor bubbles and films in polymeric solutions explain the efficiency of quenchants, based on water-soluble polymers. The main reason is stabilization of the film-boiling regime at initial stage of quenching. Such stabilization is connected with elastic properties of the liquid skin layer, adjacent to the interface that is enriched by polymer due to solvent evaporation. Appearance of this layer leads to fast growth of longitudinal viscosity and normal stresses, when perturbations of the interface arise, thus increasing the vapor film stability. A similar mechanism is responsible for stabilization of jets of polymeric solutions[9] as well as for retardation of bubble

collapse in a viscoelastic liquid (Section 7.2.1). In systems with LCST this effect can be still enhanced due to phase separation, induced by interaction of the liquid with high-temperature body. Additional reason that governs the decrease in heat removal rate at quenching is connected with reduction of heat conductivity in aqueous solutions of polymers with growth of concentration of the high-molecular additive.

After the body temperature is lowered sufficiently, the film boiling gave way to the nucleate one. According to data, presented in the previous section, over the polymer concentration ranges, typical for high-molecular quenchants, the α value must decrease in comparison with water. In fact, this is normally observed in experiments. Rise of the temperature, characterizing transition from nucleate boiling to convective heat transfer, is associated with the increase in liquid viscosity.

Abbreviations

HEC	hydroxyethylcellulose
LCST	lower critical solution temperature
PS	polystyrene
PIB	polyisobutylene
PAA	polyacrylamide
PEO	polymethyleneoxide
POE	polyoxyethylene
PVA	polyvinyl alcohol
TTS	time-temperature superposition

REFERENCES

1 A.B.Bird, R.C.Armstrong, and O.Hassager, **Dynamics of polymeric liquids**, *J.Wiley & Sons*, New York, 1977.
2 R. M.Christensen, **Theory of viscoelasticity. An introduction**, *Academic Press*, New York, 1982.
3 G. Astarita, and G. Marucci, **Principles of non-Newtonian fluid mechanics**, *McGraw-Hill Book Co*., London, 1974.
4 L. D. Landau, and E. M. Lifshits, **Statistical physics**, *Pergamon Press*, Oxford, 1980.
5 C. Truesdell, **A first course in rational continuum mechanics**, *Johns Hopkins University*, Baltimore, 1972.
6 K. Walters, **Rheometry**, *Chapman and Hall*, London, 1975.
7 C.J.S. Petrie, **Elongational flows**, *Pitman*, London, 1979.
8 P. J. Carreau, and D. De Kee, *Can. J. Chem. Eng*., **57**, 3 (1979).
9 Z.P. Shulman, and B. M. Khusid, **Non-stationary convective transfer processes in hereditary media**, *Nauka i Technika*, Minsk, 1983.
10 K.M. Baid, and A. B. Metzner, *Trans. Soc. Rheol.*, **21**, 237 (1977).
11 R.Y. Ting, *J. Appl. Polym. Sci.*, **20**, 1231 (1976).
12 J.M. Dealy, *Polym. Eng. Sci*., **11**, 433 (1971).
13 M.M. Denn, and G. Marrucci, *AIChE J.*, **17**, 101 (1971).
14 J.D. Ferry, **Viscoelastic properties of polymers**, *J.Wiley & Sons*, New York, 1980.
15 M. Doi, and S. F. Edwards, **The theory of polymer dynamics**, *Clarendon Press*, Oxford, 1986.
16 P.-G. de Gennes, **Scaling concepts in polymer physics**, *Cornell University Press*, Ithaca and London, 1979.
17 T. W. Spriggs, *Chem. Eng. Sci.*, **20**, 931, (1965).
18 G. V. Vinogradov, and A. Ya. Malkin, **Rheology of polymers**, *MIR*, Moscow, 1980.
19 Ya.I. Frenkel, **Kinetic theory of liquids**, *Dover Publications*, New York, 1955.
20 V.P. Budtov, and V.V. Konsetov, **Heat and mass transfer in polymerization processes**, *Khimiya*, Leningrad, 1983.
21 D. W. Van Krevelen, **Properties of polymers: correlations with chemical structure**, *Elsevier Publishing Co.*, Amsterdam, 1972.
22 R. S. Marvin, and J. E. McKinney in **Physical Acoustics: Principles and Methods, vol.II**, p.B, W. P. Mason, Ed., *Academic Press*, New York, 1965, pp. 193-265.
23 B. Froelichb, C. Noelb, and L. Monnerie, *Polymer*, **20**, 529 (1979).
24 D. Pugh, and D.A. Jones, *Polymer*, **19**, 1008 (1978).

25 S.P. Levitsky, and Z.P. Shulman, **Dynamics and heat and mass transfer of bubbles in polymeric liquids**, *Nauka i Tekhnika*, Minsk, 1990.
26 W.J. Yang, and H.C. Yeh, *Phys. Fluids*., **8**, 758 (1965).
27 H.S. Fogler, and J.D. Goddard, *Phys. Fluids*., **13**, 1135 (1970).
28 J.R. Street, A.L. Fricke, and L.P. Reiss, *Ind. Eng. Chem. Fundam*., **10**, 54 (1971).
29 S.P. Levitsky, and A.T. Listrov, *J. Appl. Mech. Techn. Phys*., **15**, 111 (1974).
30 G. Pearson, and S. Middleman, *AIChE J.*, **23**, 714 (1977).
31 S.P. Levitsky, *J. Appl. Mech. Techn. Phys*., **20**, 74 (1979).
32 G. Ryskin, *J. Fluid Mech*., **218**, 239 (1990).
33 R.C. Reid, J.M.Prausnitz, and T.K. Sherwood, **The properties of gases and liquids**, *McGraw-Hill*, New York, 1977.
34 R.I. Nigmatulin, and N.S. Khabeev, *Fluid Dynamics*, **9**, 759 (1974).
35 S.P. Levitsky, and Z.P. Shulman, **Bubbles in polymeric liquids**, *Technomic Publish. Co*., Lancaster, 1995.
36 R.Y. Ting, and A.T. Ellis, *Phys. Fluids*, **17**, 1461 (1974).
37 G.L. Chahine, and D.H. Fruman, *Phys. Fluids*, **22**, 1406 (1979).
38 A. Shima, Y. Tomito, and T. Ohno, *Phys. Fluids*, **27**, 539 (1984).
39 W.D. McComb, and S. Ayyash, *J. Phys. D: Appl. Phys*., **13**, 773 (1980).
40 S.L. Peshkovsky, M.L. Fridman, V.I. Brizitsky et al., *Doklady Akad. Nauk SSSR*, **258**, 706 (1981).
41 R.T. Knapp, J.W. Daily, and F.G. Hammit, **Cavitation**, *McGraw-Hill*, New York, 1970.
42 P.R. Williams, P.M. Williams, and S.W. Brown, *J. Non-Newtonian Fluid Mech*., **76**, 307 (1998).
43 J.W. Hoyt, Trans. *ASME. J. Fluids Eng*., **98**, 106 (1976).
44 R.Y. Ting, A*IChE J.*, **20**, 827 (1974).
45 R.Y. Ting, *Phys. Fluids*, **21**, 898 (1978).
46 L.E. Scriven, *Chem. Eng. Sci.*, **10**, 1 (1959).
47 P.J. Bruijn, *Physica*, **26**, 326 (1960).
48 R.A. Shock, in **Multiphase science and technology**, *Hemisphere Publishing Corporation*, New York, 1981, pp. 281-386.
49 J.R. Thome, and R. A. W. Shock, *Adv. Heat Transfer*, **16**, 60 (1984).
50 S.G. Kandlikar, Trans. *ASME., J. of Heat Transfer*, **120**, 380 (1998).
51 J. Crank, **The mathematics of diffusion**, *Clarendon Press*, Oxford, 1975.
52 Z.P. Shulman, and S.P. Levitsky, *Int. J. Heat Mass Transfer*, **39**, 631 (1996).
53 L.W. Florshuets, and A. R. Khan, Heat Transfer-70, v.6, p. B7, 31970, Paris, 1970, pp.1-11.
54 R.I. Nigmatulin, **Dynamics of multiphase flow**, *Hemisphere Publishing Corporation*, New York, 1990.
55 J.L. Duda, J.S. Vrentas, S.T. Ju, and H.T. Liu, *AIChE J.*, **28**, 279 (1982).
56 P. Kotchaphakdee, and M.C. Williams, *Int. J. Heat Mass Transfer,* **13**, 835 (1970).
57 H.J. Gannett, and M.C. Williams, *Int. J. Heat Mass Transfer*, **14**, 1001 (1971).
58 H. Wei, and J.R. Maa, *Int. J. Heat Mass Transfer*, **25**, 431 (1982).
59 A.T. Papaioannou, and N.G. Koumoutsos, 7th Int. Heat Transfer Conf. Proc., 1982, Munchen, 1982, v.4, pp. 67-72.
60 B.P. Avksent'yuk, and Z.S. Mesarkishvili, Boiling of aqueous PEO solutions at reduced pressures under the conditions of natural convection, Institute of Thermophysics, RAS, Novosibirsk, 1983, preprint No. 108.
61 D.D. Paul, and S.I. Abdel-Khalik, *J. Rheol.*, **27**, 59 (1983).
62 **Heat exchanger design handbook**, v.1, contributors D.B. Spalding and J. Taborek, *Hemisphere Publishing Corporation*, New York, 1987.
63 R.Y.Z. Hu, A.T.A. Wang, and J.P. Hartnett, *Exp. Therm. Fluid Sci.*, **4**, 723 (1991).
64 Yan Yu Min, *Int. Commun. Heat and Mass Transfer*, **17**, 711 (1990).
65 Z.P. Shulman, B.M. Khusid, and S.P. Levitsky, *Heat Transfer Research*, **25**, 872 (1996).
66 S.P. Levitsky, B.M. Khusid and Z.P. Shulman, *Int. J. Heat Mass Transfer*, **39**, 639 (1996).
67 M.G. Cooper, and A.J.P. Lloyd, *Int. J. Heat & Mass Transfer*, **12**, 895 (1969).
68 Z.P. Shulman, and S.P. Levitsky, *Int. J. Heat & Mass Transfer*, **35**, 1077 (1992).
69 S.P. Levitsky, and Z.P. Shulman, *Soviet Phys. Acoust.*, **31**, 208 (1985).
70 N.R. Suttie, *Heat Treat. Metals*, **6**, 19 (1979).
71 K.Y. Mason, and T. Griffin, *Heat Treat. Metals*, **9**, 77 (1982).
72 F. Moreaux, and G. Beck, *Heat Transfer*, **4**, 2067 (1986).
73 F. Morou, and P. Arshambol, *Prom. Teplotekhn.*, **11**, 48 (1989).
74 G.B.Okonishnikov, N.V. Novikov, P.A. Pavlov, and S.L. Tsukrov, Heat and Mass Transfer - 92, v.6, Heat and Mass Transfer Institute, Minsk, 1992, pp. 3-6.
75 S.P. Levitsky, and Z.P.Shulman, *Thermophys. of High Temperatures*, **33**, 616 (1995).

7.3 DRYING OF COATED FILM

Seung Su Kim
SKC Co., Ltd., Chon-an City, Korea
Jae Chun Hyun
Department of Chemical Engineering, Korea University, Seoul, Korea

7.3.1 INTRODUCTION

Thin film coating and drying technology are the key technologies for manufacturing diverse kinds of functional films, such as photographic films, adhesives, image media, magnetic media and recently lithium battery coating. Coating applied to a substrate as a liquid need some degree of solidification in order to be final products. The degree of solidification can be low in the case of pressure-sensitive adhesives (PSA) and it ranges to high in the case of dense metal-oxides.[48] The final structure and properties of coating are greatly influenced by the drying conditions.[21] Poorly chosen operating conditions of drying cause unwanted internal gradients,[6,7] phase separations,[29,35,36] colloidal transformations that lead to the wrong microstructure,[43,51,56] inappropriate non-uniformities, and stress-related defects.[12-15,21,22]

Here we address a subject of solvent removal, or drying, which is a part of solidification processes.

Typically a formulation of coating solution is consisted of pigments, binders (polymer resins) and solvents. The solvents are used to solubilize the coating formulation and to give the coating solution(or dispersion) the rheology necessary for the application. The coating solution is deposited onto a substrate or web at the coating station and is dried by passing through a series of separate ovens (zones). A substrate can be an impermeable material such as plastic film and permeable in the case of paper coating. The dryer is consisted of ovens

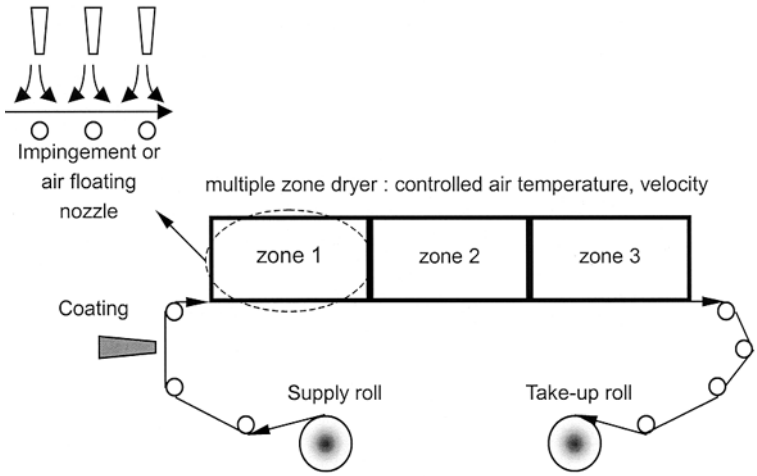

Figure 7.3.1. An example of industrial coating and drying apparatus. A coated liquid is deposited onto a substrate which is unwound from a supply roll at the coating station and passes through the three separate ovens(dryer) where the temperature and velocity of air is controlled independently. Finally dried coated substrate is taken up by a take-up roll.

(zones) in which the temperature and velocity of air are controlled independently. The air impinges the coated and back side surface of the substrate through the nozzles and sweeps away the solvent vapor from the coated surface. In a case of single sided impingement dryer, the air impinges only on the coated surface. The coated film must be dry before the rewind station. The residence time of coated substrate in the dryer is as short as several seconds in a case of high speed magnetic coating processes and it ranges to as long as several minutes in a case of lithium battery coating processes.[28] Finally the dried coated substrate is taken up by a take-up roll (Figure 7.3.1).

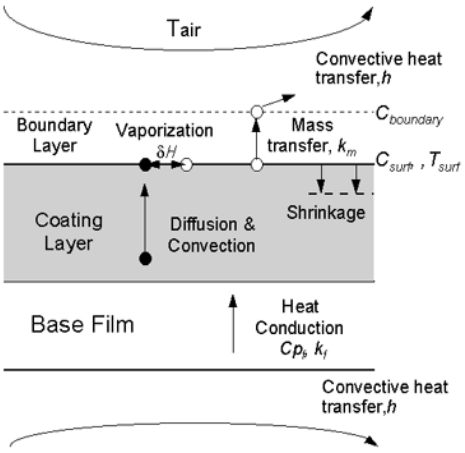

Figure 7.3.2. Elemental process of drying and typical parameters of drying. [After references 28,30].

The elemental process of drying is depicted in the Figure 7.3.2. Solvent is evaporated from the exposed surface of a liquid coating into the adjacent air. Diffusion of evaporating solvent into stagnant air is a comparatively slow process. Commonly the rate of diffusion of solvent vapor is greatly enhanced by the forced convective sweeping of the exposed surface. The rate of solvent evaporation per unit area is a product of the two factors : 1) the difference in partial pressure of the solvent at the surface of coating and in the bulk of nearby gas and 2) the mass transfer coefficient, which represents the combined action of convection and diffusion.[16]

The energy, which is needed to supply the latent heat of solvent evaporation, is delivered mainly by blowing hot air onto the coating surface. This convective heat transfer not only can deliver the needed energy to the coating, but also can enhance the transport of solvent vapor away from the surface of the coating. Commonly the conductive and radiative heating are accompanied with convective heating if they are necessary.

As long as the temperature and the concentration of solvent at the exposed surface of coating is constant, so does the evaporation rate of solvent. This is true during the initial stages of drying when the exposed surface of coating is fully wetted with the solvent. This period is commonly called as constant drying rate period (CDRP).[10] In CDRP, all the heat, which is supplied to the coating, is used to supply latent heat of vaporization. Thus the temperature of coating surface is nearly constant. In a case of aqueous coating, the temperature of coating surface is equivalent to the wet bulb temperature of a given air humidity.[9,10] Therefore in CDRP the external mass transfer resistance to drying limits the rate of drying.

As the solvents depart the coating, the rate controlling step for the drying steadily shifts from the external mass transfer to the mass transfer within the coating. The solvents within the coating can move to the exposed surface by diffusion along with diffusion-induced convection[1,8,17] and pressure gradient-driven flow in a porous coating.[43,44] In polymeric solutions, the diffusion coefficient of solvent dramatically drops as solvent concentration falls.[17] Thus the concentration of solvent at the exposed coating surface falls with drying proceeded, and so does the vapor pressure of solvent there. Therefore the drying

rate steadily falls. This period is called as falling drying rate period (FDRP). Generally the diffusion coefficient of solvent in a polymeric solutions is a strong function of solvent concentration, temperature and molecular size.[53-55,60] The binary diffusion coefficient can be estimated by the free volume theory of Vrentas and Duda[17] and can be measured by the NMR. However, there are many difficulties to measure or estimate the ternary diffusion coefficient.

The evaporated solvents are swept away by the hot air and are exhausted to the outside of the dryer. The vapor concentration of solvent of a zone (oven) must be lower than the lower explosive level (LEL) of solvents to meet the safety. Thus enough fresh air should be supplied to each zone to meet this LEL safety.[10,28] However, too much supply of fresh air brings about too much energy consumption to heat the fresh air, and it also increases the VOC containing waste gas which should be treated by VOC emission control unit. The LEL of a zone can be controlled within appropriate LEL ranges by measuring and predicting of drying rate.[28]

We are going to deal with some important features of drying a liquid coated film in the subsequent sections.

First, we will introduce theory for the drying and method of modeling of the drying process. A drying process of liquid coated film can be simulated by setting up heat and mass transfer equations[8,9,40,59] and vapor liquid equilibrium equations[19,39] with appropriate heat and mass transfer coefficient.[37,45]

Secondly, we will try to give examples of drying rate measurements in laboratory experiments and in a pilot or production scale dryer. Traditionally, the rate of drying was obtained by measuring weight loss using a balance under the controlled experimental conditions of air velocity and temperature.[5,40,51] However, it is difficult to obtain such data in the high airflow rate experiments, for the balance is disturbed by the high airflow motion. Therefore the alternative way of measuring was proposed in which hydrocarbon analyzers[57] or FT-IR[47,50] was used instead of balance. Moreover, the weight changes of each solvent in a multi-solvent coating system could be found by applying rapid scanning FT-IR method.[50]

However, rare data has been given about measuring the actual drying rate and solvent concentration profile along the dryer while operating.[28] The drying rate of coated film in an industrial dryer is measured by analyzing dryer exit gas, and we will illustrate how the solvent concentration profiles of coating at the exit of each zone are estimated from the experimentally measured drying rate data.[28]

In third, we will try to illustrate the dependence of dried coating structure on the drying path by means of the basic phenomena, phase equilibrium.[29,35,38,41,42,56,58] We will also briefly introduce the mechanisms behind the formation of microstructure of various kind of functional films.[44,51]

Finally, we will categorize the drying related defects according to the origin of defects, and we will show some examples of defects and the cause and curing of them.[8,15,21,25]

7.3.2 THEORY FOR THE DRYING

7.3.2.1 Simultaneous heat and mass transfer

Because evaporation is an endothermic process, heat must be delivered to the system, either through convection, conduction, radiation, or a combination of these methods. The solvents are evaporated from the coating surface and at the same time the latent heat of solvent cool

down the coating surface. Thus the heat and mass are transferred simultaneously through the surface of coating.

Assuming that the heat is supplied only by convection of hot air and the substrate is impermeable. Further if we neglect the internal resistance of solvent transport to the coating surface, the heat and mass balance consist a lumped parameter system.

A schematic diagram of the modeled system is shown in Figure 7.3.3. The corresponding mass and heat balance of the systems are as follows[28]

$$R_{mass,i} = \rho_i b_C \frac{dz_i}{dt} = k_m \left(C_i^{sat} - C_i^{\infty} \right) \qquad [7.3.1]$$

$$\left(\rho_f b_f C_{Pf} + \sum_{i=1}^{k} \rho_i z_i b_C C_{Pi} \right) \frac{dT}{dt} = h\left(T - T^{\infty} \right) - \sum_{i=1}^{k} R_{mass,i} \left(-\delta H_{evap} \right)_i \qquad [7.3.2]$$

where:

$R_{mass,i}$	evaporation rate of component i
z_i	volume fraction of component i
ρ_i	density of pure component i
b	thickness
C_i^{sat}	saturated solvent concentration of component i
C_i^{∞}	solvent concentration of component i in the bulk air
k_m	mass transfer coefficient
h	heat transfer coefficient
T	temperature of coated film
T^{∞}	temperature of drying air
δH	latent heat of solvent
C_p	heat capacity

Subscript f and C mean the substrate and coating layer respectively. Equation 7.3.1 and 7.3.2 apply to the each component of coating.

7.3.2.2 Liquid-vapor equilibrium

The equilibrium saturated solvent concentration is related to the concentration of solvent at the coating surface by thermodynamic equilibrium relations, such as Henry's law, Raoult's law and the Flory-Huggins equation.[8] The Raoult's law is

$$C_i^{sat} = \gamma_i z_i \frac{P_i^{sat}}{RT} \qquad [7.3.3]$$

where:

γ_i	activity coefficient of component i
P_i^{sat}	saturated vapor pressure of component i
R	gas constant

The saturated vapor pressure is calculated from the Antoine equation at the specific temperature.

$$\log_{10} P^{sat} = A - \frac{B}{T + C} \qquad [7.3.4]$$

The Antoine equation coefficients A, B, C for various organic solvents can be found elsewhere.[19] The UNIFAC group contribution method was used to calculate the activity coefficient of each solvent.[49]

7.3.2.3 Heat and mass transfer coefficient

The rate of heat transfer to the coating depends on the two factors as shown in Equation 7.3.2: the difference between the temperature of coating and ambient air (the driving force) and the geometry where the heat transfer occurs (heat transfer coefficient). The heat transfer coefficient is a function of the nozzle geometry and blowing air properties. Many variables affect the heat transfer coefficient of nozzles, such as nozzle geometry and size, nozzle to coating surface distance, nozzle to nozzle spacing, velocity of air at the nozzle exit and air motion above the coating surface.[37,45]

Therefore the average heat transfer coefficient of a zone can be expressed as follows,

$$\bar{h} = f(\textit{Geometry of nozzle}, \textit{Properties of air}) \times f(w) \qquad [7.3.5]$$

where:

$\bar{h}$	average heat transfer coefficient of a zone
w	velocity of air at the nozzle exit.

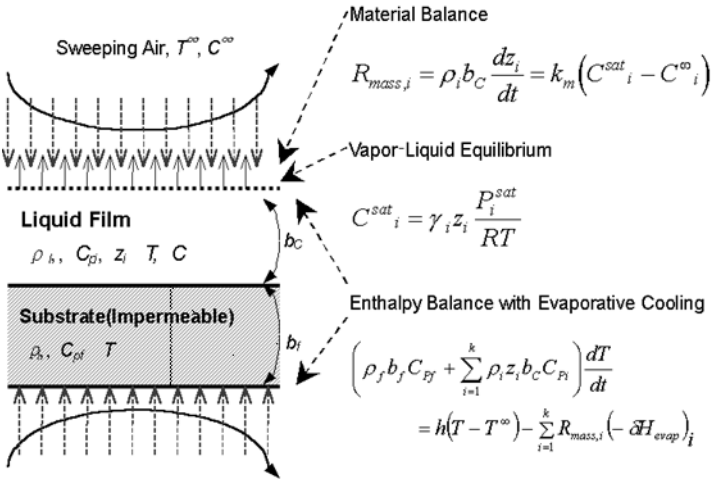

Figure 7.3.3. Schematic diagram of modeled drying of coated film. [After reference 28].

The accuracy of drying rate calculation greatly depends on the proper estimation of the heat and mass transfer coefficient of nozzles. Many researches have been done to find out the heat transfer coefficient of nozzles, among them the Martin's correlation is the notable one which correlates the geometry of impinging jet nozzle and air velocity to the heat and mass transfer coefficients.[37] For a multiple slot jet nozzles, which is depicted in Figure 7.3.4, Martin suggested following empirical correlation,

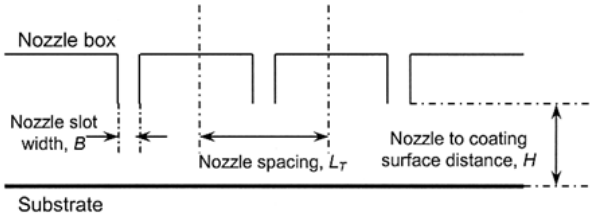

Figure 7.3.4. Geometry of slot nozzles for the Martin's correlation [After reference 37].

$$\frac{\bar{N}u}{Pr^{0.42}} = \frac{2}{6} f_O^{3/4} \left(\frac{4Re}{\frac{f}{f_O} + \frac{f_O}{f}} \right)^{2/3} \qquad [7.3.6]$$

where:

$\bar{N}u$	average Nusselt number over a zone ($2\bar{h}B/\kappa_a$)
Re	Reynolds number ($2wB/\nu_a$)
Pr	Prandtl number of air (ν_a/α_a)
f	Fraction open area (B/L_T)
f_O	$[60 + 4(H/2B - 2)^2]^{-1/2}$
B	Nozzle slot width (Figure 7.3.4)
L_T	Nozzle spacing (Figure 7.3.4)
H	Nozzle to coating surface distance (Figure 7.3.4)

Range of applicability is

$1{,}500 \le Re \le 40{,}000$

$0.008 \le f \le 2.5 f_O$

$2 \le H/B \le 80$

The heat transfer coefficient of the arrays of round jet nozzles and the other shapes of nozzles can be found elsewhere.[37,45] In general the heat transfer coefficient can be written in the following form[9,10]

$$\bar{h} = Kw^n \qquad [7.3.7]$$

where:

K	a constant that depends on the physical properties of the air and geometric properties of the dryer
n	0.6 ~ 0.8 (depending on the nozzle geometry)

One can easily calculate the actual heat transfer coefficient of a zone by running a heavy gauge web through a dryer and measuring temperature rising of web using non-contacting infrared thermometer in the early part of the dryer where the web is heating up.[10] The procedures of measuring and accompanied calculation are illustrated in Table 7.3.1.

The mass transfer coefficient is related to the heat transfer coefficient through the Chilton-Colburn analogy.[16] Thus,

$$\frac{\bar{S}h}{\bar{N}u} = \left(\frac{Sc}{Pr} \right)^{0.42} = (Le)^{0.42} \quad or \quad \bar{k}_m = \frac{\bar{h}}{k_a} Le^{0.42} \qquad [7.3.8]$$

where:

$\overline{Sh}$	average Sherwood number of a dryer zone
$\overline{Nu}$	average Nusselt number of a dryer zone
Sc	Schmidt number of air
Pr	Prandtl number of air
Le	Lewis number of air
$\overline{k}_m$	average mass transfer coefficient of a dryer zone
k_a	heat conductivity of air

Table 7.3.1. Procedure for calculating h in dryer. [Adapted, by permission, from Cohen, E. D. and E. B. Gutoff, Modern Coating and Drying Technology, VCH Publishers, Inc., New York, 1992]

1	Set dryer air conditions and measure air inlet temperature
2	Run heavy gauge polyester web through dryer
3	Install two infrared thermometers relatively close together at initial part of drying zone
4	Run web at varying line speeds and measure temperature rise in web

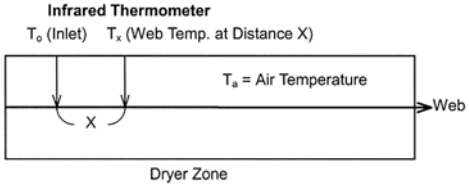

$$\frac{T_a - T_x}{T_a - T_o} = \exp\left(-\frac{200hx}{\rho C_p t U}\right)$$

where:

C_p	heat capacity,
h	heat transfer coefficient
t	thickness of web
T_a	temperature of hot air
T_o	initial temperature of web
T_x	temperature of web at distance x
U	line speed,
x	distance between infrared thermometers
ρ	density of web

The typical value of heat transfer coefficient of modern industrial dryer ranges from 50 to 150 J/m^{2}sec^{o}C. Figure 7.3.5 shows the calculated heat transfer coefficient of an impingement dryer with varying nozzle exit velocity of air and fraction open area (nozzle spacing), calculation was done according to the Martin's correlation.

7.3.2.4 Prediction of drying rate of coating

The drying rate of coating and the subsequent residual solvent amount along with dryer length can be found by applying above equations. In magnetic media manufacturing pro-

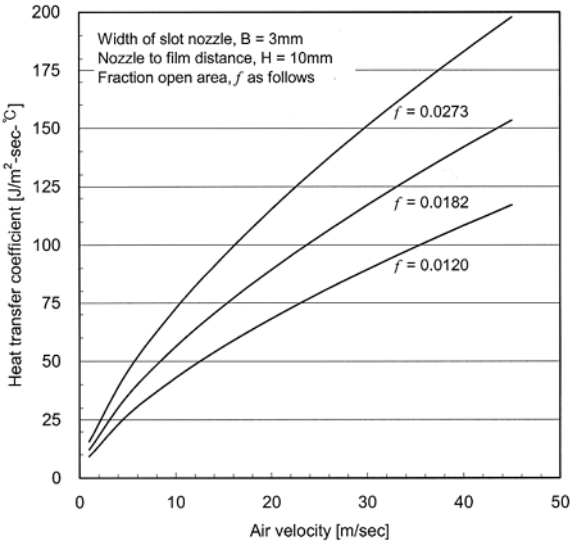

Figure 7.3.5. Calculated heat transfer coefficient of industrial dryer with varying air velocity.

cess, magnetic particulate dispersed solution is coated on the PET (polyethlylene terephthalate) film. The wet coating thickness is about 5 to 6 μm and the thickness of substrate is 14 to 15 μm. The line speed is normally 400 m/min to 1000 m/min. Usually several kinds of solvents are used for the coating solution, here we used three kinds of solvents - toluene, methyl ethyl ketone (MEK) and cyclohexanone (CYC). Equations 7.3.1 and 7.3.3 are applied to each solvent component. The temperatures of dryer zones were 50 to 130°C, and the air velocities at the nozzle exit were 10 to 20 m/sec. The average heat transfer coefficient of a zone could be found by applying Martin's correlation for the slot nozzles, however in this case we had the empirical coefficient for the Equation 7.3.7 which was supplied by the dryer nozzle manufacturer. And we obtained average heat transfer coefficients which were ranging from 80 to 140 J/m^{2}s°C according to the air velocities of the zones.

The coupled and non-linear set of equations is solved by standard numerical method (such as Runge-Kutta-Gill method). The temperature and concentration of coating at time 0 was given as the initial concentration of coating. The concentration of coating at the next time step was calculated by solving Equation 7.3.1 with assuming that there was no significant temperature change of coating. This is a plausible assumption if the time step is small enough. Then the result of concentration of coating was substituted to the Equation 7.3.2 and the temperature of coating at that time step was calculated.

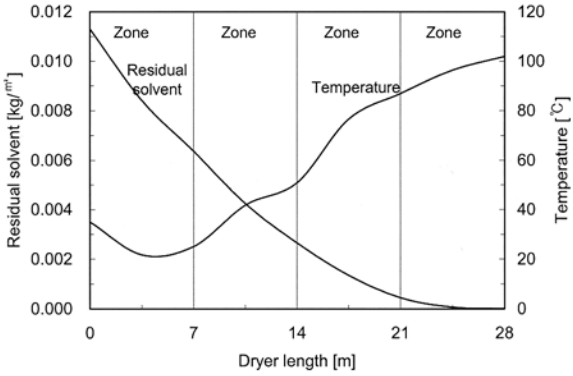

Figure 7.3.6. Predicted residual solvent and temperature profile along with the dryer length.

The calculated concentration and temperature profile of coating are given as in the Figure 7.3.6. The concentration of solvent gradually decreases along with the dryer length. The slope of solvent concentration profile at zone 1 was nearly constant, but the slop was changed within the zone 1 though there were no changes in the drying conditions. It was due to the fact that the less volatile solvent (cyclohexanone)

began to evaporate only after significant amount of more volatile solvents (MEK, toluene) were evaporated in the first part of zone 1. Therefore the slope was changed in zone 1. The temperature profile shows the effect of evaporative cooling in the first part of dryer. The temperature of coating at zone 1 was lower than that of coating at the entrance of dryer, but after significant amount of solvent was evaporated, the temperature of coating began to rise and eventually it approached to the temperature of zone. The temperature and concentration profile successfully explain the drying regimes - constant drying rate period (CDRP) and falling drying rate period (FDRP).

7.3.2.5 Drying regimes: constant drying rate period (CDRP) and falling drying rate period (FDRP)

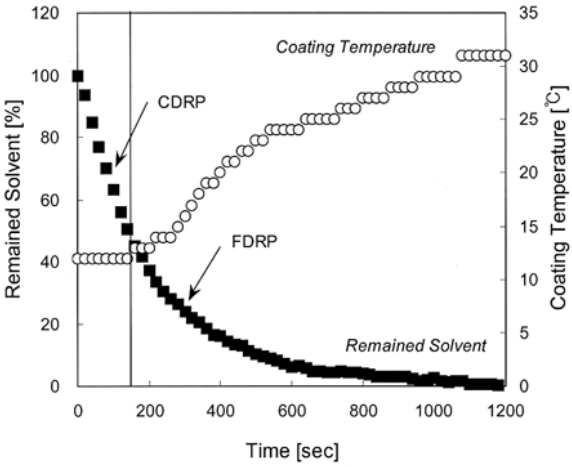

Figure 7.3.7. Characteristic drying curve of polymeric solution (methanol - ethyl acetate - acrylic resin solution).

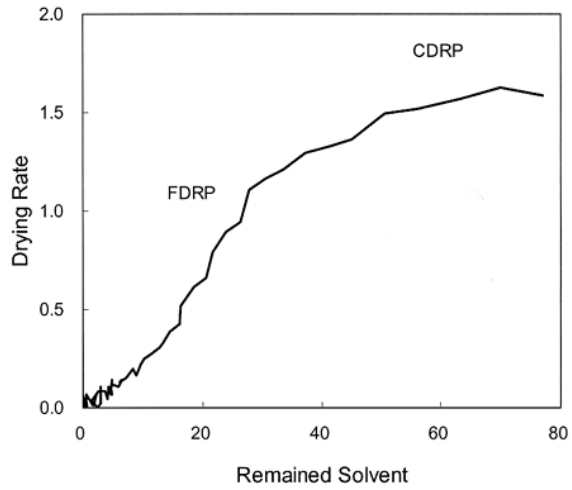

Figure 7.3.8. Typical drying rate curve (methanol - ethyl acetate - acrylic resin solution).

As we mentioned earlier in this chapter, the drying process can be divided into two or four distinct and easily identifiable processing regions: pre-dryer, constant drying rate period (CDRP), falling drying rate period (FDRP) and equilibration, or simply CDRP and FDRP.[10] The pre-dryer and equilibrium regions denote the part of dryer which is located between the coating station and the dryer, and between the dryer exit and the take up roll, respectively.

In the early stages of drying of polymeric solution coating, the surface of coating is fully wetted with solvent, thus the evaporation of solvent takes place as if there were no polymer or solute in it, as in the case of evaporation of pure solvent. The only factor that affects the drying rate of coating is the external mass transfer resistance such as the diffusion process of solvent vapor into the bulk air. The drying rate increases proportional to the temperature and velocity of blowing air. All the heat input is used to supply the latent heat of evaporation, therefore with constant heat input the temperature of coating remains constant as shown in Figure 7.3.7. Figures 7.3.7 and 7.3.8 represent typical drying curve of polymeric

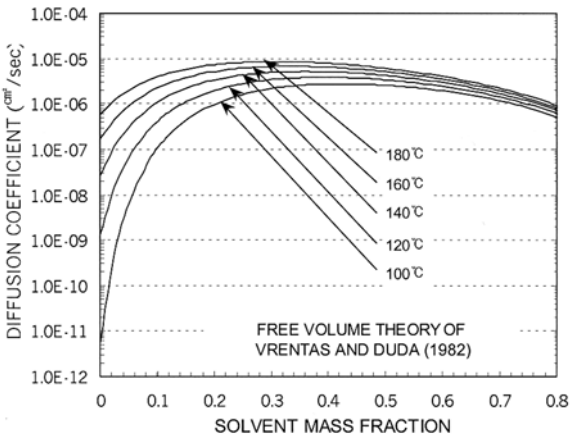

Figure 7.3.9. Concentration and temperature dependence of the binary diffusion coefficient of a polystyrene-toluene solution according to the free volume theory of Vrentas and Duda. [After References 17].

coating solution. In CDRP, as shown in the figures the slope of solvent content loss with time (drying rate) and the coating temperature are nearly constant. These drying rate curves were obtained by measuring weight changes of coating in an oven with blowing hot air above the coating samples - see Section 7.3.3.1.

However, as the solvent content decreases the drying rate of coating also decreases gradually as shown in Figure 7.3.8. In this falling rate regime, mass transfer within the coating becomes the limiting factor, and with constant heat input the temperature of coating rises and drying rate decreases. The solvent is transported to the exposed coating surface by diffusion and convection, where the solvent evaporates to the bulk air in a polymeric coating system. In most drying processes of thin film coatings the convection of solvent within the coating is negligible, thus the diffusion of solvent is the only method for solvent to reach the coating surface. The diffusivity of solvent in a polymeric solution falls dramatically when the solvent content is low as shown in Figure 7.3.9. Therefore the diffusion process of solvent within the coating controls the rate of drying in FDRP.

To understand and improve the drying process during the FDRP, it is important to estimate diffusion coefficient of solvent within the coating. Vrentas and Duda predicted the binary diffusion coefficient by using free volume theory.[17] Figure 7.3.9 shows the binary diffusion coefficient of toluene in the polystyrene-toluene solution that was found by applying free volume theory. The diffusion coefficient falls by a number of magnitudes in the low solvent concentration range, and it increases with increasing temperature. By the way the concentration dependency of diffusion coefficient at the low solvent concentration range declines at a high temperature. For example, at the temperature of 100°C the diffusion coefficient of toluene falls 5 orders of magnitude (about 10^{-5}) from its highest value, but at the temperature of 180°C it falls only one order of magnitude. This shows us that it is highly required to eliminate residual solvent of coating at the low solvent concentration range the temperature of oven should be high enough. Therefore the temperatures of final zones keep high enough to achieve complete dryness in a multiple zone dryer. Normally the temperature of oven is restricted by the onset of deformation of substrate such as wrinkles and it is also restricted by the properties of coated material, such as melting point of binders.

The parameters for the free volume theory of binary solution systems can be found in the literatures,[17,53-55,60] and they have been effectively used in modeling drying process.[1,2,6-8] But there are many difficulties in estimating diffusion coefficient for the ternary systems. Until now, almost all the empirical and theoretical correlations are restricted to the binary solution systems.

7.3.3 MEASUREMENT OF THE DRYING RATE OF COATED FILM

The drying rate of coating is easily measured by simple experimental equipment. In a controlled air condition, the weight loss of coating due to the solvent evaporation is measured by electrical balance and filed at the PC. The weight loss with time is converted to drying rate of coating per unit area. The commercialized experiment equipment is commonly used to obtain the drying rate, such as thermo-gravimetric analyzer (TGA). Nowadays commercial TGA equipped with FT-IR or gas chromatography is available and readily used to obtain not only the overall drying rates of coatings but also the relative drying rate of each solvent in a multi-solvent system. However it is difficult to obtain such data at a high air velocity, because the air stream disturbs the balance and cause to oscillate the balance reading. Practically the available air velocity of this kind would be 1 m/sec or lower.

Fourier-Transform-Infrared (FT-IR) spectrometer is used to obtain the drying rate at a higher air velocities.[47,50] FT-IR is commonly used for the analysis of organic materials. Recently, FT-IR is applied to measure the drying rate of coating. This specially designed FT-IR with coating apparatus and air blowing system made it possible to measure solvent content without disturbances of airflow, and moreover it enabled us to find the content of each solvent with drying proceeded.[47,50] This can be used to study selective evaporation of solvent and phase separation phenomena in a multi-solvent system.[50]

The air velocity of industrial dryer is up to 20 m/s or more and the temperature of oven is normally up to 200ºC. A specially designed drying chamber was suggested to measure solvent concentration in these drying conditions.[52,57] The chamber is equipped with flame ionization detector (FID) total hydrocarbon analyzer, and the oven exit gas which contains the evaporated solvent flows to the analyzer. The drying rate is calculated by multiplying the solvent concentration with exit gas flow rate. It provides access to a wider range of drying conditions that approximate industrial conditions.

However, it is much more difficult to find out the actual drying rate of coating in an industrial dryer. In a continuous industrial dryer it is impossible to measure the drying rate by any of the above methods, because the coated substrate is running through the dryer at the speed of several hundreds meter per minute. To measure the drying rate of coating in such a condition, the dryer exit gas of each zone is analyzed by gas chromatography. Then the drying rate of each zone is calculated by multiplying solvent concentration with exit gas flow rate. From the drying rate of each zone, the evaporated amount of solvent is calculated. Thus the solvent concentration of coating is found at the point of each zone end.[28,30]

7.3.3.1 Thermogravimetric analysis

The drying rate of a coating could be easily found by measuring coating weight loss during drying in a laboratory. The set-up of experimental equipment is relatively easy, and the commercial equipment can be readily available such as thermogravimetric analyzer (TGA).[5,53] As drying proceeded, the weight of coating decreases due to the solvent evaporation. The amount of solvent loss with time is monitored by the balance. The schematic representation of the equipment is shown in Figure 7.3.10. The sample, such as coated films or a tray that contains the coating liquid, is mounted on the balance to be monitored. The temperature of coating is measured by non-contact infrared thermometer. A thin wire type thermocouple can be used to measure the temperature, and the thermocouple is attached to the coating or sample tray. The air is made up by conventional blower and is heated up to a certain temperature by electrical heater. The air is supplied to the coating surface through

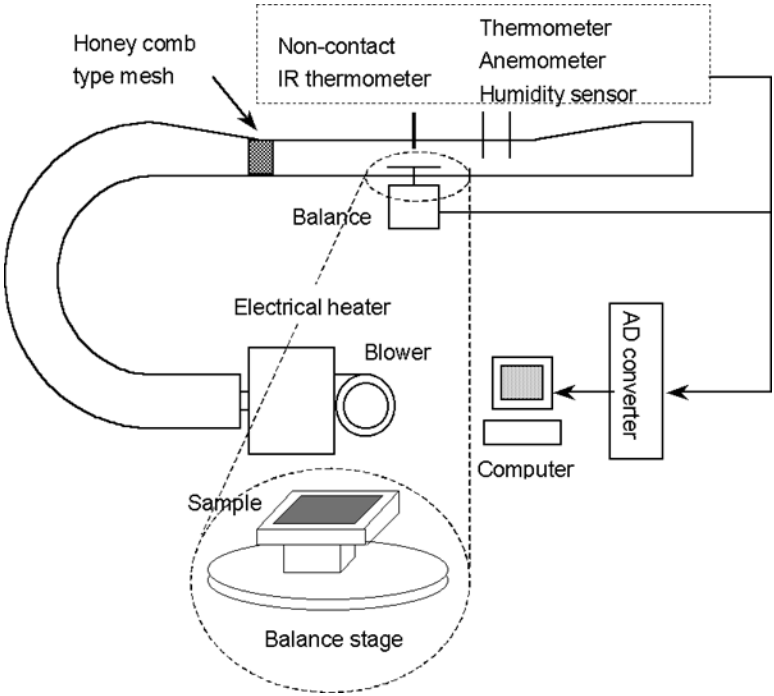

Figure 7.3.10. Schematic diagram of drying experiment apparatus.

ducts. To make the laminar airflow over the balance, the length of ducts and sizes are determined. The experiment is usually conducted in a low air velocity so as the air not to disturb the balance. Honeycomb style mesh is often helpful to filter the air and make the airflow a laminar one. It enabled us to do the drying experiment at a higher velocity of air. The air velocity can be as high as 1 ~ 2m/sec.

Actually the air velocity of industrial dryer is much higher than the experimental conditions and the directions of flow are normally perpendicular to the coating surface, not parallel with coating surface. Thus we can hardly expect to conduct a quantitative simulation from this experiment, but we can find the characteristic drying curve and mechanisms of drying of the given materials.

The drying rate of coating is the weight of solvent loss per time divided by the area of evaporation.

$$R_{mass} = -\frac{dW}{Adt} \approx -\frac{W_{t+\Delta t} - W_t}{A\Delta t} \qquad [7.3.9]$$

where:

R_{mass}	evaporation rate
W	weight of sample at a specific time
t	time
Δt	time interval between measurements
A	evaporation area

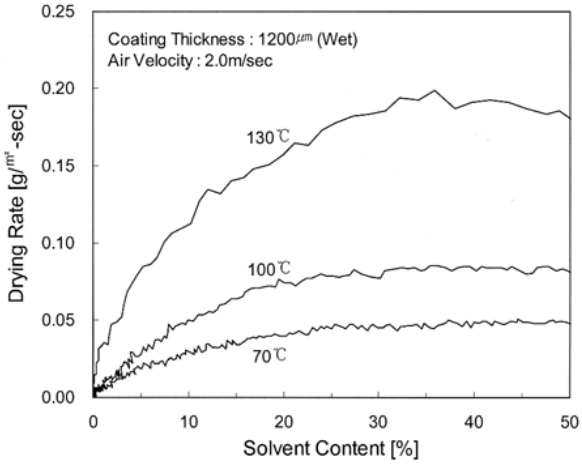

Figure 7.3.11. Drying rate curve of low volatile solution: N-methylpyrrolidone (NMP) - $LiCoO_2$ - PVDF solution.

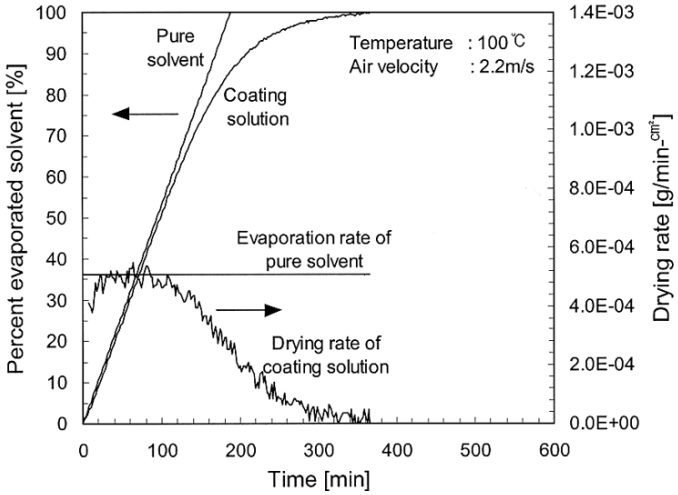

Figure 7.3.12. Comparison of drying rate between coating solution and pure solvent : N-methylpyrrolidone (NMP) - $LiCoO_2$ - PVDF solution and pure NMP.

The example of measurement is shown in Figure 7.3.7. The remained solvent means the percent of remained solvent to the total solvent load, and the drying rate of coating is readily calculated using Equation 7.3.9. The drying rate at the specific time equals the slope of the drying curve of Figure 7.3.7, and it is depicted in Figure 7.3.8. The drying rate of coating shows constant and falling rate period with solvent content decreases. The temperature of coating is nearly constant at the beginning of drying where the slope of weight loss remains constant. As shown in Figure 7.3.7, most of the solvent is evaporated during the constant rate period.

Figure 7.3.11 is the drying rate profile according to the solvent content at the various drying temperatures. The coating solution is consisted of $LiCoO_2$ and poly(vinylidene fluoride) (PVDF) solution. Polymer is dissolved in N-methylpyrrolidone (NMP), and this solu-

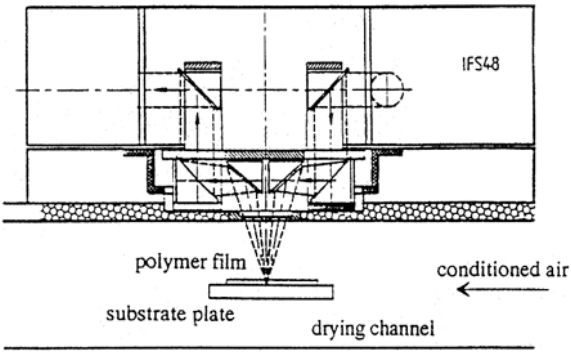

Figure 7.3.13. Schematic diagram of FT-IR spectrometer for the measurement of solvent content. [Adapted, by permission, from Saure, R. and V. Gnielinski, *Drying Technol*., **12**, 1427 (1994)].

tion is originally prepared for the anode cell of the lithium ion battery. The solvent content represents the percent of remained solvent to the weight of non-volatile component, $(W-W_o)/W_o$, where W and W_o represent the wet weight during drying and dry weight, respectively. NMP has very high boiling temperature (about 202°C) and low volatility, thus the drying of coating shows long period of constant rate. Figure 7.3.12 shows the comparison of drying rate between pure solvent and coating solution. The drying rate of coating solution is nearly equal to that of pure solvent during the CDRP. But the drying rate of coating gradually decreases as the solvent concentration falls, while the evaporation rate of pure solvent is constant throughout the evaporation.

7.3.3.2 Rapid scanning FT-IR spectrometer analysis

Recently Fourier-Transform-Infrared (FT-IR) spectrometer is applied to drying studies to obtain the drying rate at a higher air velocities.[47,50] FT-IR is a widely used analytical instru-

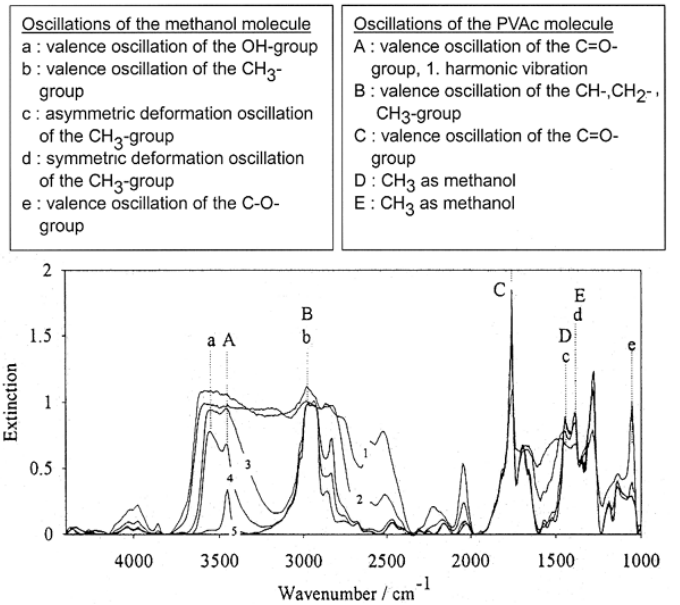

Figure 7.3.14. An example of FT-IR spectra of drying film. The methanol bands disappear slowly while the polymer bands remain constant. The ratio of the band height contains information on concentration. Methanol contents spectrum1 54 g/m^2, spectrum2 19 g/m^2, spectrum3 3.7 g/m^2, spectrum4 1.5 g/m^2, and spectrum5 0 g/m^2, PVAc content 57 g/m^2. [Adapted by permission, from Saure, R. and V. Gnielinski, *Drying Technol*., **12**, 1427 (1994)].

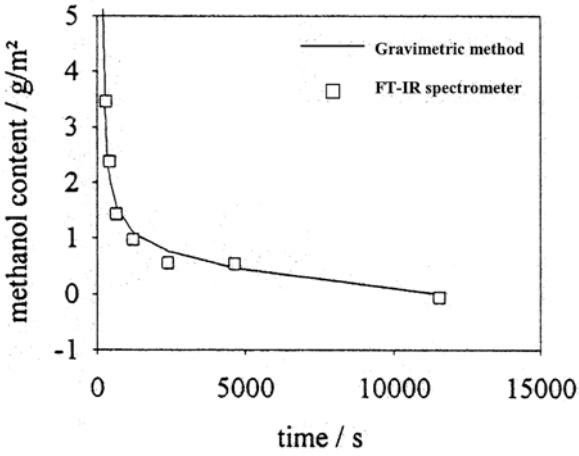

Figure 7.3.15. Comparison between gravimetric and FT-IR data. [Adapted, by permission, from Saure, R. and V. Gnielinski, *Drying Technol.*, **12**, 1427 (1994)].

ment to analyze organic materials. Development of powerful methods for the quantitative analysis made it possible to use the FT-IR technique for the drying studies. Moreover, with the aid of rapid scanning FT-IR the concentration of coating is measured with high resolution and sensitivity. The FT-IR spectrometer was modified for the drying experiment as shown in Figure 7.3.13.[47] A typical spectra of a coated film, which contains methanol and polyvinyl acetate (PVAc), is shown in Figure 7.3.14. The typical absorption bands of PVAc and methanol can be identified from the literature and is shown in the Figure 7.3.14 for a reference.[47] Basically the plot of FT-IR spectra and the ratio of band heights between the solvent and nonvolatile material give the information of concentration. The calculated methanol contents along with methanol bands are also seen in the Figure 7.3.14. The comparison between FT-IR and gravimetric data shows a good agreement as shown in Figure 7.3.15.[47] The calibration method affects the qualitative analysis result, so care should be given in selecting the spectra to evaluate, baseline correction of the spectra and selection of the wavenumber ranges to evaluate.[47]

Besides the usefulness of FT-IR method to measure the solvent content at the high airflow ranges, it gives the concentration of each solvent in a multi-solvent system. Suzuki et al. applied the rapid scanning FT-IR technique to obtain the individual solvent concentration of binary solvent containing coating.[50] The process path and phase diagram can be drawn from the FT-IR data. Figure 7.3.16 shows the phase diagram of MEK-toluene-polyvinylchloride and polyvinylacrylate copolymer (VGAH) system. The initial and final coating composition are given as an initial condition and a measured residual solvent content of a coating respectively. With the aid of FT-IR technique the drying process path between the two points can be found, and it enables us to investigate the phase separation phenomena during drying and the mechanism of structure formation of coating. Figure 7.3.16 shows how the coating of various initial solvent compositions is dried. The drying process path of toluene rich coating, sample 1, go through inside region of spinodal line in the early drying stages, but the drying process path of MEK rich coating do not go through the inside of binodal or spinodal region until the most of the solvent is evaporated. While the appearance of sample 3 and 4 kept clear after dried up, sample 1 whose drying process path was number 1, looked like a frosted glass due to the phase separation.[50]

Though the FT-IR technique is useful to study the various kinds of drying phenomena, the application of FT-IR spectrometer is restricted to a certain solvent system because the bands of spectrometer of each component of a solution must be separated. While the above

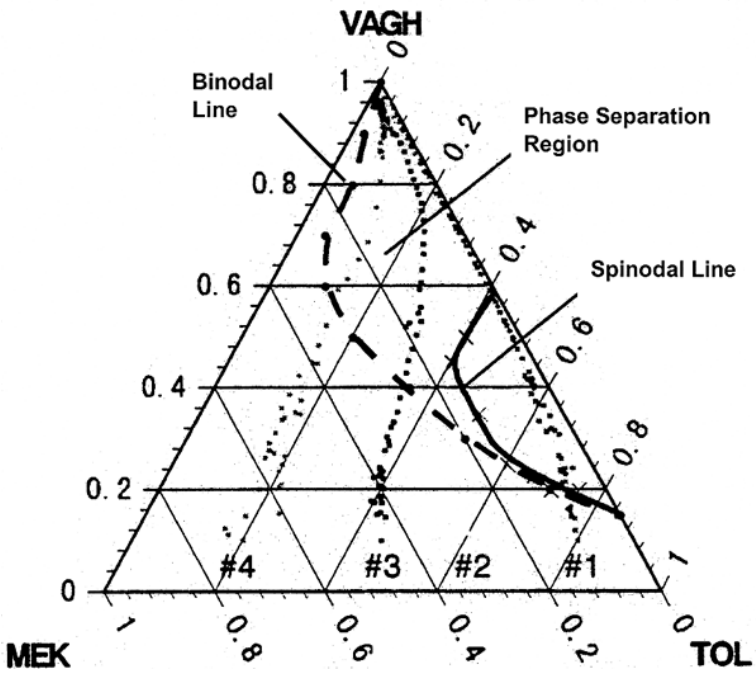

Figure 7.3.16. Phase diagram of MEK-toluene-VAGH system with the different initial solvent compositions. The concentration is measured by rapid scanning FT-IR method. [Adapted, by permission, Suzuki et al., Proceedings of 9th International Coating Science and Technology Symposium, Delaware, USA, May 17 - 20, 1998, pp. 21-24].

example of PVAc-methanol system is suitable for the FT-IR spectroscopy because of their separated bands, it is difficult to extend FT-IR technique to the other solvent systems.

7.3.3.3 High-airflow drying experiment using flame ionization detector (FID) total hydrocarbon analyzer

The gravimetric method is limited to a certain air velocity level due to the oscillation of balance in the high airflow stream. However most of the industrial drying process accomplished by passing the coating under high air velocity jet of hot air. Thus to simulate the industrial drying conditions and according drying phenomena better, high airflow drying experiment setup (HADES) was suggested by Cairncross et al.[52,57]

Low air velocity results in low heat transfer coefficient, the heat transfer coefficient of conventional laboratory drying experiments ranges from 1 to 10 J/m^2s^oC, while that of industrial dryer is ranges about 20 to 200 J/m^2s^oC. The high heat and mass transfer at the evaporation surface may result in 'trapping skinning' because the surface evaporation is too high in compared with the rate of diffusion of solvent within the coating. The heat transfer coefficient of HADES is up to 26.4 J/m^2s^oC which is equivalent with that of usual single-side impingement dryers,[52] and it was reported that the HADES successfully simulates the skinning phenomena with the solution of PMMA-toluene.[52]

HADES measures solvent concentration of exhaust gas from the sample chamber where the solvent is evaporated from the coating. Then the rate of evaporation is equal to the

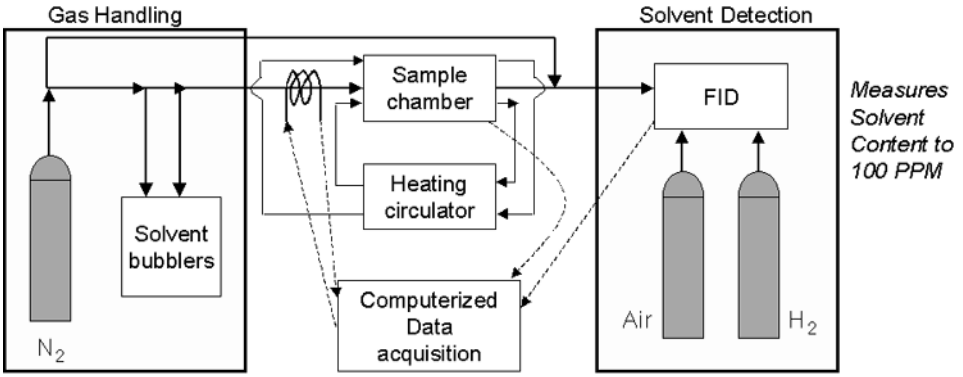

Figure 7.3.17. Schematic of HADES. HADES contains several sections. [Adapted, by permission, Vinjamur and Cairncross, Presented at the AIChE national meeting, Dallas, Texas, November 1, 1999].

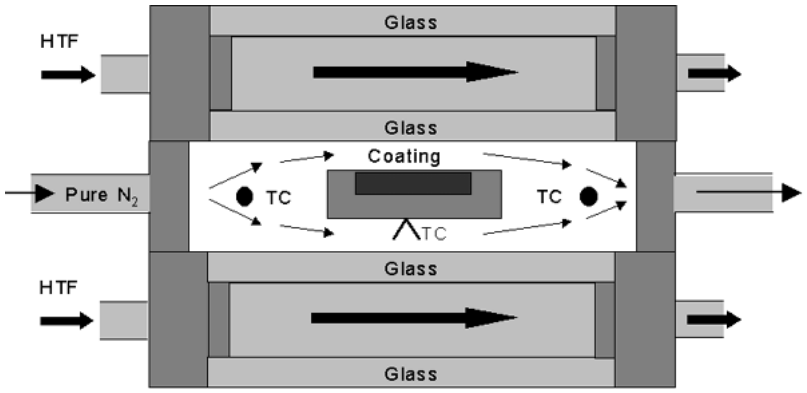

Figure 7.3.18. Schematic of sample chamber of HADES. Dry nitrogen flows in from the port on the left side and the exhaust flows out through the port on the right to a FID. [Adapted, by permission, Winward and Cairncross, 9th International Coating Science and Technology Symposium, Delaware, USA, May 17 - 20, 1998, pp.343 - 346].

solvent vapor concentration times the gas flow rate, and the solvent loss is found by integrating the evaporation rate.

The HADES is consisted of several sections as shown in Figure 7.3.17; gas handling system, a sample chamber and several process measurements.[52,57] The nitrogen gas flows into the sample chamber as shown in Figure 7.3.18. The temperature and rate of gas flow are controlled and the gas temperatures before and after the coating sample tray are measured with thermocouples. The coating temperature is measured with thermocouple which is installed at the coating sample tray, and the solvent laden gas flows into the total hydrocarbon analyzer which is equipped with flame ionization detector (FID). The concentration of solvent at the exhaust gas is measured by total hydrocarbon analyzer, which is calibrated with known concentration of solvent vapor (via solvent bubblers).

Figure 7.3.19 and Figure 7.3.20 show the examples of HADES running.[52] Figure 7.3.19 shows the measured solvent concentration of the PVAC-toluene system, as shown in the figure the residual solvent decreases according to the rate of airflow. However, over the 36 cm/s of airflow rate the drying rate wasn't changed, above this airflow rate, the residual

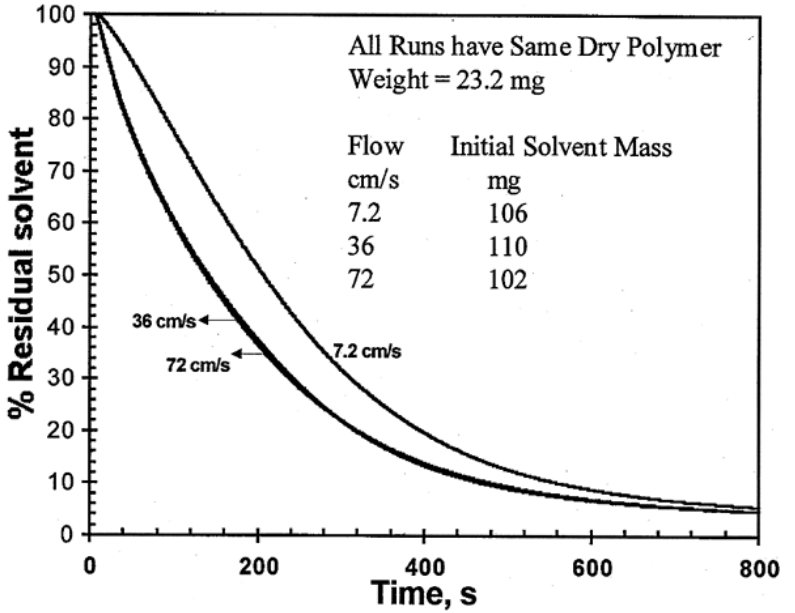

Figure 7.3.19. Measured solvent loss of PVAC-toluene system by HADES. [Adapted, by permission, Vinjamur and Cairncross, Presented at the AIChE national meeting, Dallas, Texas, November 1, 1999].

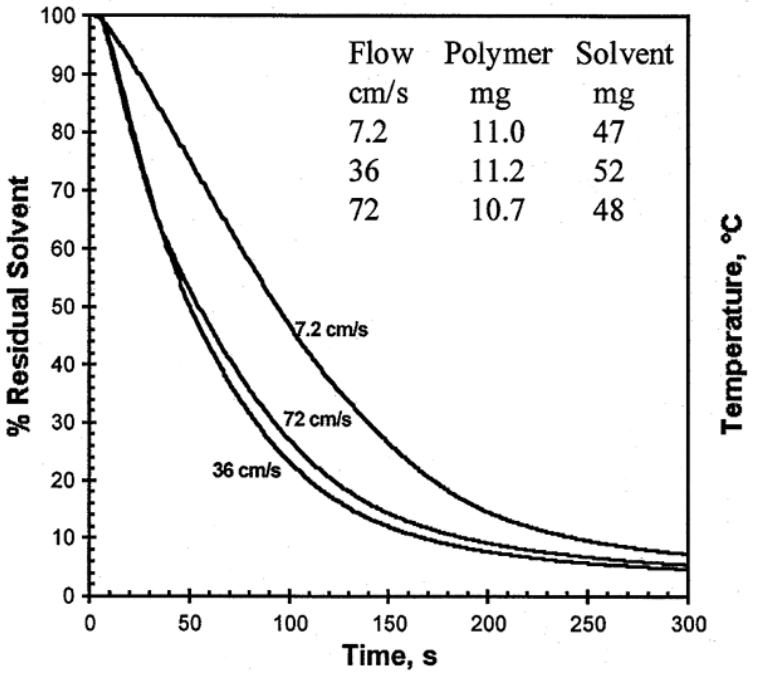

Figure 7.3.20. Measured solvent loss of PMMA-toluene system by HADES. [Adapted, by permission, Vinjamur and Cairncross, Presented at the AIChE national meeting, Dallas, Texas, November 1, 1999].

solvent wasn't decreased by enhancement of airflow rate. From these results we can infer that the drying rate is controlled by internal mass transfer above this airflow rate.

In a case of PMMA-toluene system, the drying rate at the airflow rate of 72 m/sec is lower than that of airflow rate of 36 m/sec (Figure 7.3.20). These are the contrary results to what we expected. It shows that this system exhibits 'trapping skinning' at the high airflow rate. Thus the residual solvent of final dried coating may be minimized at middle airflow as shown in the Figure 7.3.20. As shown in these HADES experiments, it is often the solution to lower the airflow rate or temperature of drying air when trapping skinning is suspected to occur.

7.3.3.4 MEASUREMENT OF DRYING RATE IN THE PRODUCTION SCALE DRYER

Numerous drying rate data have been obtained in laboratory drying experiments using thermo-gravimetric analyzers as shown in the previous chapters. However it was difficult to know the actual drying rate or solvent concentration profiles in the pilot or production scale dryer from these experimental results.

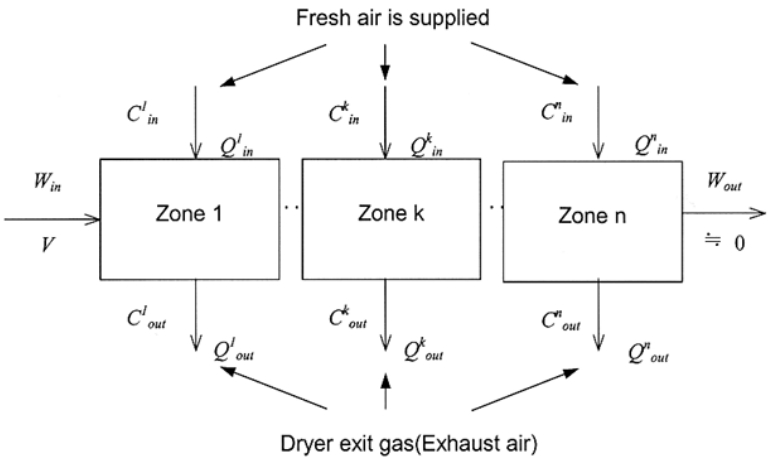

Total amount of evaporated solvent per minute

$$ER^{per} = (W_{in} - W_{out}) \times V \times WD \quad \text{[kg/min]} \qquad \text{(A)}$$

C^k_{in}, C^k_{out} Measured solvent concentration in the supply and exhaust air respectively, at zone k [kg/m^3]

ER^{per} Evaporation rate of solvent calculated by equation A [kg/min]

Q^k_{in}, Q^k_{out} Volumetric supply and exhaust airflow rate at zone k, respectively[m^3/min]

V Line speed [m/min]

W_{in}, W_{out} Initial and final solvent coating amount respectively [kg/m^2] and W_{out} is practically zero in this drying application (less than 1000 ppm)

WD Coating width [m]

Figure 7.3.21. Construction of material balance to calculate the solvent concentration of the coating at each zone end from the measured solvent concentration of exit gas. [After reference 30].

However, in a multiple zone dryer the solvent concentration of coating at the end of each zone could be found by analyzing the dryer exit gas with measured airflow. This experimental method provides concentration profile of each solvent with drying as well as the total drying rate of coating. It gives precise measurement value at the early stages of drying in which the concentration of solvent in the dryer exit gas is high, and the length of each zone is long enough to ensure negligible intermixing of air between adjacent zones.

The solvent concentrations of the exit gas are measured by portable gas chromatography (GC), and the gas samples are taken at the exhausted air duct of each zone. From these concentration data and the airflow rate of each zone, the evaporation rate of solvent at each zone is calculated. (Figure 7.3.21)

$$\textit{Evaporation rate of solvent at zone k, } ER^k \ [kg/min]$$

$$= \textit{Solvent concentration, } C^k_{out} \ [kg/m^3] \times \textit{Airflow rate, } Q^k_{out} \ [m^3/min] \quad [7.3.10]$$

The example of solvent concentration measurement and the accompanying results of drying rate calculation are shown in Table 7.3.2., and the accompanying specification of dryer and the formulation of coating solution is given in Table 7.3.3 and 7.3.4. The solvent concentrations at the exhaust duct are measured by gas chromatography(MTI Analytical Instrument 200, Portable GC). The solvent concentrations were measured three times at the same point, and the deviations from the average value were less than ±5%.

Table 7.3.2

Zone	Concentration, ppm			Evaporation rate, kg/h			
	MEK	Tol.	Cyc.	MEK	Tol.	Cyc.	Total
1	1655	740	142	47.6	27.2	5.6	80.4
2	1150	988	359	40.5	44.4	17.2	102.0
3	485	1243	1866	14.0	46.0	73.5	133.6
4	308	157	2223	1.5	1.0	15.2	17.7
5, 6	269	99	278	6.6	3.1	9.4	19.2

Table 7.3.3

Operating conditions	Drying air temperature, °C	50 ~ 120
	Line speed, m/min	900
Dryer specification	Total number of zones	6
	Total dryer length, m	45
	Dry coating thickness, μm	2.6
	Dryer type	Air floating dryer

Table 7.3.4

Component	Weight fraction, %	Initial coating amount, g/m^2
Pigment and binder	35.5	6.23
Methyl ethyl ketone	21.5	3.77
Toluene	21.5	3.77
Cyclohexanone	21.5	3.77

The solvent concentration of coating at the entrance of dryer is known with coating formulation and the solvent concentration of final dried coating could be measured offline, thus the percent evaporated solvent at each zone can be calculated. In this example of drying of magnetic coated film, the final dried coating contains less than 1000 ppm solvent, so we assumed that all the coated solvent was evaporated within the dryer. Finally, we estimated how much percent of solvent that was evaporated at each zone. The fractional amount of the evaporated solvent at zone, k, is

$$F^k = \frac{ER^k}{\sum_{k=1}^{n} ER^k} \qquad [7.3.11]$$

where:

F^k fractional evaporated solvent amount in zone k
ER^k evaporation rate at zone k
n number of zone

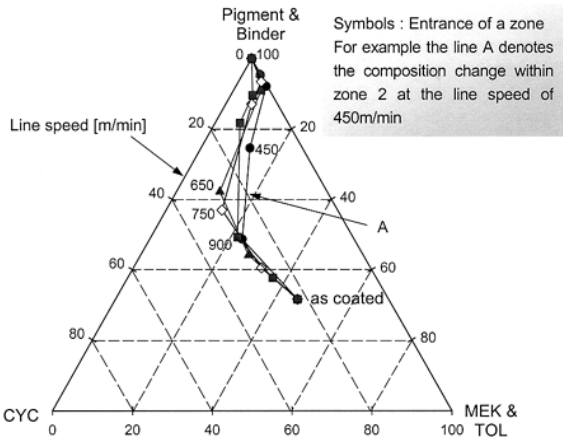

Figure 7.3.22. Measured coating composition changes with drying.

From these fractional solvent evaporation data we estimate the solvent concentration in the coated film at the end of each zone. The solvent content per unit area decreases according to the fractional solvent evaporation data at each zone, for example, if the fractional evaporation rate of solvent is 50% in zone 1 and the initial solvent content is given as 10 g/m^2, then the solvent content at the end of zone 1 should be 5 g/m^2, thus we can find the solvent concentration at the end of each zone. Moreover the measurements and calculations are applied to the each solvent in multiple solvent systems, therefore we can find the solvent content of each solvent at the end of zone. The resulting coating composition changes with drying are shown in Figure 7.3.22.

The theoretical evaporation rate to dry a given solvent load at the specified line speed can be calculated as in Figure 7.3.21. Theoretically and experimentally found evaporation

rate should be equal in ideal case. We can check the measurement error by comparing measured and theoretical evaporation rate through the whole dryer. ER^{per} is calculated by equation A in Figure 7.3.21.

$$\frac{ER^{per} - \sum_{k=1}^{n} ER^{k}}{ER^{per}} = \varepsilon \qquad [7.3.12]$$

In most cases the value of ε is about 0.05 ~ 0.10. ER^{per} is the theoretical evaporation rate which assumes that all the solvent is evaporated only in the dryer. But in the real situation, some of the solvent is evaporated before the dryer, such as in the coating head and the pre-zone (between the coating head and the first dryer zone), and some of the solvent vapor leaks out of the dryer through the gaps where the substrate running in and out. Therefore measured ER was less than ER^{per} by about 10%.

This experimental method gives precise results at the early stages of drying where the concentration of solvent at the exit gas is high. And it is a unique method to measure the solvent concentration of coating in the production and pilot scale dryer.

7.3.4 MISCELLANEOUS

7.3.4.1 Drying of coated film with phase separation

As a final process of coating process, drying plays an important role for the quality of products. The structure of coating is determined during the drying process. The structure formation of coating depends on the history of drying (drying process path) which represents the composition changes of coating during drying. The drying process path depends on the drying conditions such as temperature and velocity of hot air, residence time of coating in the dryer, humidity or solvent concentration of drying air, the initial composition of coating etc. Figure 7.3.23 shows the two different structures of coating according to the extremely different drying conditions (cellulose acetate solution of 10 wt% prepared in acetone 80 wt%

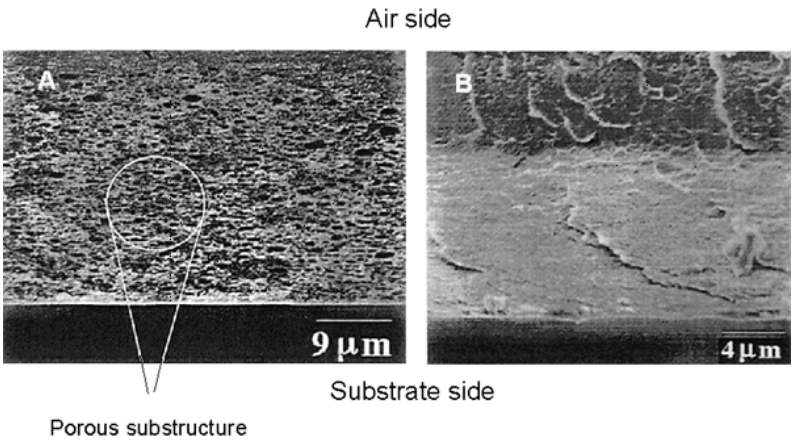

Figure 7.3.23. Cross-sectional SEM images of final coating microstructures prepared under slow and fast rates of external gas-phase mass transfer conditions. [Adapted, by permission, Mahendra et al., Proceedings of 9th International Coating Science and Technology Symposium, Delaware, USA, May 17 - 20, 1998, pp. 177 - 180].

and water 20 wt%).[35] Sample A was dried under the room conditions of free convection mass transfer, and sample B was dried under impinging high velocity air which corresponded to intense forced convection. Though the initial coating compositions were same for the two samples, the coating structures were totally different with each other after drying. As shown in the figure, sample A had a porous structure at the bottom (substrate side) and dense structure at the top (air side) while sample B had a dense structure trough the coating layer.[35]

The structure of coating is determined by the competition of phase separation and solidification phenomena. The final structure is determined by the onset of solidification.[35] The phase behavior of polymer solution is divided into three regions according to the thermodynamic stability; binodal (metastable region), spinodal (unstable region) and stable region. And the area of unstable and metastable region decreases with increasing temperature of solution.[48,49] The phase separation can also be induced by the saturation of polymer in the solution. When a polymer is saturated in a good solvent, we can easily observe the precipitation of polymer by adding some non-solvent to the system. The phase separation region can be found by thermodynamic relations such as Flory-Huggins equation,[35] and it is also be measured by adding non-solvent and observing the turbidity of solution (cloud point method).

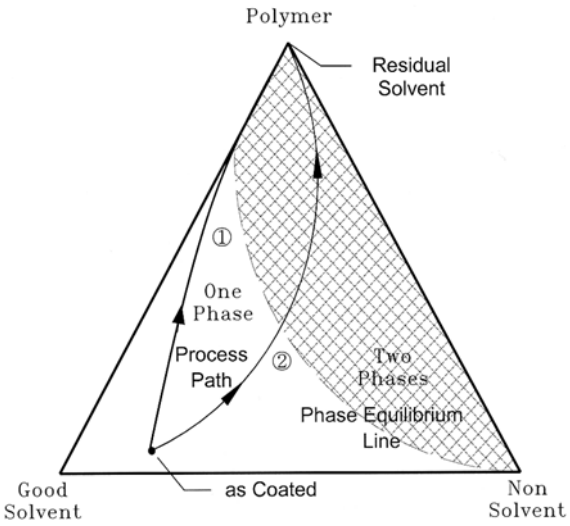

Figure 7.3.24. Conceptual representation of phase separation phenomena during drying.

In these polymer-solvent-solvent system, the drying induced phase separation can be explained by process path and phase equilibrium line. During the drying of coating the phase separation occurs when the isothermal drying path intersects two-phase region as shown in Figure 7.3.24. Let's say that the good solvent is more volatile than the non-solvent, then as the drying proceeded the fraction of non-solvent weight to the good solvent weight is steadily increased. Thus the drying process path intersects the phase equilibrium line as line ② in Figure 7.3.24. However, if the good solvent is less volatile than the non-solvent, then the process path doesn't intersect the phase equilibrium line until the significant amount of solvent is evaporated (line ①).

In most clear coating system, the drying induced phase separation is unwanted phenomena. Therefore formulators are careful about the selection of solvent to avoid the defect. However in some applications, phase separation is needed to have desirable properties for the coating. In the coating of adhesive layer of hot stamping foil, the layer should have discontinuous porous structure as shown in Figure 7.3.25.[29] Humidified air can be used to control the process path. In most polymer-solvent coating systems, the water acted as

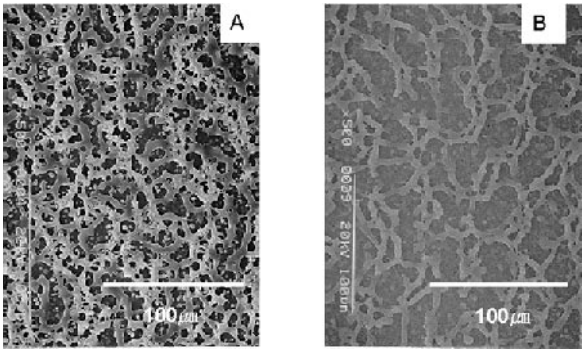

Figure 7.3.25. Surface structure of coatings with different drying conditions (SEM ×500). Humidity of air [kg water/kg dry air] : A - 0.062, B - 0.036, Initial solid content : 10.0 wt%.

non-solvent. But it is difficult to handle or store the water laden coating solution, since the state of solution is very unstable. Therefore to supply water to the coating the highly humidified air is sometimes used at the early stages of drying (in most cases the first and the second zone of dryer). The water was condensed at the coating surface and it acted as non-solvent. By adjusting air humidity various kind of coating structures can be obtained as in Figure 7.3.25.

The phase separation phenomena in polymer-polymer-solvent system can be called as polymer incompatibility.[41,42,56,58] The relative solubility of two polymer in the common solvent determines the surface structure of dried coating. Diverse kinds of surface structure can be obtained by adjusting drying rate, substrate surface properties, relative solubility of solvent.[56,58] The shapes of surface structure can be simulated by Cell Dynamic System.[41,42]

7.3.4.2 Drying defects

The maximum line speed of drying and operating conditions of dryer are often restricted by the onset of defects. The drying related defects could be classified according to the cause of defects - stress induced defects, surface tension driven defects, defects caused by air motion.

7.3.4.2.1 Internal stress induced defects

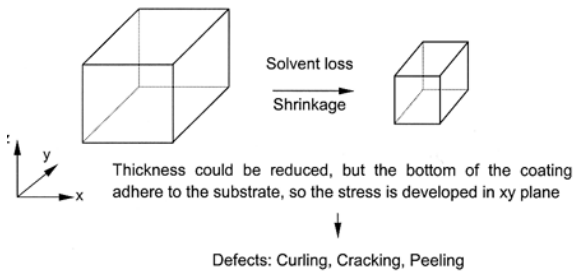

Figure 7.3.26. The origin of internal stress in a conventional polymer solution coating.

Evaporation of solvent is necessarily accompanied with the shrinkage of coating in volume as illustrated in Figure 7.3.26. This shrinkage can be only allowed in the coating thickness direction, because the adhesion of coating to the substrate prevents coating from shrinking in the plane of coating. Thus the stress is developed in the plane of coating. This stress brings about the defects which is known as curling, cracking and peeling.[10-15,21-23,34,46]

Curling and cracking

The internal stresses are build up with drying of wet coating. When the coating has enough mobility, the stresses that are developed during drying can be relieved by flow. After the coating solidified stresses will build up in the lateral dimensions. The solidification point equals the concentration at which the glass transition temperature of coating has risen

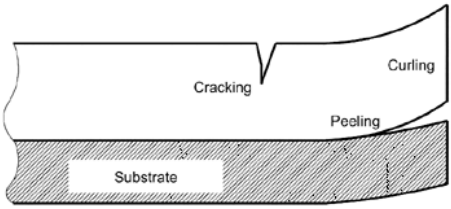

Figure 7.3.27. Internal stress related defects.

to the experimental temperature.[13-15] These stresses bring about the defects such as cracking, curling and peeling. If the local strength is overwhelmed by the local stress, the response is cracking. It is often called as 'mud cracking', because it looks like a field of mud in a dry period. And if the local stresses exceed the adhesion strength of coating to a substrate, the response is peeling or delamination as shown in Figure 7.3.27. At the edge of the coating the internal residual strength rises sharply, hence the stresses bring about the curling of coating at the edge if the adhesion strength of coating is sufficient to endure the peeling or delamination. The curling and peeling are also used to measure the internal stress of coating.[12,14,15,22]

With solvent evaporation, the coating becomes to be concentrated with polymers, and the coating becomes to have solid like nature (viscoelasticity). Thus the stresses depend not only on the strain rate, but also strain. Strain is deformation from the stress-free state.[49] After the solidification point, the solvent evaporation continues, so the stresses persist. Croll analyzed the origin of residual internal stress during drying and correlated the internal stress with the coating properties.[13-15] The residual internal stress, σ, for a coating is

$$\sigma = \frac{E}{1-\nu}\frac{\phi_s - \phi_r}{3} \qquad [7.3.13]$$

where:

E	Young's modulus
ν	Poisson's ratio
ϕ_s	volume fraction of solvent at the point of solidification
ϕ_r	volume fraction of solvent in the dried coating

As shown in the Equation 7.3.13, the internal stress depends on the difference of solvent volume fraction before and after solidification point. Croll's experiment confirms that the internal stress does not depend on the coating thickness until the coating thickness is so large that the net force on the interface exceeds adhesion. At this point stress is relieved by peeling.[12-15]

Adding plasticizer can often be helpful to reduce the internal residual stress of coating, because it makes coating more flexible to the later stages of drying.[13-15] The residual internal stress depends on the solvent volume loss from the solidification point, we can shift the solidification point to the later stages of drying by using plasticizers. Adding plasticizers makes the coating more flexible, but it is not always the desirable property of final products.

The residual internal stress is a result of combined action of stress and stress relaxation process. Therefore to give a sufficient relaxation time for the coating, we often dry a coated film in a mild operating conditions, e.g., dry at lower temperature and velocity of air.

Peeling

If the local stresses exceed the adhesive strength of coating to a substrate, then the coating is delaminated from the substrate. Peeling easily occurs when the coating is thick. With increasing thickness, one can find a critical thickness where the peeling occurs spontaneously. This critical thickness for the spontaneous peeling can be used as a method of measuring internal residual stress.[12]

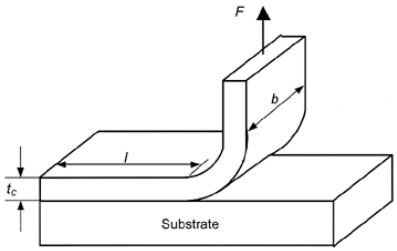

Figure 7.3.28. 90° Peel test configuration [After reference 12].

Croll illustrated that interfacial work of adhesion could be found by peeling test.[12] If the coating is peeled at a constant rate, the rate of change of total internal energy of coating is equal to zero. Thus the peeling strength is related to the interfacial work of adhesion as follows (Figure 7.3.28),

$$\frac{F}{b} = \gamma - t_C U_R \qquad [7.3.14]$$

where:

γ	interfacial work of adhesion
b	sample width (Figure 7.3.28)
F	measured force of peeling
t_C	thickness of sample (Figure 7.3.28)
U_R	recoverable strain energy per unit volume stored in the coating

In a case of spontaneous peeling,

$$\gamma = t_p U_R \qquad [7.3.15]$$

where:

t_p	critical thickness for the spontaneous peeling

Interfacial work of adhesion, γ, can be measured by spontaneous peeling test using above equation. Spontaneous peeling thickness, t_p, can be directly measured, and the recoverable strain energy, U_R, for an elastic material under a one-dimensional strain is,

$$U_R = \frac{1}{2} E \varepsilon_i^2 \qquad [7.3.16]$$

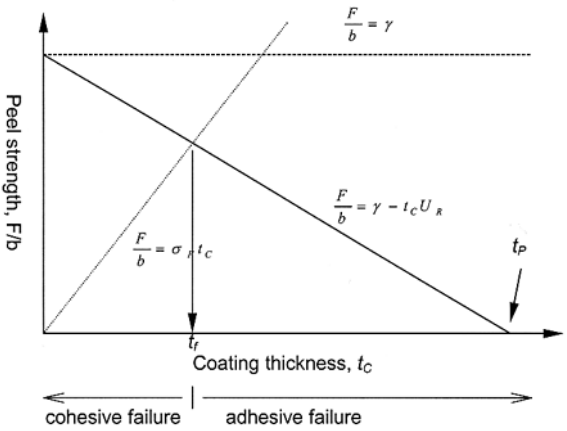

Figure 7.3.29. Graphical representation of the equations governing the 90° peel test. [Adapted, by permission, from Croll, S.G., *J. Coating Technol.*, **52**, 35 (1980)].

where:

E	modulus of coating
ε_i	internal strain in coating

As shown in Figure 7.3.29 the interfacial work of adhesion and recoverable strain can also be found by measuring peeling strength at several different coating thickness. If the adhesive strength of the interface exceeds the cohesive strength of one of the coating component materials, there occurs cohesive failure - the coating layer loses the adhesive strength within the layer itself. At a small thickness, cohesive failure often occurs during the peeling test illustrated in Figure 7.3.28.

The spontaneous peeling thickness can be found by extrapolating the experimental data to the zero peeling strength. The validity of interfacial work of adhesion and recoverable strain which is obtained from this experiment can be tested by comparing this spontaneous peeling thickness with obtained from independent measuring of spontaneous peeling thickness.

To enhance the adhesive strength, the surface properties of substrate are very important. The surface treatments are often used to enhance the adhesive strength between the coating and the substrate, as well as to enhance the surface energy of substrate - improving wettability of coating. If adhesive problem occurs, check out the surface treatment processes such as flame, plasma, or corona.[21] Corona treatment does not persist permanently, therefore it should be done in-line, the corona is often applied directly before the coating station.

Sometimes a thin, high surface energy adhesive or subbing layer is coated on the substrate to improve the adhesion of coating.[21] As often the case, this layer is coated in-line during manufacturing of substrate - such as in-line coating of acrylic resin during bi-axial extension of PET film. If the adhesive failure occurred when one used these kind of treated substrate, one should check that the correct side was used where the subbing layer was coated and the status of coated subbing layer was perfect. Simple peel tests with adhesive tape can give a clue to the coating status of subbing layer. First laminating the adhesive tape with substrate where the coated material is applied, then pull off the tape rapidly. If there are problems with the subbing layer such as the partial un-coating of subbing layer, then the coating will be peeled off according to the un-coated pattern. By analyzing un-coated pattern, one can find the steps of process which have problems. If the substrate is suspected, change the substrate lots.

7.3.4.2.2 Surface tension driven defects

Defects can arise during drying of a coated film by building non-uniform surface tension gradient over the coating. They include convection or Benard cells, fat edges or picture framing, etc.

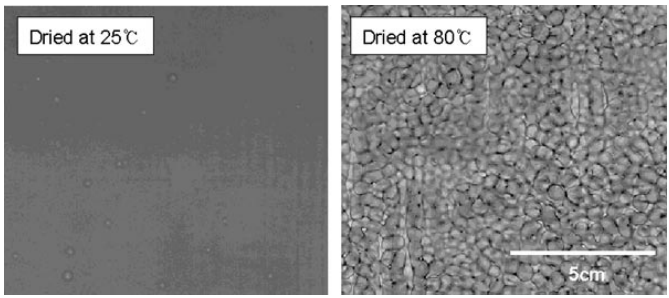

Figure 7.3.30. Surface tension driven defect: Convection cells.

Convection cells

Convection or Benard cells can arise when the coating is heated from the bottom of the coating, and the density or surface tension gradients are built across the coating thickness. These gradients lead to convection cells which look like regular close-packed hexagonal surface patterns (Figure 7.3.30).[10,21] The evaporative cooling can also be the cause of the temperature gradient. This gradient arises the density and surface tension gradient, which brings about the internal flows within the coating to form the convection or Benard cells.

The convection cells, which come from the surface tension gradient, can arise when the Marangoni number (Ma) exceeds 80.[10] The Marangoni number is

$$Ma = \frac{(d\sigma / dT)(dT / dy)h^2}{\mu\kappa} \qquad [7.3.17]$$

where:

σ	surface tension
μ	viscosity
κ	heat conductivity
T	temperature
h	thickness of coating
dT/dy	temperature gradient in the thickness direction

Convection cells can arise at a lower Marangoni number when the coating thickness is above 2 mm.[21] Convection or Benard cells can be reduced or eliminated by adjusting operating conditions and formulation of coating solution. The possibility of having convection cells is reduced at the following conditions[21]

- Lower surface tension of coating liquid
- Reduce the thickness of the wet coating
- Increase the viscosity of coating liquid
- Reduce the drying rate by adding low volatile liquid or reducing the temperature of drying air

When the thickness of wet layer of coating is less than 1 mm, as is often the case with almost all coatings, convection cells are almost always due to the surface tension gradients.[10,21]

However, it is not desirable to lower the drying rate because it decreases the line speed of coating process. Frequently it is helpful to use surfactant to reduce the convection cells due to the surface tension gradients. Care should be given in selection of the surfactant and the amount of it not to deteriorate the final quality of products. The amount of surfactant should be minimized, excess surfactants can migrate to the coating surface and react with humidity at a coating station to form a haze coating surface. Moreover, the remaining excess surfactant, which is in the final products, can migrate to the coating surface while the products in use in a some environmental conditions to ruin the final quality of the products.

Fat edges

Fat edges can be built during drying of coating with non-uniform surface tension distribution at the edges of coating. Figure 7.3.31 illustrates the mechanisms of fat edge defects. The edges are usually thinner than the bulk of coating, thus as the evaporation proceeded the concentration of polymer is increased faster at edges than in the bulk of coating. Usually the surface tension of solid is much higher than that of polymer, the surface tension is higher at the edges than the bulk. The higher surface tension at the edges will

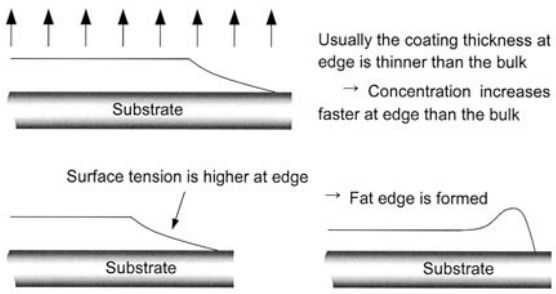

Figure 7.3.31. Formation of fat edge or picture framing.

cause to flow to the edges, giving fat edges. The surfactants are often helpful to eliminate the fat edges.

7.3.4.2.3 Defects caused by air motion and others

Dryer bands

At the early stages of drying, where the coating has enough mobility to flow, the coating layer is apt to being disturbed by the motion of drying air.[21] This defect is observed in the dryer which uses the arrays of round jet nozzles rather than the slot nozzles. Often it looks like a lane running in the machine direction and the width of bands is nearly equal to the nozzle diameter. When the air comes out of slots, bands are less likely if the flow across the slot is uniform.[10,21,25] The bands are more likely to be developed with low viscosity solution, thick coating and high air velocity. Thus we can reduce the bands by reducing air velocity (but this also decreases the drying rate) and by increasing the initial solid content so as to increase the viscosity of solution and to coat thinner layer with concentrated solution.

The geometry of arrays of round jet nozzles should be designed to avoid this defect by applying nozzles of larger diameters in the first part of zones. Large amount of fresh air is needed in the first part of zones of the multiple zone-dryer, because in the first zone the amount of evaporated solvent vapor is large, hence one should supply enough fresh air to ensure the dryer is operated below the lower explosive level (LEL) of a given solvent. Therefore the diameters of round jet nozzles are gradually decreased along the dryer length.

Skinning

If the drying rate of solvent is extremely high, then the solvent concentration at the surface of coating falls rapidly, for the rate of solvent evaporation is much higher than that of diffusion of solvent within the coating. This rapid decrease of solvent concentration at the surface causes to form a thin solid layer near the coating surface. This phenomena called as 'skinning', and it retards the drying of coating.[4,5,8-10] Skinning can be reduced by using solvent laden gas as a drying air,[4,8,10] but it isn't applicable to the conventional drying process in which uses the volatile organic compound as a solvent. Most of the solvent has the possibility of explosion above a certain concentration in the air. Thus solvent laden drying gas should be applied in a inert environment, in which no oxygen is present. If the skinning occurs in a aqueous coating system, it is possible to use humid air to reduce the skinning.

7.3.4.3 Control of lower explosive level (LEL) in a multiple zone dryer

If the solvent concentration of a zone exceeds certain level, then the system becomes to be in danger of explosion due to the flammability of organic solvent vapor. This level of solvent concentration is called as lower explosive level (LEL), and the dryer should be operated below the LEL prior to any constraints. Thus each zone needs sufficient airflow rate to meet these needs. However, too much airflow rate results in waste of energy to heat the excess air, and it increases the load of waste gas facilities (e.g., VOC emission control units). Therefore the airflow rate of each zone and the ratio of recycled to fresh air should be optimized. The typical airflow system for a multiple zone dryer is shown in Figure 7.3.32. The supplying air of each zone is consisted of fresh and recycled (used or returned from the exit gas) air as shown in the figure. LEL can be calculated if we know the evaporation rate of solvent of a zone. The evaporation rate of solvent can be measured or calculated as we explained in previous sections. Thus we can distribute the fresh air to each zone to meet the LEL safety without substantial increase in the total exhaust air.

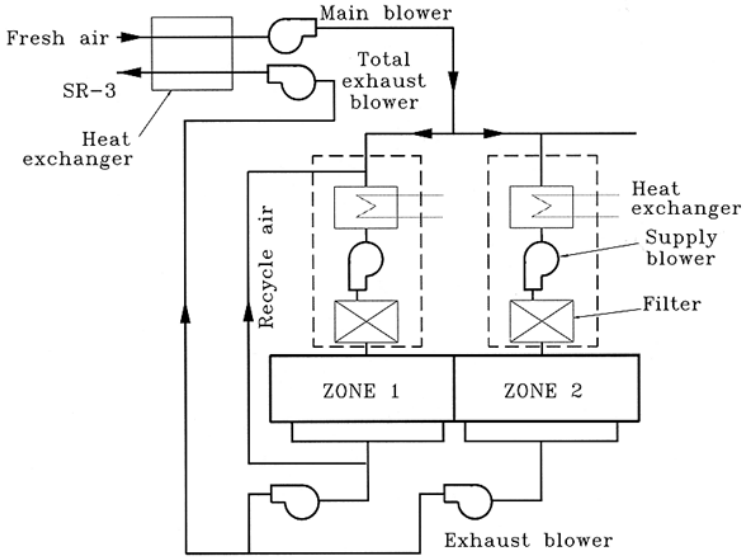

Figure 7.3.32. Schematic diagram of airflow system to a zone. [After reference 30].

7.3.5 NOMENCLATURE

B	Nozzle slot width
b	Thickness [m]
C	Concentration of solvent at a gas phase [kg/m^3]
C_P	Specific heat [J/kg]
E	Young's modulus
ER	Evaporation rate of solvent [kg/min]
F	measured force of peeling
f	Fraction open area (B/L_T)
f_O	$[60 + 4(H/2B - 2)^2]^{-1/2}$
G	Mass flow rate of dry air [kg/sec]
h	Heat transfer coefficient [J/m^{2}s^{o}C]
H	Nozzle to coating surface distance
k	Heat conductivity [J/m^{o}C]
k_m	Mass transfer coefficient [m/sec]
L_T	Nozzle spacing
P	Vapor pressure [atm]
Q	Volumetric flow rate of air [m^3/min]
R	Gas constant
T	Temperature [^{o}C]
t	Time [s]
t_C	Thickness of sample
U_R	Recoverable strain energy per unit volume stored in the coating
V	Line speed [m/min]
W	Solvent coating amount [kg/m^2]
w	Velocity of air at the nozzle exit [m/sec]
WD	Coating width [m]
z	Volume fraction of component [-]

Dimensionless Numbers

Sh	Sherwood number

Nu	Nusselt number
Le	Lewis number
Sc	Schmidt number
Pr	Prandtl number
Ma	Marangoni number

Greek letters

ϕ_s	Volume fraction of solvent at the point of solidification
ϕ_r	Volume fraction of solvent in the dried coating
γ	Interfacial work of adhesion
γ	Activity coefficient
δH	Heat of vaporization [J/kg]
ε_i	Internal strain in coating
κ	Heat conductivity
μ	Viscosity
ν	Poisson's ratio
ρ	Density of pure component [kg/m^3]
σ	Surface tension

Subscripts

a	Pertinent to dry air
C	Pertinent to coating layer
f	Pertinent to substrate, PET film
fn	Outlet condition
i	Component
in	Inlet condition

Superscripts

k	Zone number
∞	Bulk air condition

REFERENCES

1 Alsoy, S. and J. L. Duda, *Drying Technol*., **16**, 15, (1998).
2 Aust, R., F. Dust and H. Raszillier, *Chem. Eng. Process*., **36**, 469 (1997)
3 Bird, R. B., W. E. Stewart and E. N. Lightfoot. **Transport Phenomena**, *John Wiley & Sons*, 1960.
4 Bornside, D. E., C. W. Macosko, and L. E. Scriven, *J. Appl. Phys.*, **66**, 5185, (1989).
5 Cairncross, R. A., A. Limbert, L. F. Francis, and L. E. Scriven, 24th annual meeting of Fine Particle Society, 24-28 August 1993, Chicago, IL.
6 Cairncross, R. A., L. F.Francis, and L.E. Scriven, *AlChE J.*, **42**, 55 (1996).
7 Cairncross, R. A., S. Jeyadev, R.F. Dunham, K. Evans, L.F. Francis, and L.E. Scriven, *J. Appl. Polym. Sci.*, **58**,1279 (1995).
8 Cairncross, R. A., Ph.D. thesis, University of Minnesota, Minneapolis (1994).
9 Cary, J. D. and E. B. Gutoff, "Analyze the Drying of Aqueous Coatings" *Chem. Eng. Prog*., **2**, 73 (1991).
10 Cohen, E. and E.Gutoff, **Modern Coating and Drying Technology**, *VCH Publishers, Inc*., New York, 1992.
11 Cohen, E., E. J. Lightfoot and K. N. Christodoulou, *Ind. Coating Res.*, **3**, 45 (1995).
12 Croll, S.G. *J. Coating Technol*., **52**, 35 (1980).
13 Croll, S.G. *J. Coating Technol*., **51**, 64 (1979).
14 Croll, S.G. *J. Coating Technol*., **50**, 33 (1978).
15 Croll, S.G. *J. Appl. Polym. Sci.*, **23**, 847 (1979).
16 Cussler, E. L. **Diffusion Mass Transfer in Fluid Systems**, 2nd Ed., *Cambridge University Press*, 1997.
17 Duda, J. L., J. S. Vrentas, S. T. Ju, and H. T. Lu, *AIChE J*., **28**, 279 (1982).
18 Evans, K. J., Smith, W. R., Dunham, R. F., Leenhouts, T. J., Ceglinski; B. D., and Cairncross, R. A., **US Patent 5,394,622**.
19 Felder, R. M. and R. W. Rousseau. **Elementary Principles of Chemical Processes**, 2nd Ed., *John Wiley & Sons, Inc*., 1986.
20 Gutoff, E. B., *Drying Technol*., **14**, 1673 (1996).
21 Gutoff, E. and E. Cohen, **Coating and Drying Defects - Troubleshooting Operating Problems**, *John Wiley & Sons*, Inc., 1995.

22 Hoffman, R.W., *Surf. Interface Anal*., **3**, 62 (1981).
23 Hu. S. M., *J. Appl. Phys*., **50**, 4661 (1979).
24 Huelsman, G. L. and W. B. Kolb, **US Patent 5,694,701**.
25 Hunt, B. V., R. A. Yapel and R. K. Yonkoski, 9th International Coating Science and Technology Symposium, Delaware, USA, May 17 - 20, 1998, pp. 93 ~ 96.
26 Imakoma, H. and M. Okazaki, *Ind. Coating Res.*, **1**, 101 (1991).
27 Imakoma, H. and M. Okazaki, *Ind. Coating Res.*, **2**, 129 (1992).
28 Kim, S. S. and M. H. Kwon, 9th International Coating Science and Technology Symposium, Delaware, USA, May 17 - 20, 1998, pp. 353 - 356.
29 Kim, S. S., H. S. Park, I. C. Cheong and J. S. Hong, 3rd European Coating Symposium , Erlangen, Germany, Sep. 7 - 10, 1999.
30 Kim, S. S., M. H. Kwon, submitted to the *Drying Technol*. (1999).
31 Kolb, W.B. and G. L. Huelsman, 9th International Coating Science and Technology Symposium, Delaware, USA, May 17 - 20, 1998, pp.209 ~ 212.
32 Kolb, W.B. and M.S. Carvalho, 9th International Coating Science and Technology Symposium, Delaware, USA, May 17 - 20, 1998, pp.9 ~ 12.
33 Koschmieder, E.L., and M.I.Biggerstaff, *J. Fluid Mech*., **167**, 49, (1986).
34 Lei, H, L. F. Francis, W. W. Gerberich and L. E. Scriven, 9th International Coating Science and Technology Symposium, Delaware, USA, May 17 - 20, 1998, pp.97 ~ 100.
35 Mahendra D., L. F. Francis and L. E. Scriven., 9th International Coating Science and Technology Symposium, Delaware, USA, May 17 - 20, 1998, pp 177 ~ 180.
36 Mahendra D., L.F.Francis and L.E. Scriven., 1st Asian and 7th Japan Coating Symposium, Fukuoka, Japan, Sept. 1997, pp 8 ~ 9.
37 Martin, H., **Advances in Heat Transfer**, 13, pp.1~60, *Academic Press*, New York, 1977.
38 Ohta, T., H. Nozaki and M. Doi, *J. Chem. Phys*., **93**, 2664 (1990).
39 Oishi, T. and J. M. Prausnitz, *Ind. Eng. Chem. Process Des. Dev*., **17**, 333 (1978).
40 Okazaki, M., K. Shioda, K. Masuda, and R. Toei, *J. Chem. Eng. Japan*, **7**, 99 (1974).
41 Oono, Y. and S. Puri, *Phys. Rev. A: At. Mol. Opt. Phys*., **38**, 434, (1988).
42 Oono, Y. and S. Puri, *Phys. Rev. A: At. Mol. Opt. Phys*., **38**, 1542, (1988).
43 Pan, S. X, H. T. Davis, and L. E. Scriven, *Tappi J*., **78**, 127 (1995).
44 Pan, S. X., Ph.D. thesis, University of Minnesota, 1995.
45 Polat, S. *Drying Technol.*, **11**, 1147 (1993).
46 Sato, K., *Prog. Org. Coat*., **8**, 143 (1980).
47 Saure, R. and V. Gnielinski, *Drying Technol.*, **12**, 1427 (1994).
48 Scriven, L.E. and W.J. Suszynski, Coating Process Fundamentals, Short course. June 19-21, 1996. University of Minnesota.
49 Smith, J. M and H. C. Van Ness, **Introduction to Chemical Engineering Thermodynamics**, *McGraw-Hill*, 1987.
50 Suzuki, I., Y. Yasui and A. Udagawa, 9th International Coating Science and Technology Symposium, Delaware, USA, May 17 - 20, 1998, pp. 21 - 24.
51 Takase, K., H. Miura, H. Tamon and M. Okazaki, *Drying Technol.*, **12**, 1279 (1994).
52 Vinjamur, M. and R. A. Cairncross, Presented at the AIChE national meeting, Dallas, Texas, November 1, 1999.
53 Vrentas, J. S. and C. M. Vrentas, *J. Polym. Sci. Part B : Polym. Phys*., **32**, 187 (1994).
54 Vrentas, J. S. and J. L. Duda, *AIChE J*., **25**, 1 (1979).
55 Vrentas, J. S. and J. L. Duda, *J. Appl. Polymer. Sci*., **21**, 1715 (1977).
56 Walheim, S., Böltau, M., Mlynek, J., Krausch, G. and Steiner, U, *Macromol*., **30**, 4995 (1997).
57 Winward, T. and R. A. Cairncross, 9th International Coating Science and Technology Symposium, Delaware, USA, May 17 - 20, 1998, pp.343 - 346.
58 Yamamura, M., K. Horiuchi, T. Kajiwara, and Adachi, K, 3rd European Coating Symposium, Erlangen, Germany, Sep. 7 - 10, 1999.
59 Yapel, R. A., M.S. Thesis, University of Minnesota, Minneapolis, 1988.
60 Zielinski J.M. and J. L. Duda, *AIChE J*., **38**, 405 (1992).